UNIVERSITY OF CALIFORNIA,
IRVINE

Tracing Anthropogenic Emissions from Cities Using Atmospheric Measurements and Plant Radiocarbon

DISSERTATION

submitted in partial satisfaction of the requirements
for the degree of

DOCTOR OF PHILOSOPHY
in Earth System Science

by

Cindy Cristina Yañez

Dissertation Committee:
Professor Claudia Czimczik, Chair
Associate Professor Francesca Hopkins
Professor James Randerson

2024

DEDICATION

For my beloved nephew
Ethan Manuel Rojo

TABLE OF CONTENTS

Page

LIST OF FIGURES iv

LIST OF TABLES vii

ACKNOWLEDGEMENTS viii

VITA x

ABSTRACT OF THE DISSERTATION xiii

INTRODUCTION 1

CHAPTER 1 CONTRASTING TRENDS IN VEHICLE COMBUSTION EFFICIENCY IN LOS ANGELES, CA AND SALT LAKE CITY, UT 8

1.1 Introduction 8
1.2 Materials and Methods 11
1.3 Results and Discussion 16
1.4 Acknowledgements 27

CHAPTER 2 REDUCTIONS IN CALIFORNIA'S FOSSIL FUEL CARBON DIOXIDE EMISSIONS DURING THE COVID-19 PANDEMIC 28

2.1 Introduction 28
2.2 Methods 32
2.3 Results and Discussion 37
2.4 Conclusions 50
2.5 Acknowledgements 51

CHAPTER 3 PLANT RADIOCARBON ACROSS AN URBAN-RURAL CO_2 GRADIENT MATCHES SURFACE AND COLUMN CO_2 OBSERVATIONS 52

3.1 Introduction 52
3.2 Methods 54
3.3 Results and Discussion 62
3.4 Conclusions 71

CONCLUSIONS 72

REFERENCES 77

APPENDIX A 87

APPENDIX B 98

APPENDIX C 107

LIST OF FIGURES

Figure 1.1. Histograms showing the distribution of CO_{xs}/CO_{2xs} for each mobile survey: (left panels) Los Angeles in (a) 2013 and (b) 2019, (right panels) Salt Lake City in (c) 2013 and (d) 2019. The solid vertical lines indicate the median and the dashed line indicates the mean value of each survey. For visualization purposes and comparison between surveys, the x-axis has been truncated. Inset maps on each panel show the full data distribution of each survey without truncation. 17

Figure 1.2. Maps showing the ratio of CO_{xs}/CO_{2xs} for each mobile survey: (left panels) Los Angeles in (a) 2013 and (b) 2019, (right panels) Salt Lake City in (c) 2013 and (d) 2019. 19

Figure 1.3. Histograms and maps of on-road CO_{xs}/CO_{2xs} observations in Los Angeles in July (a-b) 2019, (c-d) 2020, during COVID-19 pandemic related traffic reductions, and (e-f) 2021.The dashed lines on the histograms are the median CO_{xs}/CO_{2xs} values for each survey. The x-axes on the histograms have been truncated for visualization purposes. 20

Figure 1.4. Box plots of hourly traffic speed, derived from the ratio of reported vehicle miles traveled (VMT) per vehicle hour traveled (VHT), for (a) Los Angeles freeways (I-5, I-405, I-605, I-210, SR-60, and SR-91) and (b) Salt Lake City freeways (I-15 and I-80) ver the month each mobile survey was conducted. Only daytime hours are included (11AM - 4PM local time). VMT and VHT data were downloaded from the Performance Measurement Systems data sources (CalTrans, 2022; UDoT, 2022). 23

Figure 2.1. On-road CO_{2xs} observed near midday on Los Angeles freeways before (2019) and during the COVID-19 pandemic (2020 and 2021). Choropleth maps show CO_{2xs} observations in (a) July 2019, (b) July 2020, and (c) July 2021. Green triangles show locations of plant ^{14}C samples collected in 2020 and 2021. Basemap shows topography for elevations >300 m as hillside shading based on a Digital Elevation Model from USGS. 38

Figure 2.2. The $\Delta^{14}C$ (‰) of annual grass samples collected in California, USA and the corresponding C_{ff} values in 2020. Blue points indicate locations where plants were collected in both 2020 and 2021, while pink points indicate 2020-only locations. Background colors were mapped using an ordinary kriging interpolation of 2020 plant $\Delta^{14}C$ values using the Spatial Analyst toolbox in ESRI's ArcMap software. The uncertainty in the kriging prediction is presented in Fig. B4. 43

Figure 2.3. A record of $\Delta^{14}C$ measurements from 2003-2021. Average plant 14C from various studies are shown as green points with error bars showing the standard deviation. Green circles represent statewide data (this study and Riley et al. 2008) while triangles represent only the Los Angeles metropolitan area (this study and Wang & Pataki, 2010). Air-based ^{14}C observations are shown as gray lines (X. Xu, Pers. Comm., 2021)

and blue triangles (Miller et al., 2020). Shaded green bars represent the typical annual grass growing season in California (March to May). 44

Figure 2.4. Growing season $\Delta^{14}C$ of ambient CO_2 in Pasadena, CA, a city within the northeast Los Angeles basin. The blue circles show the average growing season (March to May) $\Delta^{14}C$ of ambient CO_2 at Caltech [Newman et al., 2016], with error bars showing the minimum and maximum $\Delta^{14}C$ measurements. The line is a linear regression of these data with shading indicating the 95% confidence intervals. The green triangles show the measured $\Delta^{14}C$ of plant samples collected approximately 4 km away from the Caltech site in 2020 (n=1) and 2021 (n=6, error bars show standard deviation). 45

Figure 2.5. The difference in C_{ff} values from 2020 to 2021 between plant samples repeatedly collected in California's urban areas: (a) the San Francisco Bay Area and (b) the Los Angeles metropolitan area. Points show sample locations colored by their change in C_{ff}. Redder colors indicate CO_2 emission increases in 2021 compared to 2020. Background colors were calculated using an Ordinary Kriging interpolation of C_{ff} in ESRI's ArcMap software. C_{ff} changes by land use class are shown in (c). 46

Figure 3.1. Map showing study sites in the Los Angeles area in Southern California, USA. Background colors indicate CO_2 emissions from the Hestia-LA annual 2015 emissions inventory, which has a spatial resolution of 1 km × 1 km (Gurney et al., 2019). Grid cells with less than 1 ktC emissions yr^{-1} were excluded for visualization purposes. Diamond symbols indicate site locations, with darker red colors indicating more urbanization. Sites that were used to estimate background CO_2 levels are in gray. 56

Figure 3.2. Temporal trends in $\Delta^{14}C$, XCO_2 and surface CO_2 measurements collected in and around the Los Angeles area. (a) Points are plant $\Delta^{14}C$ observations averaged and colored by site. Lines are ambient $\Delta^{14}CO_2$ measurements from air samples collected in Utqiagvik, AK (gray) and Irvine, CA (orange). (b) Points are daily-averaged XCO_2 observations colored by site, with error bars representing the daily standard deviation. Orange and black lines are daily-averaged XCO_2 observations from the TCCON PAS and AFRC sites, respectively. (c) Points are daytime (10:00 – 16:00 PT), daily-averaged surface CO_2 measurements colored by site. Lines are daytime daily-averaged surface CO_2 measurements at SCI and VIC background sites. 63

Figure 3.3. Correlations between plant fossil fuel enhancements derived from ^{14}C analysis ("Plant C_{ff}") and (a) excess surface CO_2 based on in situ measurements collected on rooftops/towers ("Surface CO_{2xs}") and (b) total column CO_2 enhancements (ΔXCO_2) based on ground-based solar spectra measurements. The colors of the points indicate the site, with darker red colors representing more urbanized sites. 66

Figure 3.4. Isotopic mixing analysis used to determine Δ_{source}, following the same protocol as in Miller et al. (2020). Green triangles are calculated from plant $\Delta^{14}C$ and in situ CO_2 measurements aggregated by site and season (including DLA, PAS, IRV, and RIV). Gray points are measurements made by Miller et al. (2020) at three sites in LA using

flask analysis of air $\Delta^{14}CO_2$ and CO_2 in 2015-2016. The linear fits were calculated using a York regression method (York et al., 2004), which considers the error in both x and y. The slope of the fit line (Δ_{source}) and its uncertainty for each dataset is shown on the lower left, with the green line/slope calculated based on the plant ^{14}C data and the black line/slope was calculated using air $^{14}CO_2$ data from Miller et al. (2020). 68

Figure 3.5. Source attribution of C_{xs} to C_{ff} and C_{bio} for each site in (a) spring, (b) summer, (c) fall and (d) winter. Bars represent the average C_{xs} (blue), C_{ff} (gray), and C_{bio} (green) for a site and season. Uncertainty is calculated using a Monte Carlo simulation described in Appendix C. Sites with "NA" indicate that surface CO_2 observations were not available for the calculation. The net ecosystem exchange (NEE) estimates were provided by the Solar Induced Fluorescence for Urban biogenic Fluxes (SMUrF) model (Wu et al., 2021). Hourly NEE estimates from SMUrF were averaged for the LA Basin region on a monthly basis for the most recent year available (2019), specifically, May, August, November, and March for spring, summer, fall, and winter, respectively. 70

LIST OF TABLES

Table 2.1. Changes in CO_2 levels during the COVID-19 pandemic in California based on on-road mobile surveys and observations of ^{14}C in plants and/or air. _____ 39

Table 3.1. Overview of CO_2 observation sites in the Los Angeles area in relation to existing Total Carbon Column Observing Network (TCCON) and LA Megacities (LAM) network sites._____ 55

ACKNOWLEDGEMENTS

This research was supported by the National Science Foundation Graduate Research Fellowship Program (DGE-1839285) and the University of California Office of the President Lab Fees Research Program. Chapter 2 is a reprint of the material as it appears in "Reductions in California's Urban Fossil Fuel Carbon Dioxide Emissions during the COVID-19 Pandemic" *AGU Advances*, 3(6), e2022AV000732, with permission from Wiley and co-authors: F.M. Hopkins, X. Xu, J.F. Tavares, A.M. Welch, and C.I. Czimczik. Chapters 1 and 3 are currently unpublished material that is co-authored by R. Bares, C.I. Czimczik, J. Lin, J. Zhang, S.E. Bush, F.M. Hopkins, M.K. Dubey, A. Meyer, X. Xu, J. Romero, J. Kim, and H. Parker.

I would like to express my profound gratitude to my Ph.D. committee for their immeasurable guidance and mentorship over the last five years. I owe many thanks to my advisor, Dr. Claudia Czimczik, who patiently pushed me to do my best work and diligently believed in me even when I was only starting to gain experience doing research. Thank you for training me to think like a scientist and for all the great times we have had in the field and developing these projects. I am also deeply thankful to Dr. Francesca Hopkins for opening so many doors for me, starting with her response to my cold email in 2017. I will forever be grateful for all your guidance since the start of my career, and in admiration of your research creativity and active efforts to make science inclusive and open to all. I also thank Dr. Jim Randerson, who inspired me with the many great ideas that he generously shared with me.

This research was a team-effort, and I had the privilege of working with many talented people in the field and in the lab. I would like to thank the many community scientists and volunteers who donated their time and energy to assist with this work. Thank you to Caren Girguis, Arvin Ocampo, Lynette Ocampo, Valerie Carranza, Celia Limon, Audrey Odwuor, Allison Welch, and Nidia Rojas for voluntarily sitting in traffic with me for science and for the memories we made while driving around Los Angeles in the mobile lab. The plant samples in Chapter 2 were collected by community scientists across the state of California. Their active curiosity and enthusiasm for science gave me inspiration to power through this research during the trying times of the COVID-19 pandemic. The EM27/SUN measurements in Chapter 3 would not have been possible without the help of enthusiastic volunteers including Jazmin Romero, Yuan Liu, Theo Mackey, Harrison Parker, Angelu Lupascu, Maddie Haddad, Shay Syed, Isis Frausto-Vicencio, Valerie Carranza, Yaning Miao, Jinyhuk Kim, Ethan Mao, Audrey Odwuor, Allison Welch, Faith Sunga, Adrian Nunez, Uy Tran, and Arvin Ocampo. Also, I am grateful to Aaron Meyer, Sajjan Heerah, and Isis Frausto-Vicencio for teaching me how to use the EM27 instrument and always being super helpful when answering my questions.

I owe lots of thanks to my mentors and lab mates from the Hopkins Lab at UCR and the Czimczik lab at UCI. A special thanks to Isis Frausto-Vicencio and Valerie Carranza who were my initial inspiration for pursuing a Ph.D. Their mentorship helped me navigate many challenges and shape my career path. I am also very grateful for the comradery of the "lab girls", Audrey Odwuor and Allison Welch, who always made themselves available for lab discussions and venting. We will still visit Tijuana together some day. I would also like to thank Gracie Wong, who became one of my closest friends during this process. In our first year in the Ph.D. program, we quickly discovered that we are the same person. I feel very lucky for this era we spent being neighbors, going to concerts together, watching reality TV, and enjoying some tea.

This accomplishment would not have been possible without the support and encouragement of my family. I am grateful to my mother, Bertha Felix, for engraining in me a spirit of hard work, for the many sacrifices she has made for me and for always setting an example for me to power through challenging times. I thank my father, Salvador Yañez, who called me almost every day just to say "te quiero hasta el mundo." I am also so grateful for my deep friendship with my siblings: Susana, Mariana, and Chava, who always remind me to have fun and for the bond we have through watching movies and playing games together. These distractions are what refueled me whenever I sabotaged myself into burn out. I am also immensely grateful to Dora Cuen and Jacob Ocampo, for embracing me into their loving family and for the countless dinner table conversations filled with many laughs and tears. They never let me struggle alone, and went out of their way to accommodate me in their house during COVID and in the last year when I moved out of Irvine. I would also like to thank Azula and Arlo for their unconditional love and warm companionship.

Last, but not least, I am incredibly grateful to my best friend and partner in life, Arvin Ocampo, who has been my biggest supporter for the past ten years. He made this research better by sharing his perspectives as an urban planner which helped me keep this work motivated by our common goal of improving the communities that we live in. He also voluntarily assisted me with all the field work for these projects and woke up at 4 am with me in solidarity as I finalized my dissertation. His sense of humor, cooking and comforting presence kept me grounded, especially during the last year when I had no work-life balance. He witnessed all my highs and lows, and was there to celebrate all the milestones and to pick me up during all the difficult times. I am incredibly inspired by his genuine curiosity about everything and am grateful to him for consistently reminding me of my capabilities.

VITA

Cindy Cristina Yañez

EDUCATION

Doctor of Philosophy in Earth System Science, University of California Irvine 2024

Master of Science in Earth System Science, University of California Irvine 2021

Bachelor of Science in Physics, University of California Riverside 2019

PROFESSIONAL EXPERIENCE

Air Pollution Specialist, California Air Resources Board 2023 – Present
Mobile Source Technology Assessment and Modeling Section

Graduate Student Researcher, University of California Irvine 2019 – 2023
Mentor: Dr. Claudia Czimczik

Undergraduate Student Researcher, University of California Riverside 2017 – 2019
Mentor: Dr. Francesca Hopkins

Research Intern, NASA Jet Propulsion Laboratory 2018
Mentors: Dr. Kristal Verhulst and Dr. Charles Miller

PUBLICATIONS

Yañez, C. C., Dubey, M., Hopkins, F. M., Meyer, A., Romero, J., Parker, H., Xu, X., & Czimczik, C. I. (In Prep). Plant radiocarbon across an urban-rural CO_2 gradient matches surface and column CO_2 observations

Yañez, C. C., Bares, R., Czimczik, C. I., Lin, J., Zhang, J., Bush, S. E., & Hopkins, F. M. (In Review). Contrasting trends in vehicle combustion efficiency in Los Angeles, CA and Salt Lake City, UT

Odwuor, A., Yañez, C. C., Chen, Y., Hopkins, F. M., Moreno, A., Xu, X., Czimczik, C. I., & Randerson, J. T. (2023). Evidence for multi-decadal fuel buildup in a large California wildfire from smoke radiocarbon measurements. *Environmental Research Letters*.

Yañez, C. C., Hopkins, F. M., Xu, X., Tavares, J. F., Welch, A., & Czimczik, C. I. (2022). Reductions in California's urban fossil fuel CO_2 emissions during the COVID-19 pandemic. *AGU Advances*, 3(6), e2022AV000732.

Yañez, C. C., Hopkins, F. M., & Porter, W. C. (2020). Projected impacts of climate change on tourism in the Coachella Valley, California. *Climatic Change*, 162, 707-721.

PRESENTATIONS

Poster Presentation. "Evaluating improvements in vehicle combustion efficiency using mobile on-road CO/CO_2 measurements." American Geophysical Union Meeting. San Francisco, CA. December 2023

Oral Presentation. "Plant radiocarbon as an indicator of urban decarbonization." NASA Jet Propulsion Laboratory Carbon Club Seminar. Pasadena, CA. March 2023

Oral Presentation. “Multiscale observations of fossil fuel CO2 along an urban-rural gradient.” American Geophysical Union Fall Meeting. Chicago, IL. December 2022

Oral Presentation. “The Climate Gap in the Coachella Valley.” Commission on the Status of Women. New York, NY. March 2022.

Oral Presentation. “Impacts of California’s Stay-at-Home order and economic recovery on fossil carbon emissions in California.” American Geophysical Union Fall Meeting. Washington D.C., December 2020.

Oral Presentation. “The Impact of Climate Change on Tourism in the Coachella Valley.” UCR Undergraduate Research Symposium. Riverside, CA. May 2019.

Poster Presentation. “Exploring variability in CO2 and CO measurements due to episodic emissions in the Los Angeles Megacity.” American Geophysical Union Fall Meeting. Washington D.C., December 2018.

Oral Presentation. “Impact of Climate Change on Tourism in the Coachella Valley.” Fourth Climate Change Assessment Symposium for the Inland Deserts Region. Palm Desert, CA. October 2018

Poster Presentation. “The Impact of Climate Change on Tourism in the Coachella Valley.” UCR Undergraduate Research Symposium. Riverside, CA. May 2018

AWARDS AND HONORS

UC Lab Fees Graduate Research Fellowship	2022 – 2024
Latino Excellence and Achievement Award, UCI School of Physical Sciences	2022
SACNAS National Diversity in STEM Conference Travel Scholarship	2022
National Science Foundation Graduate Research Fellowship Program	2019 – 2023
UC Irvine Provost PhD Fellowship	2020
UC Irvine Diversity Recruitment Fellowship	2019
UC Irvine Minority Serving Institution Enhancement Fellowship	2019
UC Riverside Chancellor’s Research Fellowship	2018
NASA Fellowships and Internships in Extremely Large Data Sets	2018, 2019

OUTREACH AND SERVICE

AGU Voices for Science program	Mar 2023 – present
UCI Earth System Science Graduate Student Representative	Aug 2021 – Jun 2022
Climate, Literacy, Empowerment And iNquiry (“CLEAN”) Education	Sep 2020 – present
Día del Estudiante – Mexicali, BC, Mexico	May 2021
MPNA-GREEN Toxic Tour Day – Santa Ana, CA	May 2021
Graduate Student Panel – Riverside, CA	Apr 2021
Graduate Student Mentor	Sep 2020 – Jun 2023
Vice President, Society of Women Engineers at UCR	Jun 2018 – Jun 2019
Secretary, Society of Women Engineers at UCR	Jun 2017 – Jun 2018
Historian, Society of Women Engineers at UCR	Jun 2016 – Jun 2017
Outreach Committee, Society of Women Engineers at UCR	Sep 2015 – Jun 2016
Supplemental Instruction Mentor	Jun 2018 – Jun 2019
One Future Coachella Valley Leadership Team	Jun 2015 – Jun 2017

SKILLS

Data analysis: Proficient in Python, R, Matlab, Excel, and ArcGIS

Instrumentation: Cavity ringdown spectrometers (Picarro, Inc), Fourier transform spectrometer (EM27/SUN, Bruker), $NO/NO_2/NOx$ monitor (2B Technologies), mobile laboratory experience

Laboratory analysis: Preparation of samples for radiocarbon analysis including cryogenic CO_2 extraction on a vacuum line system and graphitization using zinc-reduction method. Prepared samples for elemental analysis in EA-IRMS

Languages: Fluent in English and Spanish

PROFESSIONAL ASSOCIATIONS

American Geophysical Union
Society for the Advancement of Chicanos/Hispanics and Native Americans in Science
Graduate Women United
Society of Women Engineers

ABSTRACT OF THE DISSERTATION

Tracing Atmospheric Emissions from Cities Using Atmospheric Measurements and Plant Radiocarbon

by

Cindy Cristina Yañez

Doctor of Philosophy in Earth System Science

University of California, Irvine, 2024

Professor Claudia Czimczik, Chair

Human activities release greenhouse gases and air pollutants into the atmosphere, causing global climate change and other widespread impacts on the Earth System. These emissions are concentrated in cities, where most humans live and where most transportation, energy generation and consumption occur. While many cities are taking action to reduce their emissions, verifying the success of such efforts is difficult, especially at local scales in complex urban environments. Without reliable monitoring of urban emissions trends, it is uncertain whether attempted solutions are effective and our ability to steer climate policy is limited.

In my dissertation, I provide novel information about spatial and temporal patterns of anthropogenic gas emissions and our capacity to monitor emissions in urban environments. In my first study, I used a mobile laboratory to measure on-road carbon monoxide (CO) and carbon dioxide (CO_2). The ratio of these two gases (CO/CO_2) is a useful metric for assessing the success of regulations intended to reduce air pollutant emissions from vehicles. The results show that California's policies and technological advancements have made the Los Angeles traffic fleet more efficient. However, combustion efficiency worsened during the COVID-19 pandemic and in Salt Lake City, likely because of changes to traffic conditions and fleet composition that offset progress in reducing vehicle CO emissions.

In Chapter 2, I focus on quantifying fossil fuel CO_2 ($ffCO_2$) emission reductions that occurred during the COVID-19 pandemic using the mobile measurements from Chapter 1 and a community-sourced dataset of plant radiocarbon (^{14}C). These two datasets reveal a significant reduction in $ffCO_2$ in California's urban areas in 2020 due to social distancing measures imposed by the pandemic. Furthermore, $ffCO_2$

emissions rebounded to pre-pandemic levels by 2021, but not uniformly, with some areas taking longer to return to "normal" than others. The study demonstrated the capacity for plant ^{14}C samples to capture $ffCO_2$ emission reductions with shifts in human behaviors. This implied that plant sampling could be an informative and accessible tool for $ffCO_2$ monitoring in cities that lack CO_2 monitoring infrastructure as climate change mitigation policies take effect. This motivated us to conduct further tests comparing $ffCO_2$ patterns indicated by plant ^{14}C analysis with more established $ffCO_2$ monitoring approaches.

In Chapter 3, I collected turfgrass ^{14}C samples along an urban to rural gradient in Southern California alongside measurements of *in situ* surface CO_2 and remotely sensed total column CO_2. The $ffCO_2$ patterns indicated by each of these metrics agreed well with each other, suggesting that plant ^{14}C analysis can independently provide similar quality information about urban $ffCO_2$ emissions, but at a finer resolution since it is more operationally feasible to sample plants. In conjunction with surface CO_2, plant ^{14}C can also provide insight on CO_2 contributions from biogenic fluxes, but more work is needed to inform nature-based climate solutions in cities. Future work should use the insights in these studies to monitor trends in urban $ffCO_2$ emissions and guide policymakers during the transition away from fossil fuels.

INTRODUCTION

Climate Change and Cities

Greenhouse gas (GHG) emissions from human activities are causing global climate change, leading to profound and widespread damage to the environment and society. The buildup of GHG's in the atmosphere has already warmed the Earth's average temperature by 1°C relative to the period 1850 to 1900 (Masson-Delmotte et al., 2021). Unless large-scale systemic changes to our energy, transportation, and land use practices are made to limit further greenhouse gas (GHG) emissions, an additional 1-4°C of global warming could occur by the end of the century (IPCC, 2023).

The outcome of the climate crisis heavily depends on the extent to which fossil fuel carbon dioxide ($ffCO_2$) emissions are reduced. CO_2 is of critical focus because it is the dominant GHG contributing to global temperature increases, accounting for approximately 75% of warming (Masson-Delmotte et al., 2021). Atmospheric CO_2 levels have risen by approximately 50% by 2024 compared to pre-industrial levels primarily due to combustion of fossil fuels. While non-CO_2 greenhouse gases like methane (CH_4) and nitrous oxide (N_2O) have a stronger warming potential than CO_2 over short timescales, CO_2 constitutes the vast majority (approximately 80%) of GHG emissions and has a long and variable lifetime in the atmosphere (Archer et al., 2009; United States Environmental Protection Agency, 2023). However, reducing $ffCO_2$ emissions is challenging because they are deeply ingrained into our economy and mobility. The majority of energy used by modern society is produced by combustion of fossil fuels. The main sources of anthropogenic CO_2 emissions in the United States are transportation (35%), electricity generation (31%), industrial processes (15%), and commercial and residential buildings (11%) (United States Environmental Protection Agency, 2023). Rapid and deep interventions are needed in each these sectors to mitigate $ffCO_2$ emissions, such as electrifying transportation systems, transitioning into renewable energy sources, reducing energy demand/reliance, incorporating sustainable urban planning, and adopting efficient building infrastructure (IPCC, 2023).

The majority of $ffCO_2$ emissions originate in cities, where fossil fuel combustion is still the primary fuel for transportation and building heating systems. Fossil fuel combustion is also the primary source of air pollution. Addressing both GHG emissions and the health risk posed by air pollution makes urban areas a key priority for emission mitigation efforts (Crippa et al., 2021; Gurney et al., 2022). Many cities have declared plans to reach low-carbon or net-zero emissions targets within the next few decades and are taking action to decrease their consumption of fossil fuels (Seto et al., 2021). Some cities have started making progress in reducing their emissions after centuries of increasing $ffCO_2$ emissions that were coupled with economic growth (Crippa et al., 2021). However, at the city scale, it is challenging to quantify spatiotemporal trends in $ffCO_2$ emissions and to gauge the success of local policy initiatives.

Challenges for Monitoring Urban CO_2 Emissions

Quantifying $ffCO_2$ emissions is critical to determine whether actions to reduce emissions are effective, and thus, whether we are on track to meet emission reduction targets. Additionally, $ffCO_2$ monitoring is needed to inform policymakers and stakeholders of specific locations or processes that should be of highest priority for mitigative action. However, quantifying urban $ffCO_2$ emissions remains a severe challenge. Studies have identified concerning discrepancies in $ffCO_2$ estimates between scientific assessments and self-reported city emission inventories (Gurney et al., 2021; Lauvaux et al., 2020).

City accounting efforts typically estimate $ffCO_2$ emissions using activity and consumption data (e.g., population, vehicle miles traveled, electricity usage) that is scaled by emission factors (e.g., grams of CO_2 emitted per mile traveled). However, such self-reported inventories may not be standardized across cities, are difficult to test for accuracy or predict uncertainty, and tend to under-report emissions by 20% on average (Gurney et al., 2021; Seto et al., 2021).

Within the scientific community, data-driven modeling approaches and environmental measurements are used to quantify urban $ffCO_2$ emissions. Atmospheric measurements are advantageous over inventories because they can provide uniform, independent information and represent all emission sources (and sinks) that may be overlooked in an inventory, providing the capacity to detect unknown

sources or fugitive emissions (Duren & Miller, 2012). Such atmospheric monitoring systems have made progress in quantifying city-wide emissions to within 10% uncertainty, a scale that is relevant for evaluating emission mitigation trends (Turnbull et al., 2019). However, the application of atmospheric measurements for city $ffCO_2$ monitoring in practice still faces significant obstacles. Maintaining these measurements requires large infrastructural and financial commitments coupled with sustained long-term involvement of scientific experts, making them unfeasible for all but the biggest cities in affluent countries.

One major problem for urban $ffCO_2$ monitoring is disentangling the fossil fuel derived contributions from the total CO_2 signal. This challenge arises because CO_2 is a long-lived, well-mixed gas with large natural sources including outgassing from the ocean, respiration of living organisms, decomposition of organic matter, and wildfires. CO_2 also has large natural sinks such as dissolution into the ocean, photosynthesis, and weathering. On a global, annual scale, these sources and sinks would be in balance if not for anthropogenic CO_2 emissions. Still, the $ffCO_2$ emissions (~10 GtC yr^{-1} globally) are much smaller than these large and temporally variable natural fluxes (~210 GtC yr^{-1} globally) (Friedlingstein et al., 2022), making them difficult to isolate. Additional complexity arises because the atmosphere is a dynamic system that continually mixes and transports $ffCO_2$ emissions in ways that differ with geography and weather. This makes attributing spatiotemporal patterns of CO_2 to $ffCO_2$ emissions using atmospheric CO_2 measurements alone complicated, especially within a complex urban environment.

Atmospheric CO_2 Tracers: Carbon Monoxide and Radiocarbon

Measurements of other gas species can be used as tracers to distinguish the fossil fuel derived portion of observed CO_2 signals. Carbon monoxide (CO) is one useful proxy. CO is co-emitted with CO_2 during the incomplete combustion of fossil fuels. However, CO has a much shorter atmospheric lifetime than CO_2 (two months vs 300 – 1000 years, respectively) due to its chemical sinks (i.e., reaction with hydroxyl radical). Direct CO emissions (excluding chemical production in the atmosphere) mainly come from anthropogenic sources (50% globally) and biomass burning (36%), while the natural sources of direct CO emissions are small (16%) (Zheng et al., 2019). These attributes make CO a useful proxy for recently

emitted $ffCO_2$, since it can be more directly tied to fossil fuel combustion than CO_2 measurements (Silva et al., 2013; Turnbull et al., 2006; Warneke et al., 2012). However, the effectiveness of CO as a tracer varies in space and time. This is because the amount of CO that is co-emitted with $ffCO_2$ depends on combustion conditions and emission control systems. As CO is a toxic gas, there are regulations in place to minimize CO emissions during combustion processes. For example, in many places, cars are required to have catalytic converters that destroy CO before it is released from the vehicle tailpipe. Thus, the effectiveness of using CO as a $ffCO_2$ tracer depends on how stringently it is regulated and the technology that is in place to prevent its emission. The resulting variability in combustion ratios limits the use of CO for tracking $ffCO_2$ emissions (Djuricin et al., 2010).

A more direct $ffCO_2$ tracer is radiocarbon (^{14}C), a radioactive isotope of carbon that is produced naturally by nitrogen interactions with cosmogenic radiation in the stratosphere (Libby, 1955; Schuur et al., 2016). Fossil fuels originate from ancient plant material that stopped exchanging carbon with the atmospheric millions of years ago. Since radiocarbon has a short half-life of only 5,730 years, it only takes about 50,000 years for a dead organism to lose all its ^{14}C by radioactive decay (at least to a point that we can no longer distinguish it from background). Thus, fossil fuels have long lost their ^{14}C content, giving them a unique signature (Levin et al., 2003). The other major CO_2 sources (biosphere and ocean exchange), have much greater (younger) ^{14}C values, reflecting the timescales of their ongoing exchange with the atmosphere (Graven et al., 2020a).

While ^{14}C is recognized as the "gold standard" tracer for $ffCO_2$ emissions, its biggest limitation is the laborious and expensive cost of measuring it, which leads to low resolution datasets. ^{14}C is a rare isotope, accounting for only 1 out of every trillion carbon atoms. Accumulating enough ^{14}C for adequate measurement in air (at ~420 ppm CO_2 in the clean atmosphere at the time of writing) requires large volume samples. Air samples collected in 5 – 6 L flasks require a lot of time and manual labor to prepare for ^{14}C analysis, since the CO_2 needs to be purified and extracted from the air sample. Cost-effective sampling approaches, such as analyzing plant ^{14}C instead of air, can potentially make ^{14}C analyses more accessible and operationally feasible, given that plants concentrate atmospheric CO_2 during growth.

Plant ^{14}C analysis is an alternative approach for monitoring $ffCO_2$. Plants integrate the atmospheric $^{14}CO_2$ signature into their tissue when they conduct photosynthesis. They also have a much higher carbon content than air samples, making their ^{14}C easier to measure with lower sample volumes. Thus, plants have potential to serve as cost-effective $ffCO_2$ monitors in urban environments, where there are heterogeneous emissions over short spatial gradients (Gurney et al., 2012). However, while plant ^{14}C analysis has been demonstrated to effectively map spatial $ffCO_2$ patterns (Hsueh et al., 2007a; Riley et al., 2008; Santos et al., 2019; Wang & Pataki, 2010), limited work has utilized plant ^{14}C to track temporal trends in $ffCO_2$ emissions. Further research is needed to advance its applicability for monitoring $ffCO_2$ emission trends in cities.

Organization of Research

This dissertation includes three studies that measure spatiotemporal $ffCO_2$ patterns within complex urban environments and in the context of human activity. Spatial patterns are assessed along urban-rural gradients within large metropolitan areas and sampling near known emission sources. Temporal trends in response to changes in human activity are assessed, such as policy interventions and the COVID-19 pandemic. In quantifying these spatial and temporal patterns, this research elucidates our capacity to monitor urban $ffCO_2$ emissions using atmospheric CO_2 measurements and tracers.

In Chapter 1, I evaluate trends in on-road CO/CO_2 ratios in two cities: Los Angeles (LA), CA and Salt Lake City (SLC), UT, USA. The study is based on on-road measurements of CO and CO_2 that I collected using a mobile laboratory and compared against similar measurements collected in SLC and in 2013. These measurements indicate that LA's on-road CO/CO_2 ratios have decreased over time, aligning with the anticipated outcomes of California's stringent regulation of CO emissions from mobile sources. However, CO/CO_2 ratios increased in SLC, indicating that the combustion efficiency of the SLC traffic fleet got worse over time. To elucidate the cause of the worsening trend, the COVID-19 pandemic provided more clues since it also led to increases in CO/CO_2. These results suggest that progress in CO-reducing technology in vehicles can be outpaced by traffic conditions, such as speed, and the fleet composition. The

results also imply that CO's effectiveness as a tracer for $ffCO_2$ emissions is diminishing, as CO emissions are decreasing and variable.

In Chapter 2, I combine the mobile measurements presented in Chapter 1 with plant ^{14}C analyses to assess whether reductions in emissions due to the COVID-19 pandemic were detectable with these atmospheric measurements. The study engaged citizen scientists across California to collect invasive annual grass samples from across the state, which we analyzed for ^{14}C content. The on-road mobile measurements show a 60% decrease in excess CO_2 on Los Angeles freeways in 2020, when mobility was reduced to limit virus spread. Additionally, plant ^{14}C indicated a reduction in $ffCO_2$ in 2020 relative to pre-2020 datasets. After COVID mobility restrictions were lifted, I observed a heterogeneous rebound in $ffCO_2$ emissions that is likely related to the various responses to the relaxation of physical distancing measures. The study demonstrated that plants are sensitive to $ffCO_2$ emission changes, both spatially and temporally, and thus a powerful tool for tracking future $ffCO_2$ emission reductions in cities.

Lastly, in Chapter 3, I compare plant ^{14}C to two prominent urban $ffCO_2$ atmospheric monitoring approaches: *in situ* observational networks and total column measurements. I collected plant ^{14}C samples alongside atmospheric CO_2 measurements across an urban to rural gradient in Southern California. I establish quantitative relationships between plant ^{14}C and atmospheric CO_2, strengthening the reliability of similar analyses in places that lack CO_2 monitoring infrastructure. This research also demonstrates that turfgrass is a suitable medium for capturing spatiotemporal $ffCO_2$ emission patterns, enabling ^{14}C analysis at intra-annual timescales and in more locations.

Together, my PhD research significantly advanced our understanding of CO and plant ^{14}C as tracers of $ffCO_2$ in cities. The findings indicate that plant ^{14}C can improve the coverage and resolution of $ffCO_2$ emissions information in urban areas. This opens new opportunities for tracking $ffCO_2$ trends in cities that lack measurements and high-resolution analyses to assess spatial disparities in emissions. In conjunction with advances in ^{14}C measuring technology, such as the Mini Carbon Dating System, plant ^{14}C samples can be measured at higher throughput using elemental analysis combined with $^{14}CO_2$. Future work can apply

these advances in plant ^{14}C analyses to validate decarbonization progress and guide local actions toward $ffCO_2$ mitigation goals.

Chapter 1 Contrasting Trends in Vehicle Combustion Efficiency in Los Angeles, CA and Salt Lake City, UT

Adapted from:

Yañez, C. C., Bares, R., Czimczik, C.I., Lin, J., Zhang, J., Bush, S.E., & Hopkins, F.M. Contrasting Trends in Vehicle Combustion Efficiency in Los Angeles, CA and Salt Lake City, UT. *Under Revision.*

1.1 Introduction

Urban areas are hotspots for the emission of trace gases that are harmful to human health and the environment. Many of these air pollutants and greenhouse gases are emitted on road from vehicles. In cities, the transportation sector accounts for a large share of anthropogenic carbon monoxide (CO) and carbon dioxide (CO_2) emissions, since both gases are co-emitted during the burning of petroleum-derived fuels in gasoline- and diesel-powered vehicles. In the United States, 38% of anthropogenic CO emissions (United States Environmental Protection Agency, 2017) and 29% of CO_2 emissions (United States Environmental Protection Agency, 2023) originate from on-road mobile sources. CO, a criteria pollutant that results from incomplete or inefficient combustion, is hazardous to human health, a precursor to other harmful air pollutants such as ozone, and contributes to climate change. CO_2 is a potent greenhouse gas and the most critical determinant of climate change in this century (Masson-Delmotte et al., 2021).

Air pollutant regulation (i.e., the 1970 U.S. Clean Air Act) and technological advances (i.e., catalytic converters) have led to significant improvements in air quality and a decline in air pollution-related mortality in many cities (Colmer et al., 2020; Sullivan et al., 2018; Zhang et al., 2018). Specifically, requirements for catalytic converters on new vehicles reduced the amount of CO and unburned hydrocarbons emitted from vehicles by oxidation reactions that convert them to CO_2. Newer vehicle models are more fuel-efficient, and CO emissions have decreased despite increases in the number of vehicles on the road and vehicle miles traveled. Ambient CO mixing ratios have substantially declined in urban areas

(Li et al., 2022; Lopez-Coto et al., 2022; McDonald et al., 2013; Warneke et al., 2012; Winkler et al., 2018), especially within jurisdictions that enforce strict emission controls, such as the State of California. In the San Francisco metropolitan area for instance, CO mixing ratios measured in vehicles traveling on a major highway decreased from 9.7 ppmv to 0.5 ppmv (a 95% reduction) between 1980 and 2011 (Flachsbart & Ott, 2019). In Los Angeles, the CO mixing ratio decreased from 20 ppmv in the 1960s to 0.4 ppmv in 2010, with an average decrease of 8% per year (Warneke et al., 2012). However, while urban CO emissions have declined, global CO_2 emissions from the on-road sector have continued to grow due to increasing transportation (Lamb et al., 2021). In contrast to technological advances that reduced CO, reducing CO_2 emissions requires higher fuel economy or fundamental changes to the vehicle fuel source (e.g., electric and hydrogen vehicles).

The ratio of CO/CO_2 is a useful metric that is indicative of vehicle combustion efficiency. Combustion efficiency denotes how effectively the vehicle engine converts fuel into energy, and consequently the degree to which polluting by-products (i.e., CO) are emitted in the process. Lower CO/CO_2 ratios indicate improvements in combustion efficiency as well as the effectiveness of catalytic converters equipped by gasoline vehicles in reducing CO emissions, and thus the ratio can be used to evaluate the success of efforts to reduce pollutant emissions from traffic. In cities, the CO/CO_2 ratio has generally been declining over time alongside reductions in CO emissions (Popa et al., 2014). However, the trend varies by location, reflecting the stringency of policies (Warneke et al., 2012) and the timing of the introduction of emission reduction policies. As such, CO/CO_2 ratios tend to be higher in places that have less stringent pollution regulations and vehicle fleets with less efficient technology (Che et al., 2022; Silva et al., 2013).

In addition to serving as an indicator of combustion efficiency, the CO/CO_2 ratio is also useful for studies aiming to quantify fossil fuel CO_2 signals based on atmospheric CO_2 measurements. Because CO is a short-lived gas relative to CO_2 and is co-emitted during incomplete combustion of fossil fuels, the CO/CO_2 ratio can be used as a tracer to distinguish fossil fuel CO_2 emissions from other sources such as biogenic fluxes, oceanic exchange and wildfires (Gamage et al., 2020; Silva et al., 2013; Suntharalingam, 2004;

Turnbull, Karion, et al., 2011). Thus, observations of temporal-spatial variations in the CO/CO_2 ratio provide critical insight regarding CO_2 sources and for validating the success of emission reduction efforts. However, spatial and temporal variations in the CO/CO_2 ratio complicate its application as a tracer. Thus, changes to the CO/CO_2 ratio over time need to be re-assessed to determine the continued usefulness of this approach.

In this study, we investigate multi-year trends in the traffic combustion efficiency using observations of the on-road CO/CO_2 ratio in greater Los Angeles (LA) and Salt Lake City (SLC), two major metropolitan areas in the western U.S. with air quality problems and contrasting vehicle emission control policies. Measurements were conducted in both cities during the summers of 2013 and 2019, and additionally in LA in 2020 and 2021 to capture changes in traffic related to the coronavirus-19 (COVID-19) pandemic. We measured on-road CO/CO_2 using mobile laboratories equipped with fast response, high precision trace gas analyzers. Alternative approaches for estimating on-road emissions rely on assumptions about the traffic fleet characteristics and driving conditions in order to extrapolate measurements made in emission testing laboratories (e.g., EPA MOVES) or on individual vehicles (e.g., portable emissions measurement systems). In contrast, our measurements represent the actual average combustion efficiency of the real-world vehicle fleet on interstate highways during daytime in these locations. We chose interstate highways to avoid the influence of non-vehicle sources, cold starts, and to keep our inter-city comparisons free of biases related to road network design. Thus, our approach allows a direct assessment of the integrated impact of vehicle emission control policies, vehicle fleet dynamics, and traffic conditions on air quality near roadways. We hypothesized that LA would have a lower and more rapidly decreasing CO/CO_2 ratio than SLC due to the earlier adoption of strict vehicle emission control policies in California compared to Utah.

1.2 Materials and Methods

1.2.1 Study areas

We focus on two urban areas in the western U.S.: Los Angeles, CA and Salt Lake City, UT. The Los Angeles (LA) metropolitan area hosts 18 million residents across approximately 88,000 km2 in Southern California, while Salt Lake City (SLC) has 1.2 million residents in approximately 20,000 km2. Both locations have historically suffered from poor air quality due to anthropogenic pollutant emissions that get trapped by atmospheric temperature inversions and surrounding mountains (Bares et al., 2018; Mackey et al., 2021; Mouteva et al., 2017). Both LA and SLC are classified as maintenance areas for ambient CO levels due to former violations of air quality standards and are thereby required by the U.S. Clean Air Act to implement measures to reduce on-road emissions. The on-road transportation sector dominates fossil fuel-derived CO_2 emissions (CO_2) in both cities, constituting 43% of LA's (Gurney et al., 2019) and 38% of SLC's emissions (Patarasuk et al., 2016). On-road mobile sources also constitute the largest source of CO emissions in the counties where the two cities reside, comprising 47% and 56% of CO emissions in LA County and Salt Lake County, respectively (United States Environmental Protection Agency, 2017).

California and Utah differ in the stringency of their statewide regulations concerning on-road emissions. The State of California was the first jurisdiction in the U.S. to regulate motor vehicle emissions of CO (1966) and CO_2 (Pavley, 2002). Since the 1960s, California has been granted waivers by the U.S. Environmental Protection Agency to write its own air pollutant regulations that are enacted separately from national laws and are more stringent. These policies include progressively stricter emission standards for vehicles sold in the state, on-board diagnostics (or "check engine" light) systems, and enhanced vehicle inspection/maintenance (I/M) programs intended to identify gross polluters (e.g., smog checks) in urban areas (California Air Resources Board, 2023b). Further, the state also has incentive programs to encourage retirement of old vehicles and the purchase of low polluting vehicles (California Air Resources Board, 2022). In addition, California has strict mandates on fuel formulations, and introduced cleaner-burning, low

sulfur fuel standards with its adoption of the LEV III standards in 2012. Thus, trends in LA's on-road CO/CO_2 ratio should be decreasing in response to strict statewide emission regulations, incentivized fleet turnover and cleaner burning fuels.

In contrast, SLC is in the State of Utah, where vehicle sales and emission regulations generally follow federal policies that are less stringent and are usually adopted years after similar policies in California. Currently, Utah has ongoing incentive programs for repair or replacement of vehicles that fail I/M checks and offers incentives for the purchase of clean air vehicles (UDEQ, 2023), albeit at a smaller scale than California. While smog checks are required in SLC as part of federally approved I/M programs since it is both an ozone and fine particulate matter nonattainment area, they are not a statewide requirement in Utah. Furthermore, federal Tier 3 fuel standards, which are highly similar to California's LEV III standard, were introduced in April of 2014 (Control of Air Pollution From Motor Vehicles: Tier 3 Motor Vehicle Emission and Fuel Standards, 2014). As Utah is a small, somewhat isolated, market for vehicle fuel, the arrival of Tier 3 fuels occurred significantly later than the federal promulgation, with arrival of these fuels largely due to local political action and incentives. As a result, Tier 3 fuels were phased into the SLC market in 2020 and later, lagging California's adoption by over seven years. Hence, due to Utah's later and less stringent adoption of on-road emission regulations compared to California, we expect that traffic combustion efficiency in SLC will not have improved as much as in LA.

1.2.2 On-road trace gas measurements

We measured the on-road mixing ratios of CO and CO_2 in LA and SLC using cavity ringdown spectrometers (Picarro, Sunnyvale, California) installed inside vehicle-based mobile laboratories following similar protocols as Bush et al. (2015) and Hopkins et al. (2016). Measurements were made on weekdays between July 15-31, 2019 in LA and August 14-29, 2019 in SLC. We compared our observations to similar data collected between June 14 - July 7, 2013 in LA and August 9-17, 2013 in SLC (Bush et al., 2015; Hopkins et al., 2016). Additionally, we collected similar measurements in LA on July 9-31, 2020 and July 15-17, 2021 to assess changes during the COVID-19 pandemic.

The mobile platform was a 2017 Mercedes Sprinter cargo van for the LA 2019-2021 surveys (Yañez et al., 2022), and a 2009 Hyundai Santa Fe Google Street View car for the SLC 2019 surveys (Miller et al., 2019). The 2013 surveys utilized the same 2011 Ford Transit Connect van in both cities. The mobile laboratories were fabricated to stream ambient air into the analyzer with the inlet sampling air several inches above the roof near the front of the vehicle. More specifically, the inlet on the LA 2019-2021 mobile laboratory was plumbed through a hole on the van's ceiling behind the driver's seat (approximately 3.5 m height above the road surface, and 10 cm above the roof of the vehicle). The SLC 2019 platform's inlet was installed several centimeters above the roof line at the rear edge of the front window (Apte et al., 2017). The 2013 mobile laboratory's inlet was attached to a telescopic mast that was extended to approximately 1 m above the vehicle roof during these surveys (Bush et al., 2015). Geospatial coordinates and meteorological information were continuously recorded during the drives using compact GPS (Garmin GPS 16x in LA 2019-2021 and SLC 2013, Garmin 18x in SLC 2019) and weather sensors (LA only) mounted to the vehicle rooftops.

For year-to-year comparisons, datasets were filtered to only include overlapping locations (measurements within a 50 m buffer of each other). We also only compared data collected on freeways ("primary" roads as defined by the U.S. Census Bureau). After these filters, our dataset represents approximately 470 km of road in LA and 60 km in SLC, most of which were sampled two or more times per survey. This includes segments of over ten freeways in LA (State Routes (SR-) 1, 22, 57, 60, 73, 91 and Interstate (I-) 5, 10, 105, 110, 210, 405 and 710) and two freeways in SLC (I-15 and 80). Our dataset is representative of an integrated traffic emissions signal, and we expect minimal influence from non-road sources. One measurement day (August 16, 2013) in SLC was affected by smoke from a nearby wildfire and excluded from the analysis (Fig. A1).

1.2.3 Data processing

Details describing the processing done on the 2013 datasets are described in Bush et al. (2015) and Hopkins et al. (2016). For the 2019-2021 LA measurements, the Picarro G2401 analyzer was calibrated

twice daily using air standard gas cylinders that contained known mixing ratios of CO_2 and CO. The mixing ratios in the standards were corrected against NOAA-certified tanks that were accurate to the World Meteorological Organization scale (WMO-CO2-X2007). The analyzer sampled directly out of the standard gas cylinder for three minutes before and after each survey. A correction was then applied to the data based on a two-point linear fit between the known and measured values.

For the 2019 SLC campaign, instrumentation was calibrated in a laboratory environment upon arriving in SLC, and again upon installation into mobile lab, to account for changes in ambient pressures and instrumentation drift during shipping. Throughout the campaign, both CO and CO_2 were calibrated at least weekly with CO calibration gases sourced from Scott-Marrin and diluted using a Teledyne T751H portable zero air system and a Teledyne T750 portable dynamic dilution calibrator. Calibration gases for CO_2 were generated at the University of Utah and are traceable to the WMO standard (Bares et al., 2019).

To synchronize the observations from the various instruments, data were integrated into 5-second averages and then gridded by averaging consecutive measurements into 100 m road intervals. Only daytime data collected between 11:00 and 16:00 (local time) was used in the analysis, when the planetary boundary layer is deep, and air is presumably well mixed.

We calculated excess values above a background (denoted with subscript "xs"; e.g., CO_{2xs}) for all gas mole fraction measurements by subtracting a regional background value from all observations. The background values are the ambient mixing ratios of CO and CO_2 of the regional atmosphere prior to being polluted by anthropogenic emissions. We characterized the background for each city and month using the "cleanest" measurements in our dataset by selecting the lowest mole fraction value of each survey day and averaging the lowest 20% of these minima (Hopkins et al., 2016). The uncertainty of the background was estimated as the standard deviation of the minima (Table A1). The LA 2019 dataset was exceptionally polluted since we only collected measurements on freeways and did not capture background conditions Therefore, we characterized its background using data from San Clemente Island (33.92°N, -118.49°E, 489 m a.s.l.), an offshore site that began collecting continuous in situ measurements of GHG mixing ratios in 2015 (J. Kim, Pers. Comm., 2022). In the summer months, the San Clemente Island (SCI) site samples

marine air masses flowing into the LA area from the Pacific Ocean, making it an adequate summer background for this region (Verhulst et al., 2017). For the non-2019 years when SCI data was available, CO_2 and CO background values derived from SCI measurements agreed within one sigma to the measured minima approach used here. For instance, in 2020 the CO_2 background was 410.0 ± 2.1 ppmv using the SCI July daytime average and 413.6 ± 6.7 ppmv using the lowest 20% of daily minima. The CO background was 82.1 ± 8.9 using SCI and 72.2 ± 36.8 using the minima. Considering the high enhancement levels of CO and CO_2 observed on the road, differences in the background estimation technique only result in a difference of 1.1 ppbv/ppmv in CO_{xs}/CO_{2xs} at most. Further, although the CO background was lower by 15-19 ppb in 2020 compared to 2019 and 2021, this does not affect our results. Even if we used a constant CO background for 2019-2021, the median CO_{xs}/CO_{2xs} values would only change by 0.01-0.15 ppbv/ppmv. Thus, the different background approach in LA 2019 should not invalidate the comparison against other years.

We focus our analysis on spatial and temporal trends in the ratio of CO_{xs}/CO_{2xs} (ppbv/ppmv), not the individual CO_{xs} and CO_{2xs} measurements. This is because the mixing ratios are not directly comparable between surveys due to differences in the fluid dynamics of the inlet configuration of the different mobile platform designs. The vehicle used for the 2013 surveys (both LA and SLC) was equipped with a telescopic mast that extended the sample inlet to 1 m above the vehicle roof, likely leading to measurements of traffic emissions that had mixed and risen above the surface. On the other hand, neither vehicle used in 2019-2021 had a mast, instead capturing air much closer to the vehicle's roof. Fluid dynamics simulations show that air captured closer to the roof line is likely composed of polluted mixtures from closer to the ground that traveled up along the vehicle body into the inlet (W. Mui, Pers. Comm., 2023). The latter configuration leads to higher CO_2 and CO mole fractions. However, this should not affect the CO_{xs}/CO_{2xs} ratios because the air mixtures originate from the same source.

1.3 Results and Discussion

1.3.1 Trends in CO_{xs}/CO_{2xs} between 2013 and 2019

Measurements of on-road CO_{xs}/CO_{2xs} ratios revealed contrasting temporal trends in the combustion efficiency of vehicle fleets in LA and SLC between 2013 and 2019 (Fig. 1.1). Values for CO_{xs}/CO_{2xs} in LA and SLC were similar in 2013 but diverged in 2019. In LA, we observed a reduction in the on-road CO_{xs}/CO_{2xs} ratio from a median CO_{xs}/CO_{2xs} value of 5.0 ppbv/ppmv in 2013 to 2.6 ppbv/ppmv in 2019 (Fig. 1.1a-b). In SLC, the median CO_{xs}/CO_{2xs} value increased from 4.1 ppbv/ppmv in 2013 to 6.4 ppbv/ppmv in 2019 (Fig. 1.1c-d). The median CO_{xs}/CO_{2xs} ratio of each city was statistically different between years according to Mood's median test (p-value < 0.05). In LA, the CO_{xs}/CO_{2xs} ratios were more variable in 2013 compared to 2019, with the interquartile range decreasing from 3.3 in 2013 to 1.4 and 2019. The opposite was observed in SLC, where the interquartile range increased from 2.4 in 2013 to 5.8 in 2019. Furthermore, the data became less skewed in LA, with skewness values decreasing from 5.0 in 2013 to 2.2 in 2019, but in SLC, skewness values increased from 3.8 in 2013 to 6.9 in 2019. The changes in skewness are also exemplified by Lorenz curves and the Gini indices of each survey's CO_{xs}, CO_{2xs}, and CO_{xs}/CO_{2xs} values (Fig. A2). Overall, the LA 2019 measurements had the lowest and least variable ratios and the SLC 2019 measurements had the highest and most variable ratios, with a maximum of 184 ppbv/ppmv. Taken together, our data shows that combustion efficiency increased from 2013 to 2019 in LA but decreased in SLC.

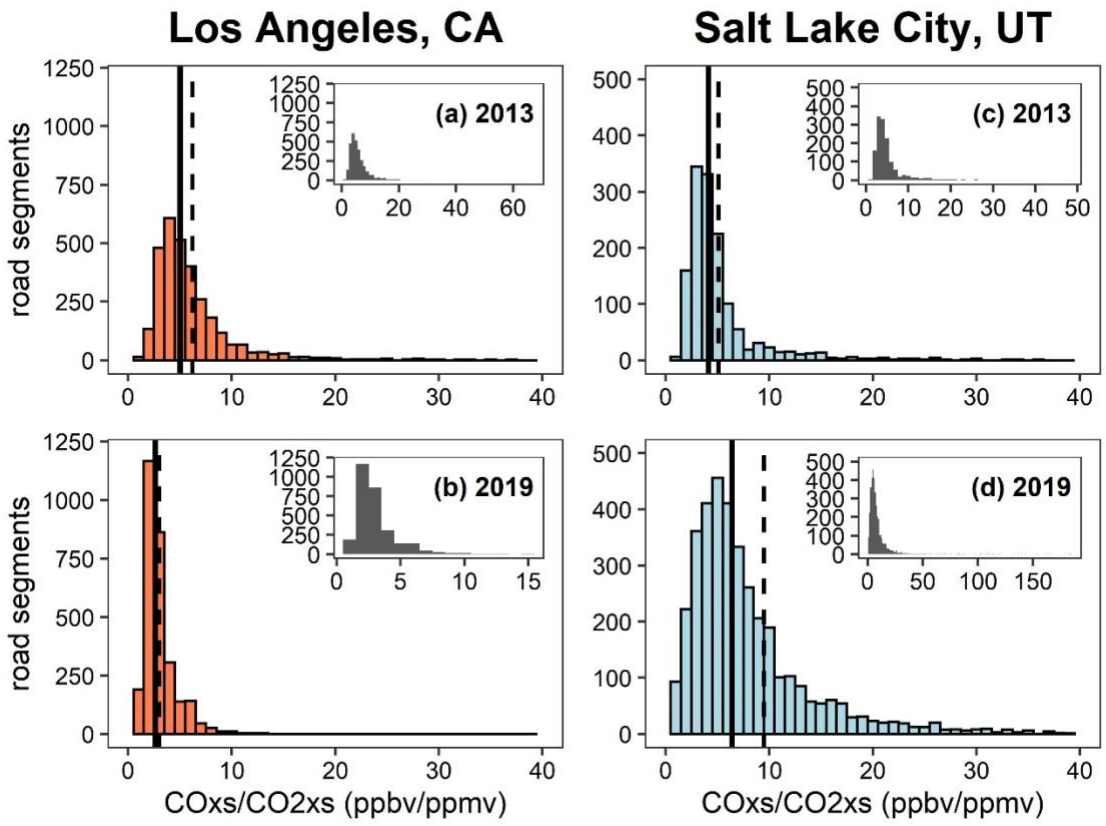

Figure 1.1. Histograms showing the distribution of CO_{xs}/CO_{2xs} for each mobile survey: (left panels) Los Angeles in (a) 2013 and (b) 2019, (right panels) Salt Lake City in (c) 2013 and (d) 2019. The solid vertical lines indicate the median and the dashed line indicates the mean value of each survey. For visualization purposes and comparison between surveys, the x-axis has been truncated. Inset maps on each panel show the full data distribution of each survey without truncation.

In LA, the reduction in CO_{xs}/CO_{2xs} ratio between 2013 and 2019 was generally observed across the entire basin, while the changes in SLC were more spatially heterogeneous (Fig. 1.2). We observed several recurring CO_{xs}/CO_{2xs} hotspots in both 2013 and 2019, indicating persistent effects of traffic features such as steep roads and major freeway junctions on combustion efficiency. We considered hotspots as locations where CO_{xs}/CO_{2xs} exceeded the 95th percentile of observations in that city and year. In LA, CO_{xs}/CO_{2xs} ratios were elevated on steep roads, such as on SR-73 and SR-241, where CO_{xs}/CO_{2xs} exceeded 12 ppbv/ppmv in 2019. This is likely because engine load is increased when driving upslope and thereby reduces the combustion efficiency. Additional reappearing hotspots were observed in LA near the junction of SR-57 and SR-60 near Pomona and near the SR-134 and SR-710 junction near Pasadena on both years.

Combustion efficiency likely decreases near freeway junctions since they often experience congestion, stop-and-go conditions, and frequent acceleration as vehicles merge. Similarly, in SLC hotspots were observed on the eastern portion of I-80 leading up to the Wasatch mountains. Additionally, new SLC hotspots were observed in 2019 that were not observed in 2013 that could potentially be due to construction or traffic conditions. Overall, SLC freeways had notably higher CO_{xs}/CO_{2xs} in 2019 compared to 2013, especially on I-15 and near its junction with SR-201 and I-80.

We compared the CO_{xs}/CO_{2xs} trends we observed to the California Air Resources Board's EMFAC model (California Air Resources Board, 2021). We downloaded annual CO and CO_2 emission estimates (in tons per year) for the South Coast Air Basin for the years 2013 and 2019-2021. We converted the emissions into molar units and calculated the CO/CO_2 ratio (in units of 1000 mol CO / mol CO_2) to match our observations in units of ppbv/ppmv. Based on the EMFAC output, the fleet-wide CO/CO_2 decreased by 42% between 2013 and 2019. This corresponds well with our observed median change of 48% over the same period. Thus, our observations and EMFAC agree that the fleetwide combustion efficiency improved between 2013 and 2019 in LA. Furthermore, assuming the reduction rate was linear and constant over the six years, this indicates a decreasing trend in CO/CO_2 of -7.1% yr^{-1} using EMFAC and -8.0% yr^{-1} based on our observations. This is on par with earlier reports of a -7.8% yr^{-1} trend from 1960 to 2010 based on regional atmospheric observations (Warneke et al., 2012). Based on EMFAC, annual on-road CO emissions decreased by 38% in 2019 relative to 2013 (or 28,500 tons CO yr^{-1}) alongside these improvements in vehicle combustion efficiency.

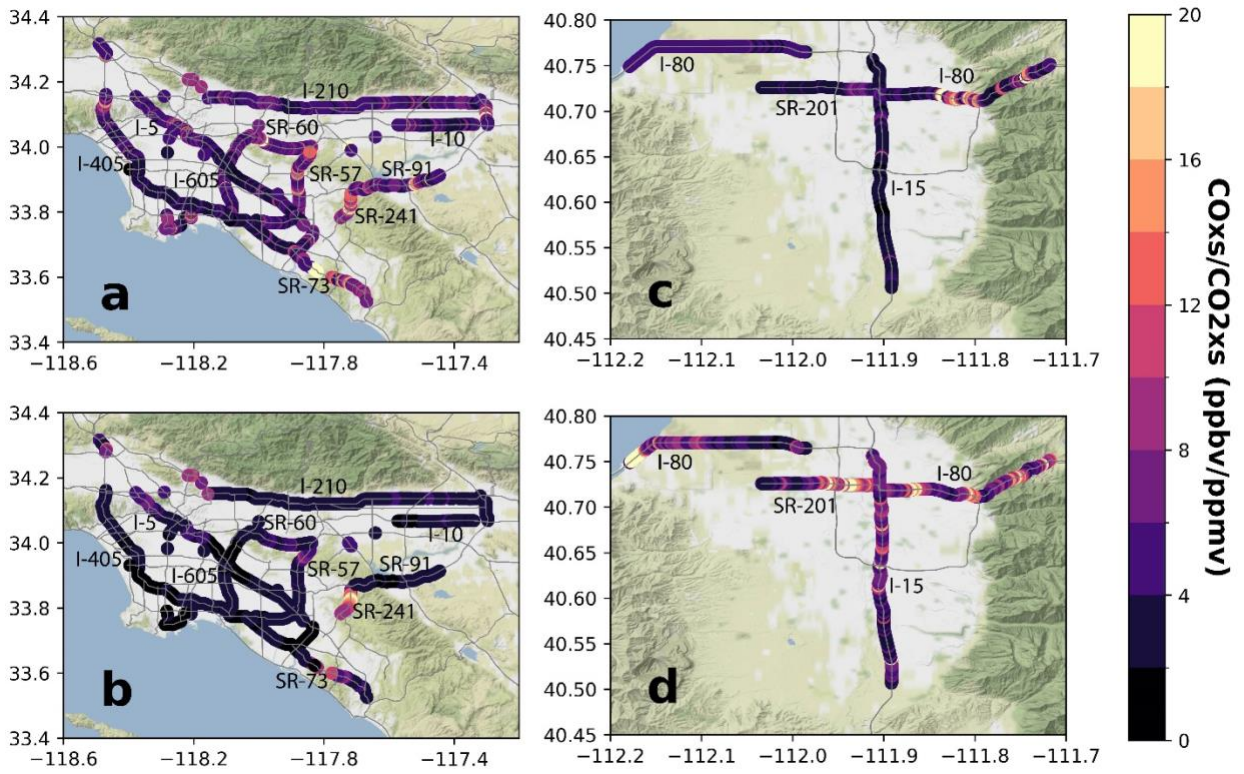

Figure 1.2. Maps showing the ratio of CO_{xs}/CO_{2xs} for each mobile survey: (left panels) Los Angeles in (a) 2013 and (b) 2019, (right panels) Salt Lake City in (c) 2013 and (d) 2019.

1.3.2 Trends in Los Angeles CO_{xs}/CO_{2xs} during the COVID-19 pandemic

The COVID-19 pandemic allowed us to further study the effects of traffic conditions on vehicle combustion efficiency. Emergency physical distancing mandates were imposed in California starting in March of 2020 to reduce rates of virus transmission (CA Executive Order N-33-20). This resulted in an abrupt shift to remote work and learning, the closure of "non-essential" businesses and entertainment venues, and strict limitations on domestic and international travel. Consequently, there was a drastic reduction in freeway traffic and congestion in the year 2020.

We repeated the LA on-road measurements in July 2020 and 2021 to assess how the combustion efficiency was affected by the sudden changes in commuter traffic (Fig. 1.3). We found that the median CO_{xs}/CO_{2xs} increased from 2.7 ppbv/ppmv in 2019 to 6.1 ppbv/ppmv in July 2020, indicating a downturn in the fleet combustion efficiency during COVID-19 restrictions. The CO_{xs}/CO_{2xs} observations were also more variable in 2020, with the interquartile range increasing from 1.4 in 2019 to 3.7 in 2020. As pandemic-

related mobility restrictions were gradually relaxed, traffic patterns eventually returned to pre-pandemic levels. By July 2021, on-road CO_{xs}/CO_{2xs} decreased to a median value of 2.5 ppbv/ppmv and an interquartile range of 1.4 which coincide with the pre-pandemic (2019) observations. This indicates that the increased CO_{xs}/CO_{2xs} ratios in 2020 were temporary and returned to the previous state of combustion efficiency by 2021.

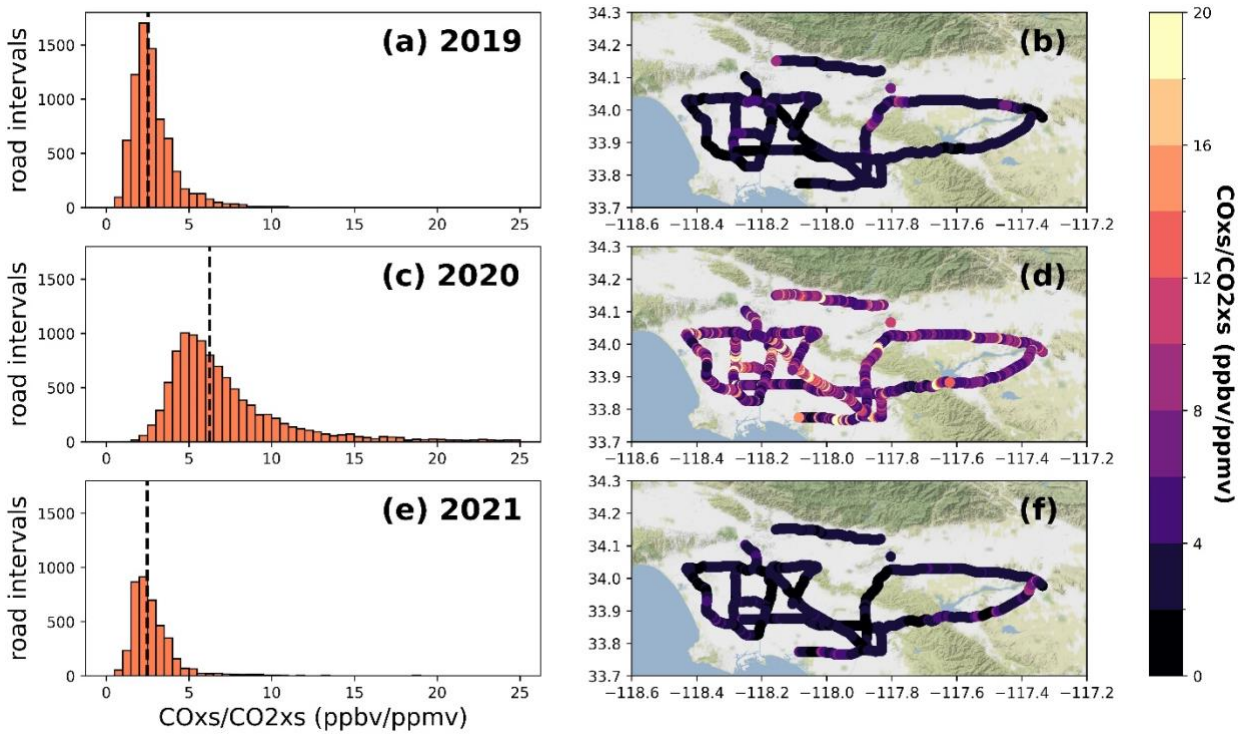

Figure 1.3. Histograms and maps of on-road CO_{xs}/CO_{2xs} observations in Los Angeles in July (a-b) 2019, (c-d) 2020, during COVID-19 pandemic related traffic reductions, and (e-f) 2021.The dashed lines on the histograms are the median CO_{xs}/CO_{2xs} values for each survey. The x-axes on the histograms have been truncated for visualization purposes.

The stark reductions in LA's traffic combustion efficiency in 2020 indicate that on-road CO_2 and CO emissions were substantially affected by changing driving patterns during the COVID-19 pandemic. In July 2020, LA's on-road CO_{2xs} levels were reduced by 60% relative to July 2019, with a near complete rebound by July 2021 (Fig. A3). We attribute the 2020 CO_{2xs} reductions to the decrease in the number of vehicles on the road, since CO_2 emissions are directly proportional to the amount of fuel burned. However, on-road CO_{xs} levels did not show a significant change between 2019-2021 (Fig. A3). This implies that

worsened combustion efficiency maintained the typical on-road CO levels despite there being fewer vehicles on the road in 2020.

Using the median CO_{xs}/CO_{2xs} observations in 2019 and 2020 as emission factors and on-road CO_2 emissions from EMFAC (65.7 million tons in 2019 and 58.5 million tons in 2020), we calculate that the worsened combustion efficiency led to 130,000 more tons of CO emitted in 2020 than would have been emitted if the combustion efficiency had remained at the 2019 level. This amounts to 20% of the South Coast Air Basin's total annual CO emissions (653,000 tons yr^{-1}), based on 2017 CO inventory estimates (California Air Resources Board, 2023a). Thus, the less efficient vehicle combustion during the pandemic led to a marked effect on CO emissions relative to the total CO budget. The potential causes of the decreased combustion efficiency in 2020 are discussed in the following section.

1.3.3 Evaluation of the potential contributors to CO_{xs}/CO_{2xs} trends

In summary, our measurements indicate an improvement in traffic combustion efficiency in LA since 2013, except for during the COVID-19 pandemic when combustion efficiency worsened. Conversely, combustion efficiency in SLC showed a decline between 2013 to 2019. Policy interventions and technological advances should be reducing CO_{xs}/CO_{2xs} in both cities, with potentially stronger reductions in LA than SLC due to stricter and earlier adoption of regulatory measures in California. However, our measurements indicate a more complex interplay of factors because CO_{xs}/CO_{2xs} increased in SLC and during COVID-19 in LA, opposing the expected decrease with emissions control measures. In this section, we discuss traffic and fleet characteristics that increase CO_{xs}/CO_{2xs} and evaluate their potential contributions based on our observations, relevant literature, and the vehicle composition in LA and SLC.

An increase in heavy-duty vehicle activity would decrease CO_{xs}/CO_{2xs} because diesel engines produce substantially less CO per unit of fuel burned than gasoline-powered engines (Held et al., 2001; Kelp et al., 2020; S. S. Park et al., 2011; Wen et al., 2019). Thus, heavy-duty vehicles cannot explain the CO_{xs}/CO_{2xs} increase we observed during COVID-19 and in SLC unless real-world CO/CO_2 emission ratios from heavy-duty vehicles differ grossly from expectation. Additionally, cold engine starts lead to higher

CO_{xs}/CO_{2xs} but are unlikely to occur during summer and on interstate freeways where our measurements took place. Construction activity may cause higher CO_{xs}/CO_{2xs} due to less efficient off-road equipment, but would have episodic effects on the data, not an overarching shift in the distribution as we observed.

Vehicle speeds. In general, CO and CO_2 emission rates increase at low (< 30 mph) and high (> 55 mph) speeds (Ammoura et al., 2014; Held et al., 2001; Jaikumar et al., 2017; Mei et al., 2021). However, the effect of speed on CO/CO_2 ratios varies with vehicle class, fuel type, and age (Fig. A4; Fig A5). Vehicles were driving faster during the two surveys in which we observed increases in CO_{xs}/CO_{2xs} (LA 2020 and SLC 2019). Based on traffic count data (California Department of Transportation, 2023; Utah Department of Transportation (UDOT), 2023), the median speed increased significantly in LA by 5 mph in 2020 compared to 2019 (Fig. 1.4; p-value < 0.05 using Mood's median test). Other reports also indicated faster driving speeds and more aggressive driving in 2020, which led to higher rates of severe crashes despite fewer vehicles on the road (Dong et al., 2022; NHTSA, 2021). When traffic conditions returned to pre-pandemic levels in 2021, both the median traffic speed and the CO_{xs}/CO_{2xs} values returned to 2019 levels. In SLC, median traffic speeds increased by 3 mph in 2019 compared to 2013, coinciding with increased CO_{xs}/CO_{2xs} ratios. This may be due to a speed limit increase on I-15 which was implemented in 2015 (Davidson, 2014; Hu, 2017). While we did not measure CO_{xs}/CO_{2xs} in SLC in 2020-2021, it is notable that the increasing speed trend continued during those years.

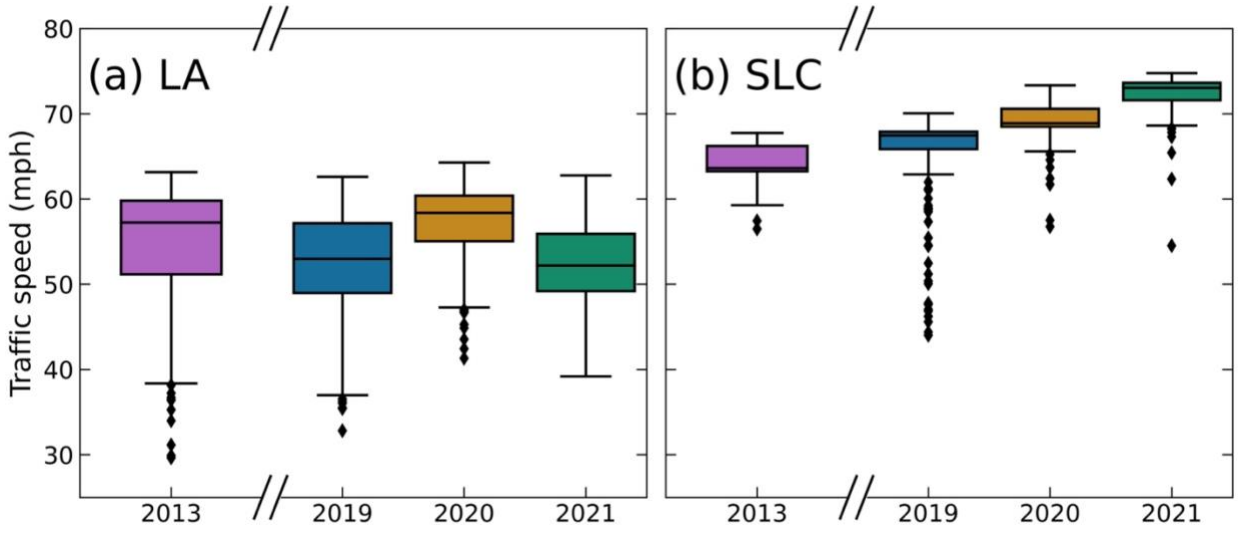

Figure 1.4. Box plots of hourly traffic speed, derived from the ratio of reported vehicle miles traveled (VMT) per vehicle hour traveled (VHT), for (a) Los Angeles freeways (I-5, I-405, I-605, I-210, SR-60, and SR-91) and (b) Salt Lake City freeways (I-15 and I-80) over the month each mobile survey was conducted. Only daytime hours are included (11AM - 4PM local time). VMT and VHT data were downloaded from the Performance Measurement Systems data sources (CalTrans, 2022; UDoT, 2022).

We tested the effect of faster speeds on CO/CO_2 the California Air Resources Board's EMFAC model by simulating annual CO and CO_2 emissions if all vehicles were driving in their nighttime speed conditions, which we assume to represent free-flow traffic. Based on this scenario analysis, EMFAC predicts that CO/CO_2 emission ratios decrease by 12% at faster speeds (Table A2; Fig. A4). However, EMFAC only models emissions for speeds up to 70 mph and many drivers commonly exceed this speed. Some studies, using portable emissions measurement systems installed on running vehicles have found that CO/CO_2 ratios increase at faster speeds, especially when the driving style is aggressive, defined by faster speeds and bursts of acceleration (S. Park et al., 2010; Suarez-Bertoa et al., 2019; Tzirakis et al., 2007; Zhu et al., 2022). However, other studies (and EMFAC) have observed that CO/CO_2 decreases or does not change significantly with speed (Ammoura et al., 2014; Lee et al., 2020; Mei et al., 2021). The discourse is probably because the effect of faster speeds on CO/CO_2 emissions varies by vehicle fuel, class, age, and driving style. Based on EMFAC, CO/CO_2 decreases with speed for modern passenger cars but increases for some light-duty trucks and older vehicles (Fig. A4 and A5). SLC's fleet mix has more passenger trucks

than LA (Fig. A6) and is older (Fig. A7). Thus, speed could be an important factor affecting our measurements, since CO_{xs}/CO_{2xs} increased for both surveys in which speed increased (LA 2020 and SLC 2019). However, the impact of speed is dependent on the fleet composition (i.e., vehicle age, fuel, and category) and likely is not the only factor contributing to CO_{xs}/CO_{2xs} increases.

Vehicle age. Older vehicles on the road would lead to increases in CO_{xs}/CO_{2xs} ratios (Table A2), especially if they are driving fast (Fig. A5). Newer vehicle models are continually improved to emit less pollutants, while older models may have outdated emission control technology (Jaiprakash et al., 2017). Further, as vehicles age, the effectiveness of their on-board emission control devices such as catalytic converters decrease. It is possible that older vehicles played a role in the two surveys in which CO_{xs}/CO_{2xs} increased. On average, SLC has older vehicles than LA (Fig. A7). During the COVID-19 pandemic, older vehicles may have become more prominent on the road, which would contribute to the increased CO_{xs}/CO_{2xs} ratios we observed. While many Californians switched to teleworking during the pandemic, "essential workers" resumed work that was essential to maintain safety, health, and sanitary services (California State Government, 2022). Those driving in 2020 may have largely been service and/or blue-collar workers who may have limited ability to purchase newer vehicles. Further, public transportation use plummeted during the pandemic due to physical distancing recommendations. Regular transit users may have increased their driving of old vehicles if they could not afford a more modern car. We simulated the impact of older vehicles in EMFAC and found that if the 2020 traffic fleet reverted to the 2013 fleet (an older-vehicle scenario), on-road CO/CO_2 ratios would increase by 84% relative to the default scenario (Table A2). If the older vehicles were driving fast and/or with an aggressive driving style, these effects occurring simultaneously could compound CO_{xs}/CO_{2xs} increases (Fig. A5).

The combination of an older vehicle fleet and higher speeds in SLC relative to LA, and during 2020 in LA relative to 2019 and 2021, is the most likely explanation for our real-world CO/CO_2 observations (Table A2). While we recognize that for most of the vehicle fleet, speed has a decreasing effect on CO/CO_2 in theory, the characteristics of the SLC fleet (older and more light-duty trucks) and the circumstances around the COVID-19 pandemic could lend toward increased CO/CO_2 at faster speeds, especially if the

driving style is aggressive. Our dataset captures the net fleet-wide CO/CO_2, and thus is not suited to distinguish which vehicles caused the increase. Further work using portable emissions measurement systems or chassis dynamometer tests is needed to isolate the vehicle-specific effects. Such tests were used to inform emission rates in EMFAC but are limited for this comparison because (1) emissions under real-world driving conditions differ from the controlled test cycles on which EMFAC is based (i.e. higher than 70 mph speeds and more aggressive driving styles) and/or (2) because the pandemic led to broad fleet composition changes that were not captured by the model. Further, very few studies measuring emissions under real-world driving directly report CO/CO_2 ratios (Zhu et al., 2022). Nonetheless, we believe the complex effects of speed on emissions could decrease combustion efficiency and warrant further research especially on emissions and combustion efficiency at high vehicle speed (>70 mph).

1.3.4 Implications for fossil fuel CO_2 quantification

Besides the use of CO_{xs}/CO_{2xs} as an indicator of combustion efficiency, the ratio can also be used to quantify emissions of fossil fuel-sourced CO_2 ($ffCO_2$). This is critical for measurements that attempt to quantify anthropogenic CO_2 emissions mostly coming from fossil fuels, given that the biosphere contributes significantly to CO_2 emissions, even in cities (Miller et al., 2020). Since incomplete combustion of fossil fuels results in co-emitted CO and CO_2, the ratio of the two gases has been used as a tracer to distinguish CO_2 emissions from non-anthropogenic CO_2 sources (Gamage et al., 2020; Lopez et al., 2013; Maier, Levin, et al., 2023; Maier, Rödenbeck, et al., 2023; Turnbull, Karion, et al., 2011; Vogel et al., 2010). The CO_2 enhancement is calculated as:

$$ffCO2 = \frac{CO_{obs} - CO_{bg}}{R_{CO/CO2}} \quad \text{Eq. 1.1}$$

where CO_{obs} is the measured CO mixing ratio, CO_{bg} is the CO background (usually determined from a remote or upwind site), and $R_{CO/CO2}$ is the ratio between CO and CO_2 in units of ppbv/ppmv. Ideally, $R_{CO/CO2}$ would be calculated based on the correlation between CO and the radiocarbon-based estimate of

the CO_2 signal, since the radiocarbon isotope is the most direct atmospheric proxy for fossil fuel emissions (Turnbull, Karion, et al., 2011).

The uncertainty in CO_2 calculations using this approach depends on the variability in $R_{CO/CO2}$ for the particular location and time period of the study. For instance, in previous work, an $R_{CO/CO2}$ value of 14 ± 2 ppbv/ppmv resulted in CO_2 values that varied by approximately ± 15% based on the upper and lower $R_{CO/CO2}$ values and background conditions in Sacramento, CA in 2009 (Turnbull, Karion, et al., 2011). However, with CO emissions declining in urban areas, uncertainty in CO_2 would increase as $R_{CO/CO2}$ approaches zero. Using the variability in measured on-road CO_{xs}/CO_{2xs} ratios to quantify uncertainty in $R_{CO/CO2}$ (i.e., 3.0 ± 1.6 in LA 2019), the resulting CO_2 values vary by 34-114%. This large uncertainty is conservative, given that LA 2019 was our least variable survey and other years and SLC had larger standard deviations ranging from 4.7 to 17.1 ppbv/ppmv. Given the spatial and temporal variability in the ratio observed in this study, the uncertainty in $ffCO_2$ using this method is substantial. This approach requires a robust correlation between CO and CO_2, which we did not observe in our data (Fig. A8). In our observations, we assumed that all of the CO_{2xs} we measured on-road was from fossil sources, yet CO_{xs} and CO_{2xs} were not strongly correlated, with R^2 values less than 0.19 (Fig. A8). The correlation weakened over time. The 2019-2021 observations had lower R^2 values (ranging from 0 to 0.16) than the 2013 measurements in both cities (R ranging from 0.17 to 0.19). Previous work has also described inconsistencies and large uncertainties in CO/CO_2 that make CO an unreliable tracer for $ffCO_2$ emissions on its own (Ammoura et al., 2014; Djuricin et al., 2010; Gamnitzer et al., 2006). Other trace gas species such as NO_2 may be suitable alternative tracers (Konovalov et al., 2016; Yang et al., 2023a), but updated studies evaluating such proxies against radiocarbon observations, the most direct tracer for CO_2, are urgently needed to ensure robust tracking of climate change mitigation measures.

In summary, using on road measurements of CO and CO_2 mole fractions, we observed changes in vehicle combustion efficiencies in two western U.S. cities (Los Angeles, CA and Salt Lake City, UT) over 2013 and 2021, a period that includes substantial changes in vehicle age and speed. Our measurements show that stricter emission regulations and mitigation incentives successfully lowered on-road CO

emissions over a six-year period in LA. In contrast, the combined effects of traffic conditions and the fleet composition led to a net worsening of fleet combustion efficiency in SLC, and during the COVID-19 pandemic in LA. Although our observations are not the ideal toolset for identifying the mechanistic drivers of the CO/CO_2 ratio for individual vehicles, they are able to uniquely measure the complex mix of sources and drivers in the real world that may differ from the model-based predictions. Future work should further evaluate the effects of traffic conditions on urban emissions and policymakers should consider the negative effects of elevated driving speeds on air quality. Furthermore, the success of CO emission regulations will make it more challenging for studies to apply CO as a tracer for quantifying fossil fuel CO_2 emissions from cities.

1.4 Acknowledgements

The authors wish to thank A. Ocampo, C. Gurguis, L. Ocampo, C. Limon, A. Odwuor, A. Welch and N. Rojas for their assistance with mobile measurements in Los Angeles. We are also grateful to M. Barth, K. Johnson, B. Wallerstein, and A. Raju for their helpful advice. C.C.Y. received support for this study from the National Science Foundation Graduate Research Fellowship Program (DGE-1839285). The Environmental Defense Fund provided funding for the 2019 mobile measurements in Salt Lake City. F.M.H. also acknowledges funding support from USDA National Institute of Food and Agriculture, CA-R-ENS-5148-H, Accession Number 1013346. We are also grateful to the California Air Resources Board EMFAC development team for providing feedback on this work. We also thank one anonymous reviewer whose feedback helped improve this manuscript.

Chapter 2 Reductions in California's Fossil Fuel Carbon Dioxide Emissions during the COVID-19 Pandemic

Adapted from:

Yanez, C. C., Hopkins, F. M., Xu, X., Tavares, J. F., Welch, A., & Czimczik, C. I. (2022). Reductions in California's urban fossil fuel CO_2 emissions during the COVID-19 pandemic. AGU Advances, 3(6), e2022AV000732.

2.1 Introduction

Carbon dioxide (CO_2) emissions associated with fossil fuel consumption ($ffCO_2$) are the dominant cause of climate change (Masson-Delmotte et al., 2021). Hence, there is an urgent need to quantify $ffCO_2$ emissions to support the success of climate change mitigation efforts. Urban areas account for 30-84% of global $ffCO_2$ emissions (Seto et al., 2014), despite encompassing less than 1% of the Earth's land area (Zhou et al., 2015). While being disproportional contributors to climate change, cities are also at the forefront of climate change mitigation actions (Rosenzweig et al., 2010), making them a top priority for quantifying and monitoring $ffCO_2$ emission reduction efforts.

Satellite-borne instruments can detect CO_2 enhancements (i.e., 6 ppm above background) over large cities (Kiel et al., 2021; Schwandner et al., 2017), and urban tower networks continuously measure CO_2 levels in a small selection of cities in more economically developed countries. However, these atmospheric observation systems are limited in their ability to detect trends in $ffCO_2$ at the neighborhood scale (~1 km^2) that is needed to inform local policy makers on the outcome of mitigation actions (Duren & Miller, 2012).

The abrupt halt of economic activity at the beginning of the coronavirus disease pandemic (COVID-19), with strictest regulations in place in the U.S. from March to May of 2020, provided an unplanned experiment on the sensitivity of atmospheric greenhouse gas (GHG) observations to changes in human behavior. Restrictions intended to prevent the spread of the virus caused a wide scale disruption of

human activities and consequently the largest reduction in global $ffCO_2$ emissions than has ever been observed, inducing rapid emission reductions larger than any historical human crisis or climate agreement (Le Quéré et al., 2021). These emission reductions provide insight on potential climate mitigation strategies, such as decreasing transportation emissions through increased flexibility in remote work. Several studies quantified emission reductions during the pandemic using activity-based models ("bottom up" estimates) that scale sector-based activity and consumption data with $ffCO_2$ emission coefficients. One study calculated a 17% (11 to 25%) reduction in daily global $ffCO_2$ emissions in April 2020 relative to 2019, based on a compilation of activity data and information on the intensity of mandated lockdowns (Le Quéré et al., 2020). Hourly to daily activity data indicated an overall global $ffCO_2$ decline of 8% in the first half of 2020 relative to 2019 (Liu et al., 2020).

Pandemic related emission reductions have also been assessed using atmospheric observations ("top-down" estimates). For instance, several cities have established *in situ* tower observation networks that continuously measure the total CO_2 mixing ratio. One such study reported a 30% reduction in the San Francisco Bay Area's CO_2 levels during the first six weeks of California's statewide Stay-At-Home Order (March 22 to May 4, 2020) relative to the six weeks before the order (Turner, Kim, et al., 2020). Similar reductions were reported for the Los Angeles (34 ± 6%) and Washington DC/Baltimore metropolitan areas (33 ± 11%) in April 2020 relative to the previous two years (Yadav et al., 2021). Alternative ground-based atmospheric measurements were also used to assess $ffCO_2$ emission reductions during the pandemic. Strong reductions in CO_2 fluxes (-5 to -87%) were observed during lockdown periods relative to the same times in previous years in 11 European cities using eddy-covariance measurements of CO_2 exchange (Nicolini et al., 2022). Atmospheric oxygen measurements were applied as novel tracers for $ffCO_2$ emissions in the United Kingdom and detected a 23% (14 to 32%) $ffCO_2$ reduction in 2020 annual emissions relative to a modeled scenario without the COVID-19 pandemic (Pickers et al., 2022).

Pandemic-related emission reductions were also observed in some remotely sensed data. One study combined bottom-up estimates and observations of nitrogen oxides (NO_x, pollutants that are co-emitted with CO_2 during fossil fuel combustion) from the Tropospheric Monitoring Instrument (TROPOMI) to

calculate a 12% decline in China's $ffCO_2$ emissions in the first four months of 2020 relative to 2019 (Zheng et al., 2020). However, studies analyzing data from CO_2-observing satellites (such as OCO-2 and GOSAT) could not conclusively detect pandemic-related emission reductions because of sparse data retrievals, low resolution, and weak signals (Buchwitz et al., 2021; Chevallier et al., 2020).

Quantifying $ffCO_2$ emission reductions (i.e., isolating fossil fuel contributions from the total CO_2 signal) remains a key challenge for climate change mitigation efforts, especially at localized spatial scales. This is because $ffCO_2$ emissions are superimposed on large and poorly constrained fluxes from land ecosystems (e.g., photosynthesis and respirations of plants and soil microorganisms) that vary seasonally and interannually in response to temperature, the timing and amount of precipitation, drought, fire, plant life stage, and management (irrigation, harvest) as well as emissions from biofuel combustion and human metabolism (e.g., respiration, sewage). Recent work in the LA metropolitan area revealed that biospheric fluxes contribute a significant proportion (up to 30%) to the excess level of CO_2 observed in the urban atmosphere (Miller et al., 2020). Thus, an effective $ffCO_2$ monitoring system requires a direct way to isolate fossil fuel sources from other entangled CO_2 fluxes, high spatial resolution, and accessibility to global cities.

One high resolution, sector-specific approach is the deployment of mobile GHG observatories that map fine scale patterns in $ffCO_2$ emissions from vehicle sources on urban roads (Bush et al., 2015). Such mobile measurements offer distinct sensitivity to traffic-related $ffCO_2$ emissions since the signal is dominated by nearby vehicle emissions and ambiguity related to transported air mixtures from other sources is reduced. During the COVID-19 pandemic, one mobile study observed dramatic reductions in on-road enhancements of CO_2 (-41 ppm or a 63% reduction) relative to a period before lockdowns in Beijing, China (Liu et al., 2021).

Radiocarbon analysis of plants is another promising approach for quantifying urban $ffCO_2$ trends at the local scale. Radiocarbon (^{14}C, a radioactive carbon isotope with a half-life of 5,730 years) is a unique tracer for $ffCO_2$ because fossil fuel-derived CO_2 is millions of years old and devoid of ^{14}C due to radioactive decay, while other sources of CO_2 have ^{14}C signatures similar to the current atmosphere (Graven et al., 2020a; Levin et al., 2003; Santos et al., 2019; Turnbull et al., 2006). Currently, an input of 1 ppm of $ffCO_2$

into the atmosphere results in a depletion of ambient $\Delta^{14}CO_2$ by 2.4‰. Since plants assimilate CO_2 during photosynthesis, plant ^{14}C reflects the $^{14}CO_2$ signature of the surrounding atmosphere integrated over the period when the plants are photosynthetically active. Where $ffCO_2$ emissions dilute ^{14}C in the atmosphere, plants are depleted in ^{14}C (appear older in ^{14}C age). Thus, plants offer a natural and efficient network of ^{14}C observations and can be used to map fine-scale spatial patterns in $ffCO_2$ in places without established CO_2 monitoring infrastructure (Hsueh et al., 2007a; Riley et al., 2008; Santos et al., 2019; Wang & Pataki, 2010).

Several studies have measured the ^{14}C of ambient air to quantify $ffCO_2$ trends in urban areas (Miller et al., 2020; Newman et al., 2016; Turnbull et al., 2011); however, plants offer time-integrated monitoring of ^{14}C that could more feasibly be used to monitor $ffCO_2$ spatial patterns in global cities than deploying air sampling stations at the same scale. Preparation for ^{14}C analysis is significantly faster for plant samples and can be done with just 4 mg of plant tissue since plants are approximately 40% C, while air samples (< 0.04% C) require expensive canisters and larger volume samples (approximately 5 L) and longer processing times to get a large enough ^{14}C sample for AMS analysis. This means that more ^{14}C samples can be analyzed leading to higher spatial resolution urban $ffCO_2$ datasets than with air samples. During COVID-19 lockdowns in New Zealand, the ^{14}C of weekly-sampled grasses tracked changes in local $ffCO_2$ emissions that coincided with the stringency of COVID-related restrictions and detected a 75% ± 3 peak reduction in $ffCO_2$ emissions (Turnbull et al., 2022).

Here, we quantify changes in $ffCO_2$ emissions during select periods of the COVID-19 pandemic (spring and summer of 2020 and 2021) in California, USA, with a focus on the state's two largest urban areas: the LA metropolitan area and the San Francisco Bay Area (SFBA). The State of California is the world's fifth largest economy (based on the state's GDP of 3.36 trillion USD in 2021, bea.gov) and has enacted landmark climate action legislation. Statewide policies that restricted mobility likely altered $ffCO_2$ emission patterns during the pandemic, such as the Stay-At-Home order that required the closing of all "non-essential" businesses from March 19 to May 4, 2020 (Executive Order N-33-20). To examine the impacts of these policies on $ffCO_2$ emissions, we use two approaches that can isolate CO_2 derived from fossil sources, are spatially resolved, and do not require establishment of CO_2 monitoring infrastructure.

First, we measured the mixing ratio of CO_2 on freeways in the LA area using a mobile GHG observatory. Second, we analyzed the ^{14}C content of annual grasses collected by community scientists across the state. Together, our data offer a unique insight into anthropogenic CO_2 emissions in California's urban regions during the COVID-19 pandemic and support the further use of plant ^{14}C analysis to evaluate decarbonization efforts in other cities.

2.2 Methods

2.2.1 On-road CO_2 measurements

We measured the on-road mixing ratios of CO_2 in the LA metropolitan area using a cavity ringdown spectrometer (G2401, Picarro) installed inside a mobile laboratory (2016 Mercedes Sprinter cargo van). The same platform has been used by previous studies to observe GHG and pollutant concentrations (Carranza et al., 2022; Thiruvenkatachari et al., 2020). Ambient air was continuously pumped into the Picarro from an inlet on the roof of the van behind the driver's seat, approximately 3 m above the road surface. We simultaneously collected position and meteorological data using a global satellite positioning device (GPS 16X, Garmin) and a compact weather sensor (METSENS500, Campbell Scientific) that were mounted on the roof of the vehicle.

Measurements were collected on freeways during daytime hours on weekdays in July 2019, 2020, and 2021. We filtered the datasets from each year to only include locations that overlapped with the 2020 dataset, focusing the analysis on approximately 750 km of road. To minimize meteorological effects on our results, we only used data collected between 11 AM to 4 PM local time, when the planetary boundary layer is well-developed and surface layer air is well-mixed (Ware et al., 2016). These times exclude typical rush hour traffic periods and make our analysis conservative since rush hour emissions were likely the most strongly reduced in 2020 as commuters switched to working from home. We also filtered out data from days that were overcast and otherwise experienced similar weather conditions during all three surveys. Different filtering strategies would be required for cities that experience different meteorology than LA.

We calibrated the analyzer before and after each survey using gas cylinders with CO_2 mixing ratios that have been corrected against the NOAA WMO-CO2-X2007 scale. For each calibration, the analyzer inlet was directed to sample air from compressed gas cylinders with known mixing ratios of CO_2 for three minutes. We used two standard tanks that spanned the range of CO_2 mixing ratios we observed on the road (Table A1). We then applied a two-point correction to the data based on the linear relationship between the known and measured values. The measurements are precise to <1 ppm for all surveys based on the standard deviation of the calibration runs. The calibrated data was aggregated into 5-second intervals and gridded into 100-m road segments to synchronize trace gas, weather, and position measurements.

Urban CO_2 enhancements (CO_{2xs}) were calculated by subtracting a background that represents the CO_2 mole fraction of air coming into the LA area before it is enhanced by local emissions. For urban studies, background characterization generally depends on latitude, seasonal wind patterns, and topography. Previous studies in other cities have used CO_2 measurements from upwind rural areas or a high elevation site to represent the background (Mitchell et al., 2018; Turnbull et al., 2019). Since westerlies prevail in LA in July, a suitable background can be represented by the inflowing marine air that originates in the Pacific Ocean (Newman et al., 2016; Verhulst et al., 2017). Thus, we characterized the CO_2 background using flask sample data from NOAA's Global Monitoring Division's site at Cape Kumukahi, Hawaii (19.54°N, 154.82°W, 15 m elevation). The NOAA GMD data is publicly available at https://gml.noaa.gov/ (Dlugokencky et al., 2021), and hosts a network of over 50 sites that monitor trace gas concentrations around the world. Previous work has found that Cape Kumukahi's CO_2 levels are similar to the local LA background for summer months (Hopkins et al., 2016). Based on the July average of all flask measurements at Cape Kumukahi, we estimate the CO_2 background was 411.0 ± 2.0 ppm in 2019, 412.9 ± 1.2 ppm in 2020, and 416.7 ± 1.7 ppm in 2021. On July 31, 2020, we measured similar CO_2 mixing ratios (413 ± 1.4 ppm) in the in-flowing marine air at Dockweiler Beach (33.94°N, -118.44°E), which supports the application of Cape Kumukahi as an adequate LA background. We assume that the observed CO_2 enhancements are solely derived from on-road emissions. It is possible that some of these enhancements

are influenced by biosphere fluxes and wildfire emissions. However, we expect that these contributions are relatively small and do not affect the results.

2.2.2 Radiocarbon analysis of plants

We measured the ^{14}C content of invasive annual grasses to map CO_2 trends across the state of California. The typical growing season of these species lasts from March to May, which coincided with California's statewide Stay-At-Home Order (March 19 to May 4, 2020) and made them useful bio-monitors of fossil fuel emission-reductions during the period of strictest COVID-19 measures in this area.

Because plant ^{14}C reflects the CO_2 assimilated from the atmosphere during photosynthesis, differences in ^{14}C depletion between plant samples are driven by local differences in ambient $^{14}CO_2$ composition and particularly the amount of fossil fuel influence. Studies around the world have mapped CO_2 patterns using a variety of plant species appropriate for their study area including tree rings in LA (Djuricin et al., 2010), evergreen tree leaves in Italy (Alessio et al., 2002), corn leaves in the United States (Hsueh et al., 2005) and Beijing, China (Xi et al., 2011), annual grasses in California (Riley et al., 2008; Wang & Pataki, 2010), ipê leaves in Rio de Janeiro (Santos et al., 2019), turfgrasses in New Zealand (Turnbull et al., 2022), and wheat crops in India (Sharma et al., 2023). Thus, cities can apply this technique to quantify CO_2 patterns by sampling a commonly found plant species that is photosynthetically active during the time integration period of interest. Unlike stable isotope signatures, plant ^{14}C content does not vary based on photosynthetic pathway, water use efficiency or other growth factors. Such factors are corrected for since the measured plant $^{14}C/^{12}C$ ratios are normalized to a $\delta^{13}C$ value of -25‰. Other than fossil fuel influence, the biggest drivers of ^{14}C differences between plant species would be from the usage of stored carbon in perennial plants (Vargas et al., 2009) and from local topographic conditions (i.e., photosynthetic fixation of soil-respired CO_2 in depressions).

We recruited community scientists to collect plant samples from their neighborhoods. We distributed a packet that contained scientific background information, sampling/mailing instructions, and photos to aid with plant identification. We also held informational webinars, gave presentations at

community college classrooms, and uploaded videos online demonstrating how to collect and mail the samples. Nearly 400 plant samples were submitted for the study. Most samples were collected on residential properties or along roadsides in public areas. The plant samples were mailed in paper envelopes along with the species, latitude, longitude, and date of collection. Collection dates for the samples ranged from late spring through the summer. Most plants were *Bromus tectorum* L. (cheatgrass), *Bromus diandrus* ROTH. (ripgut brome), *Avena fatua* L. (wild oat), or *Avena barbata* POTT EX LINK (slender oat). We inventoried all samples and information, confirmed their species (if identifiable), and recorded whether they were green or senesced. We also photographed all samples, focusing on their identifying features. These species represent a lower limit on annual $ffCO_2$ values since their growth period follows winter rain and wind events that cleanse pollution from the atmosphere.

We analyzed the ^{14}C content of 188 samples from the 2020 growing season and 82 samples from the 2021 growing season. We excluded plants that were not annual species, did not contain flowers, and any that showed signs of decay (rot, mold). We prioritized analysis of samples that were expected to have high CO_2 signals (urban areas) and were collected at similar locations in both years. To prepare the samples for ^{14}C analysis, we weighed out approximately 4 mg of plant tissue, focusing on flowers to target carbon fixed from the atmosphere during March to May. Samples were then sealed into pre-combusted quartz tubes with cuprous oxide, evacuated and combusted at 900°C for 3 h. The resulting CO_2 was purified cryogenically on a vacuum line, quantified manometrically, and converted to graphite using a sealed-tube zinc reduction method (Xu et al., 2007). The graphite was analyzed for ^{14}C at the W. M. Keck Carbon Cycle Accelerator Mass Spectrometer facility (NEC 0.5MV 1.5SDH-2 AMS) at the University of California, Irvine alongside processing standards and blanks. The measurement uncertainty ranged from 1.4 to 2.1‰. We use the $\Delta^{14}C$ notation (‰) for presentation of results [Eq. 2.1],

$$\Delta^{14}C = 1000 \cdot (FM \cdot \exp\left(\frac{1950 - y}{8267}\right) - 1) \qquad \text{Eq. 2.1}$$

where y is the year of sampling, FM is the fraction modern calculated as the $^{14}C/^{12}C$ ratio of the sample divided by 95% of the $^{14}C/^{12}C$ ratio of the oxalic acid (OX) I standard measured in 1950, 8267 years

is the mean lifetime of ^{14}C, and 1950 is the reference year for "modern". Mass-dependent isotopic fractionation of the sample is accounted for in the fraction modern term (Trumbore et al., 2016). This ^{14}C notation includes a correction for the decay of the OX I standard since 1950, giving the absolute ^{14}C content of our samples during the year they were collected.

We used a mass balance approach (Santos et al., 2019; Turnbull, Karion, et al., 2011) to quantify the fossil fuel contribution to the local CO_2 signal (C_{ff}) at each sample location. In the following equations, C_i terms denote CO_2 mixing ratios (units of ppm) from each contributing source and Δ_i terms denote the corresponding ^{14}C signature for each source in units of per mil (‰).

$$C_{obs} \cong C_{bg} + C_{ff} \quad \text{Eq. 2.2}$$

$$C_{obs}\,\Delta_{obs} \cong C_{bg}\Delta_{bg} + C_{ff}\Delta_{ff} \quad \text{Eq. 2.3}$$

$$C_{ff} \cong C_{bg}\frac{(\Delta_{bg} - \Delta_{obs})}{(\Delta_{obs} - \Delta_{ff})} \quad \text{Eq. 2.4}$$

Here, we assume the observed mixing ratio of CO_2 (units of ppm) at a location is the sum of two contributions: the CO_2 background (C_{bg}) and a fossil fuel contribution (C_{ff}) [Eq. 2.2]. The isoproduct for each CO_2 source must also be conserved [Eq. 2.3]. Combining Equations 2.2 and 2.3, we can calculate C_{ff} for each sample [Eq. 2.4]. All other values are known: Δ_{obs} is the measured ^{14}C content of the plant sample. For C_{bg} we use the average CO_2 mixing ratio measured at Cape Kumukahi (Dlugokencky et al., 2021) between March and May. C_{bg} was 416.7 ± 1.1 ppm for the 2020 and 419.4 ± 0.8 ppm for the 2021 growing season, respectively. The $\Delta^{14}C$ of background air (Δ_{bg}) is characterized by monthly-integrated air samples collected in a remote location Pt. Barrow, Alaska (X. Xu, Pers. Comm., 2021) and was -2.8 ± 1.3‰ for the 2020 and -6.2 ± 1.7‰ for the 2021 growing season, respectively. Δ_{ff} is -1000‰, the known fossil fuel ^{14}C signature. Based on the average standard deviation of replicate plant samples and error propagation of the measurement uncertainty, the uncertainty in a C_{ff} estimate is 1 ppm. Our equations assume biogenic ^{14}C inputs (such as from fires or heterotrophic respiration) are small enough to be neglected in the mass balance budget. Previous work has shown that this effect is constant and relatively small (Newman et al., 2016). The plant growing season (March to May) is outside of California's wildfire season, so we do not expect

wildfire emissions to affect the plant ^{14}C signatures. We also assume that the samples were not affected by ^{14}C emissions from nuclear power plants since there is only one such facility that is active in California (the Diablo Canyon Power Plant in San Luis Obispo County). The nearest plant sample was approximately 17 km northeast of the facility, which is not in the path of the area's dominant wind direction and is likely too far to intercept the emissions.

We expect that meteorology had minimal impact on our ^{14}C analysis since the plant samples experienced similar meteorological conditions across both study years, and because our plants only assimilate CO_2 during daytime hours. Thus, sampling excludes periods of strong atmospheric stability such as nighttime and early mornings that have increased CO_2 levels that are not driven by changes in $ffCO_2$ emissions (Djuricin et al., 2010; Newman et al., 2016; Verhulst et al., 2017).

2.3 Results and Discussion

2.3.1 Reduced CO_2 enhancements on Los Angeles freeways

We observed substantial reductions in on-road CO_2 enhancements (CO_{2xs}) in the LA metropolitan area during the pandemic (Fig. 2.1). The mean CO_{2xs} value (± SD) on LA freeways was 119 ± 50 ppm lower in July 2020 compared to July 2019 (Table 2.1), a -60 ± 16% change with CO_{2xs} reductions observed universally across all sampled freeways. By July 2021, COVID-related changes in behavior were reduced and CO_{2xs} rebounded by 153 ± 40 ppm compared to 2020 (Table 2.1). This equates to a 17 ± 29% increase in CO_{2xs} levels in July 2021 relative to July 2019. The 2021 CO_{2xs} increases were not uniformly distributed. Many freeways still had CO_{2xs} values that were lower relative to 2019, although not nearly as low as in 2020. Heavily trafficked areas had CO_{2xs} levels as much as 40% higher than 2019 (Fig. B1). Furthermore, CO_{2xs} values were less variable in 2020 (interquartile range of 33 ppm) and 2021 (interquartile range of 43 ppm) compared to 2019 (58 ppm), indicating more homogeneous CO_{2xs} on roadways during the pandemic (Fig. B2).

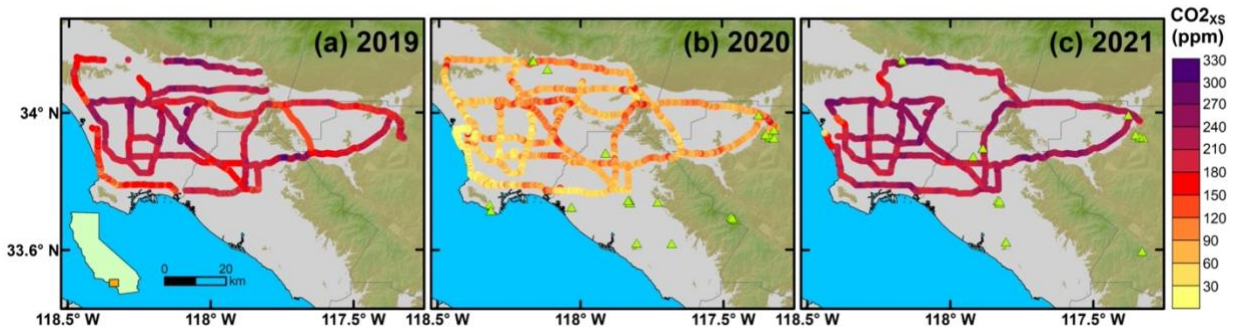

Figure 2.1. On-road CO_{2xs} observed near midday on Los Angeles freeways before (2019) and during the COVID-19 pandemic (2020 and 2021). Choropleth maps show CO_{2xs} observations in (a) July 2019, (b) July 2020, and (c) July 2021. Green triangles show locations of plant ^{14}C samples collected in 2020 and 2021. Basemap shows topography for elevations >300 m as hillside shading based on a Digital Elevation Model from USGS.

Changes in traffic patterns during the pandemic are likely the main cause of the changes in on-road CO_{2xs} values we observed. In addition to the number of cars on road, previous work has shown that on-road CO_2 mixing ratios are sensitive to traffic conditions such as speed, distance between cars and road grade (Maness et al., 2015). In July 2020, schools and businesses were operating in a remote or hybrid work model and many commercial facilities were closed, leading to substantial traffic reductions. Data from the California Department of Transportation's Performance Measurement System (PeMS) indicates that the vehicle miles traveled (VMT) on Southern California freeways was on average 12% lower in July 2020 compared to July 2019 (Caltrans, 2021). With fewer vehicles on the road in July 2020, there were wider distances between cars, fewer traffic jams, and fewer CO_2 emissions.

Table 2.1. Changes in CO_2 levels during the COVID-19 pandemic in California based on on-road mobile surveys and observations of ^{14}C in plants and/or air.

Region	Pre-pandemic	2020	2021	COVID-19[a]	Rebound[b]
CO_{2xs} (ppm) via on-road mobile surveys					
LA	199 ± 42[c]	80 ± 27	233 ± 29	-119 ± 50*	153 ± 40*
CO_2 (ppm) based on ^{14}C in plants and/or air					
CA	4 ± 5[d]	4 ± 4	5 ± 5	0 ± 6	1 ± 6
CA co-located	*n.a.*	*5 ± 5*	*5 ± 6*	*n.a.*	*0 ± 8*
LA	11 ± 9[e]	6 ± 5	9 ± 7	-5 ± 10*	3 ± 9
LA co-located	*n.a.*	*9 ± 9*	*11 ± 10*	*n.a.*	*2 ± 13*
Pasadena	23 ± 4[f]	3	13 ± 2	-20 ± 4*	10 ± 2*
Irvine	7 ± 4[g]	6	4 ± 1	-1 ± 4	-2 ± 1

Notes: Asterisk (*) indicates the means were significantly different based on Welch's t-test. Further details for these calculations are in Table B2. Uncertainties are standard deviations. Values that do not have uncertainties indicate a sample size of 1. For these cases, the uncertainty in the CO_2 estimate is assumed to be 1 ppm based on the differences in replicated plant samples. Values in regular font represent all the samples collected in that year, while values in italicized font represent only co-located plant samples that were collected in both 2020 and 2021 less than 150 m apart.

[a]Calculated as the difference between the 2020 (intense physical distancing measures and mobility restrictions) and pre-pandemic columns. The pre-pandemic observations are based on datasets from various years and are described in the subsequent footnotes and Table B2.

[b]Calculated as the difference between 2021 and 2020 (relaxation of physical distancing measures and mobility restrictions)

[c]July 2019 on-road mobile measurements.

[d]2005 plant ^{14}C observations (Riley et al., 2008).

[e]Based on 2005 plant ^{14}C observations (Wang & Pataki, 2010) and 2015-2016 air ^{14}C samples (Miller et al., 2020).

[f]Predicted value based on a linear extrapolation of 2006-2013 air ^{14}C samples (Newman et al., 2016) assuming the trend continued and there had been no pandemic.

[g]2019 air ^{14}C samples (Xu, pers. Comm., 2020).

Nationwide studies conducted during the same period deduced that CO_2 emissions started recovering after reaching minima in March or April of 2020, and that by July of 2020 (our study period), the reductions had largely diminished (Harkins et al., 2021; Le Quéré et al., 2020; Liu et al., 2020). Daily ground transportation emissions in the U.S. were estimated to only be reduced by 7-8% in July 2020 compared to 2019 (Harkins et al., 2021; Liu et al., 2020). Interestingly, our LA observations indicate much larger reductions to on-road CO_2 emissions during that period (~60%). This is likely because our measurements were collected in an area where emissions are dominated by passenger vehicles. In California and in LA, the transportation sector is the largest source of CO_2 emissions (45% of total), so changes in traffic patterns during the pandemic were more likely to have a discernable impact on this region's CO_2 budget. A 60% decrease in on-road emissions is consistent with a previous estimate that the LA area's total

emissions were reduced by 30% in the spring of 2020 relative to 2018-2019 (Yadav et al., 2021). A budget balance calculation with a 30% reduction in total LA emissions in 2020 equates to a 67% reduction in on-road emissions if we assume non-vehicle CO_2 sources were held constant and the on-road sector accounted for 45% of LA's CO_2 emissions before the pandemic. However, previous studies have shown that the pandemic-related emission reductions are not completely attributable to changes in traffic (Liu et al., 2020; Yadav et al., 2021), so our ~60% reduction result is still higher than what other studies estimated. On-road CO_2 measurements are likely to detect the transportation-sector emission changes with higher sensitivity than tower- and space-based observations since signal detection is not as dependent on atmospheric transport.

While our data revealed striking reductions in CO_2 mixing ratios, it is not trivial to translate changes in on-road CO_2 mixing ratios into reductions in ffCO_2 emissions. One reason for this is confounding effects of changes in vehicle speeds on CO_2 emissions. There is a nonlinear relationship between vehicle speeds and emission rates, such that vehicles emit more CO_2 at very low and very high speeds (Fitzmaurice et al., 2022). In 2020, our average speed was 9 km h^{-1} faster than 2019 and 12 km h^{-1} faster than 2021, which suggests a decrease in congestion in 2020. Within the range of our average speeds (64 to 76 km/hr), there is not expected to be a substantial change in CO_2 emission rates (Fitzmaurice et al., 2022). However, these averages do not capture the non-constant speeds during periods of congestion that make vehicles less efficient and increase both CO_2 emissions (Boriboonsomsin & Barth, 2008) and roadway enhancements. Faster speeds produce more CO_2 emissions because vehicle engines are doing more work and using more fuel, but they also create more turbulence near the road that effectively mixes vehicle emissions, thereby reducing on-road CO_2 enhancements. Nonetheless, we did not find a significant relationship between our measurements of CO_{2xs} and vehicle speed (Fig. B3). We estimated how much vehicle speed would affect our measurements using a model where on-road CO_{2xs} levels scale with vehicle speed to a power of -⅓ (Baker, 1996; Maness et al., 2015). Assuming that total highway emissions (Q) are related to CO_{2xs} and vehicle speed (v) by Equation 2.5 where κ is a constant of proportionality based on theoretical atmosphere and traffic conditions, a 9 km/hr increase in speed as observed in 2020 only causes total emissions to

increase by less than 5%. Thus, we attribute the measured CO_{2xs} reductions to the smaller number of cars on the road, not the changes in speed.

$$CO_{2xs} = \kappa Q v^{-1/3} \quad \text{Eq. 2.5}$$

Interestingly, our on-road observations did not scale proportionally with vehicle miles traveled (VMT), a metric that has been used to infer CO_2 emissions from the transportation sector (Gately et al., 2015; Gurney et al., 2020). While we observed a 60 ± 16% reduction in CO_{2xs} in July 2020 relative to July 2019, VMT in the LA area was only reduced by 12% during the same time periods (CalTrans, 2021). VMT does not adequately capture the strong CO_2 signal we observed because it does not account for the effects of driving behavior, congestion, vehicle speeds, and fleet composition on CO_2 emissions (Rao et al., 2017), all of which likely changed during 2020. While relationships between emissions and speed are incorporated in some models, less work has incorporated the effects of stop-and-go driving, which is likely to produce higher CO_2 emissions. Less congestion in 2020 could have reduced $ffCO_2$ emissions in ways that have not been fully explored. Other studies also reported large discrepancies between $ffCO_2$ emission estimates based on governmental traffic data, fuel-based models, and novel cell phone-based mobility datasets (Gensheimer et al., 2021; Harkins et al., 2021; Oda et al., 2021). Future work is needed to consolidate these different metrics for estimating transportation CO_2 emissions and to better understand what information each of these datasets represents.

Assuming the measured 60% reduction in on-road CO_{2xs} translates into a 60% reduction in annual interstate CO_2 emissions (7.6 Mt C yr^{-1} in 2012; Rao et al., 2017), given that interstates are the primary road type included in this analysis, this equates to an avoided 4.6 Mt C. The estimated total emissions for the LA area was 47.2 ± 5.2 Mt C yr^{-1} in 2015 (Gurney et al., 2019). This would imply that LA's total $ffCO_2$ emissions were reduced by 10% if all the pandemic-induced reductions in 2020 were solely due to changes to on-road interstate emissions (neglecting $ffCO_2$ changes in other sectors, such a residential, industry, and non-interstate roads). Interstate emissions constitute only 40% of LA's on-road emissions (Rao et al., 2017). If we instead assume the COVID-induced traffic reductions resulted in a 60% reduction in $ffCO_2$ for the

entire on-road sector (including all road types), then $ffCO_2$ emissions were reduced by 11.4 Mt C, or 24% of LA's total $ffCO_2$ emissions.

2.3.2 Reduced CO_2 emissions during the Stay-At-Home order

^{14}C analyses of plant species were used to map $ffCO_2$ patterns, whereby lower $\Delta^{14}C$ values indicate higher CO_2 inputs (Fig. 2.2). In 2020, the average $\Delta^{14}C$ (± SD) was -11.3 ± 8.6‰ (n=188) statewide, and -15.9 ± 12.5‰ (n=53) in the LA area, -10.2 ± 5.5‰ (n=91) in the SFBA, and -10.3 ± 5.6‰ (n=12) in the San Joaquin Valley. This equates [Eq. 2.4] to average fossil fuel contributions of 4 ± 5 ppm statewide, and 6 ± 5 ppm in the LA area, 3 ± 2 ppm in the SFBA, and 3 ± 2 ppm in the San Joaquin Valley. The cleanest samples were found in California's northern coast ($\Delta^{14}C$ of -5.3 ± 3.7‰, n = 5). Generally, $\Delta^{14}C$ of plants collected in urban areas were more depleted and more variable than in non-urbanized regions, indicating higher and locally variable emissions of $ffCO_2$ (Fig. 2.2). Sample collection was biased toward urban areas, with 77% of samples collected either in the LA area or SFBA, leading to higher uncertainty in predictions in other regions of the state (Fig. B4). However, we expect rural and remote areas such as northern California and the Sierra Nevada Mountains to have similar ^{14}C values as the background and little variability (Riley et al., 2008). Thus, while we do not have a lot of plant samples in these areas, we do not expect to see substantial COVID-effects on $ffCO_2$ levels.

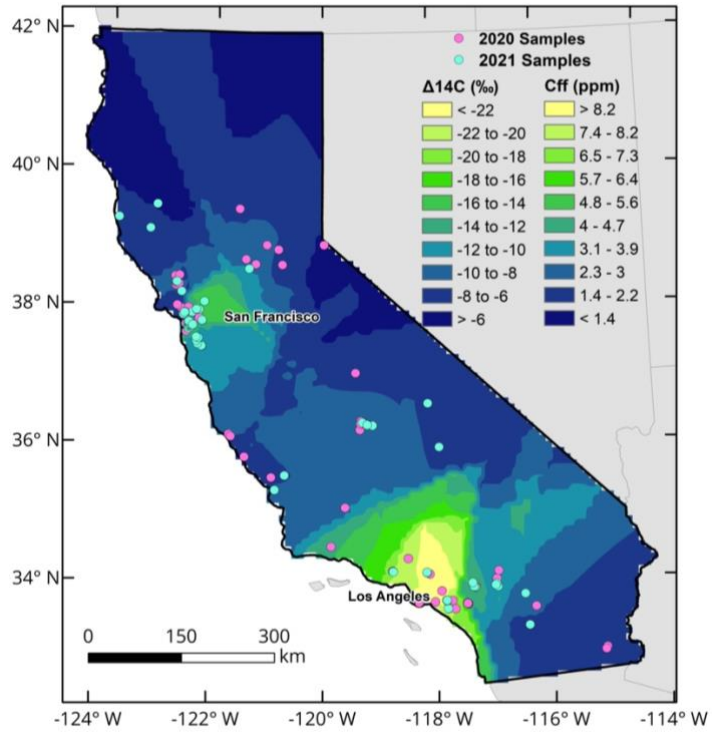

Figure 2.2. The $\Delta^{14}C$ (‰) of annual grass samples collected in California, USA and the corresponding C_{ff} values in 2020. Blue points indicate locations where plants were collected in both 2020 and 2021, while pink points indicate 2020-only locations. Background colors were mapped using an ordinary kriging interpolation of 2020 plant $\Delta^{14}C$ values using the Spatial Analyst toolbox in ESRI's ArcMap software. The uncertainty in the kriging prediction is presented in Fig. B4.

To assess our 2020 plant ^{14}C observations in the context of long-term trends in the region, we compared our data to existing records of ^{14}C in plants and/or air from Irvine, CA (a coastal city south of LA) and Pt. Barrow, AK (a remote location far from $ffCO_2$ sources) (Fig. 2.3). We infer urban $ffCO_2$ emission reductions during the 2020 Stay-At-Home order relative to the ^{14}C records shown in Figure 2.3 based on two metrics: variability in ^{14}C (standard deviation of mean) and the difference in ^{14}C from the hemispheric background (Pt. Barrow, Alaska). Reduced variability in ^{14}C indicates reduced $ffCO_2$ levels since emissions lead to anomalous and spatially variable ^{14}C values. The standard deviations of plant $\Delta^{14}C$ samples collected in the LA metropolitan area were 25.4‰ in 2005 (n=79, Wang & Pataki, 2010), 12.5‰ in 2020 (n=53), and 15.4‰ in 2021 (n=27). Thus, plant ^{14}C was less variable during California's 2020 Stay-At-Home order.

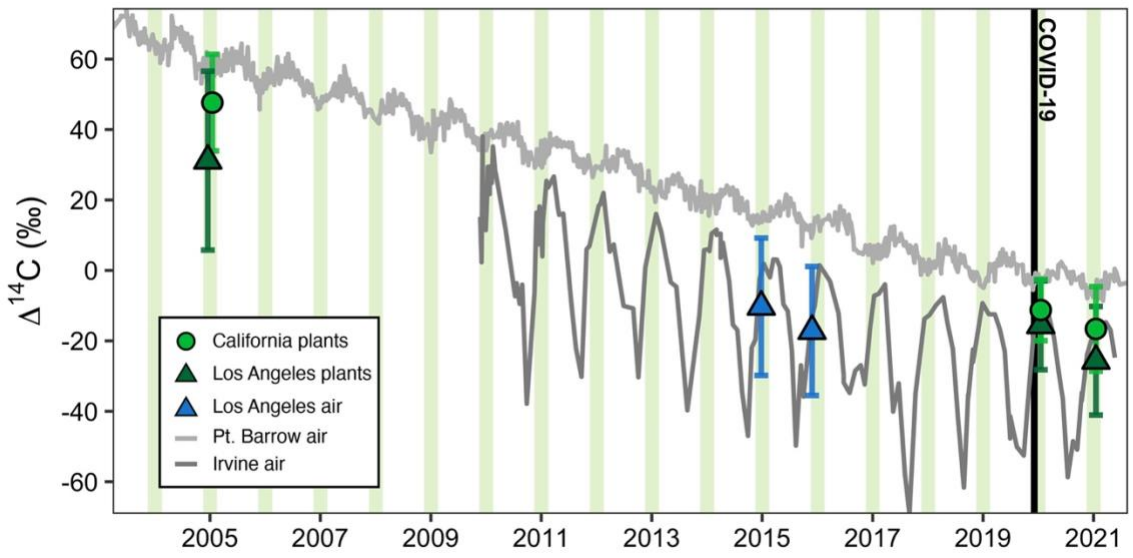

Figure 2.3. A record of $\Delta^{14}C$ measurements from 2003-2021. Average plant 14C from various studies are shown as green points with error bars showing the standard deviation. Green circles represent statewide data (this study and Riley et al. 2008) while triangles represent only the Los Angeles metropolitan area (this study and Wang & Pataki, 2010). Air-based ^{14}C observations are shown as gray lines (X. Xu, Pers. Comm., 2021) and blue triangles (Miller et al., 2020). Shaded green bars represent the typical annual grass growing season in California (March to May).

Furthermore, 2020 samples were more similar to the hemispheric background than in other years. Compared to Pt. Barrow, LA area ^{14}C samples were depleted by 26 ± 3‰ in 2005 (plant samples; Wang & Pataki, 2010), 25 ± 2‰ in 2015, 30 ± 4‰ in 2016 (flask samples; Miller et al., 2020), 13 ± 2‰ in 2020, and 19 ± 3‰ in 2021 (this study's plant samples; average depletion ± standard error of the mean). The mean 2020 depletion is significantly smaller than pre-pandemic years to a 95% confidence interval, indicating that $ffCO_2$ levels were reduced in 2020. Translating the ^{14}C depletion from background into fossil fuel-sourced CO_2 enhancements [Eq. 2.4], the mean C_{ff} in LA during pre-pandemic years ranged from 10-13 ppm (Table B2). However, during the pandemic the mean C_{ff} reduced to 6 ± 5 ppm (Table 2.1). Thus, we calculate $ffCO_2$ levels were reduced by 5 ± 10 ppm relative to pre-pandemic observations.

These samples reflect varying locations within the Los Angeles region, and hence we are assuming that both prior and current plant samples as well as previous flask samples are similarly representative of the region. To minimize the impact of these assumptions, we also estimated $ffCO_2$ emission reductions in one location, Pasadena, a city in the northeast LA basin that receives polluted air from the LA region during

afternoon hours (Newman et al., 2008). Based on a linear extrapolation of the Pasadena air record (Newman et al., 2016), the mean $\Delta^{14}C$ during the 2020 growing season (March to May) would have been -55.5 ± 8.8‰ had there been no pandemic, translating to a local enhancement of 23 ± 4 ppm CO_2 above background [Eq. 2.4], but a plant sample collected in 2020 approximately 4 km away had an enhancement of only 3 ± 1 ppm CO_2 (Fig. 2.4). This difference indicates a reduction of 20 ± 4 ppm $ffCO_2$ in Pasadena during the 2020 Stay-At-Home order. In 2021, plants were sampled in this location again and had an average $\Delta^{14}C$ of -35.7 ± 4.5 ‰ (n=6), an enhancement of 13 ± 2 ppm CO_2. This value is closer to, but still significantly different from, the predicted 2021 mean value (-60 ± 9.4‰ or 24 ± 5 ppm CO_2 enhancement), indicating a partial but not complete rebound to the pre-pandemic emissions trend. In summary, we found that plant ^{14}C data was able to capture interannual changes in local $ffCO_2$ during the pandemic.

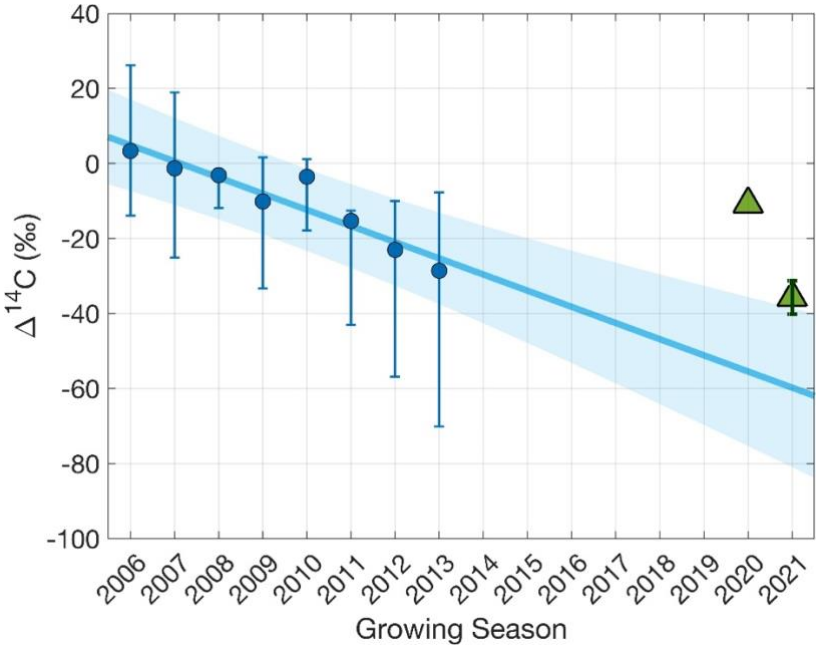

Figure 2.4. Growing season $\Delta^{14}C$ of ambient CO_2 in Pasadena, CA, a city within the northeast Los Angeles basin. The blue circles show the average growing season (March to May) $\Delta^{14}C$ of ambient CO_2 at Caltech [Newman et al., 2016], with error bars showing the minimum and maximum $\Delta^{14}C$ measurements. The line is a linear regression of these data with shading indicating the 95% confidence intervals. The green triangles show the measured $\Delta^{14}C$ of plant samples collected approximately 4 km away from the Caltech site in 2020 (n=1) and 2021 (n=6, error bars show standard deviation).

2.3.3 Changes in CO_2 during the rebound period (2020 to 2021)

Although the pandemic continued into the 2021 growing season, virus-restricting mandates were relaxed and California's vehicle miles traveled were 30% higher than the same period in 2020 (Caltrans, 2021). We observed large spatial variations and heterogeneity in ^{14}C during the second spring and summer of the pandemic. Based on a subset of samples collected at similar locations (< 150 m away) in both 2020 and 2021, we find that $ffCO_2$ levels did not change significantly between 2020 and 2021 at the statewide scale, with a mean change of 0 ± 8 ppm (Table 2.1). This average belies significant local variability in changes in $\Delta^{14}C$ between 2020 to 2021 (Fig. B5).

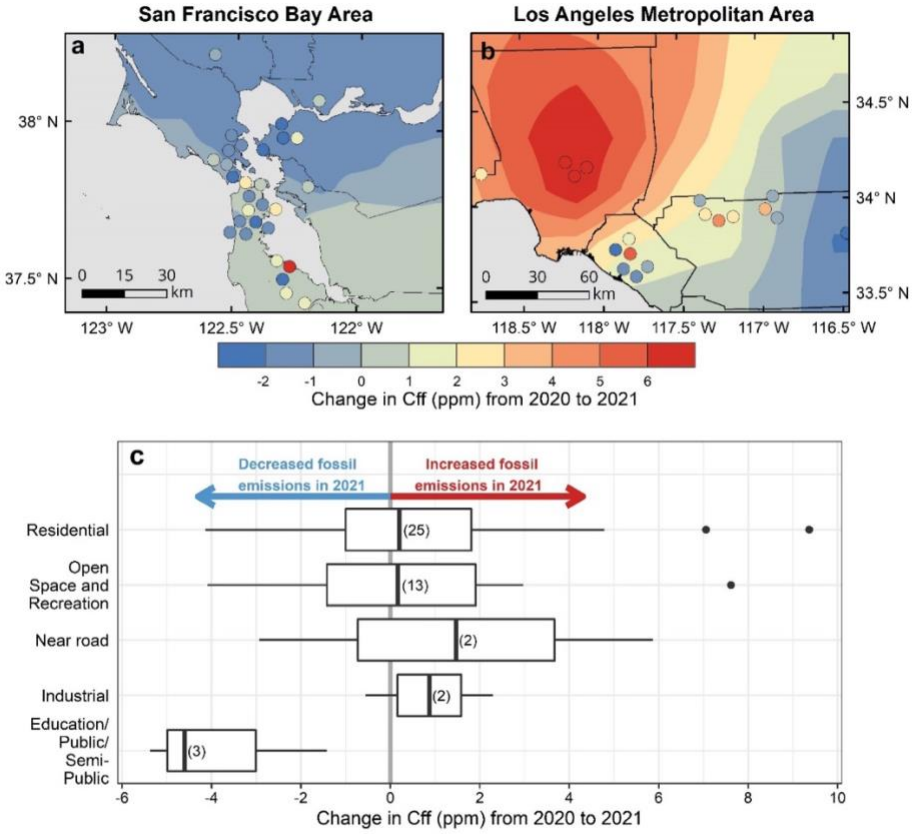

Figure 2.5. The difference in C_{ff} values from 2020 to 2021 between plant samples repeatedly collected in California's urban areas: (a) the San Francisco Bay Area and (b) the Los Angeles metropolitan area. Points show sample locations colored by their change in C_{ff}. Redder colors indicate CO_2 emission increases in 2021 compared to 2020. Background colors were calculated using an Ordinary Kriging interpolation of C_{ff} in ESRI's ArcMap software. C_{ff} changes by land use class are shown in (c).

The disparity in CO_2 emission rebounds in 2021 could be related to variations in pandemic responses as the economy recovered after the Stay-At-Home Order. We observed larger emission rebounds in LA than SFBA (Figs. 2.5 & B6). SFBA had more instances of $\Delta^{14}C$ values that either increased or only decreased as much as the long-term global ^{14}C trend between 2020 and 2021. The SFBA had a slower relaxation of COVID-19 prevention measures than other regions of California. Here, and also in Orange County in the LA area, many people continued to work from home into 2021, which may explain why emission reductions generally persisted even after lockdown restrictions were lifted (blue areas in Fig. 2.5 a,b). In LA neighborhoods, working from home was not an option for many "essential" workers, which might contribute to samples showing a stronger emission rebound in 2021 (red areas in Fig. 2.5b). These neighborhoods also have a greater density of freeways.

We used city land use data to further investigate the $ffCO_2$ emission sectors represented by plant samples collected in the LA area and SFBA (45 sample pairs, Fig. 2.5c). We found that the majority of plants were collected in areas classified as residential (58% of paired samples) or open space/recreation (29%). While there is large variation in ^{14}C within each category and results indicate that heterogeneity within regions/sectors was larger than the COVID-induced changes, there is a small trend toward higher CO_2 emissions in residential, open space/recreation and industrial areas, and a trend toward lower emissions from educational and public spaces. This is consistent with a return to normal of many activities, whereas schools in California stayed closed through the 2021 growing season and many government sector employees continued work from home. These sector-averaged trends are larger when all data is used (Fig. B7) but are on the order of ±1-2 ppm, which is not much larger than the uncertainty in our C_{ff} estimates (±1 ppm).

The heterogeneity in year-to-year changes elucidates the highly localized sensitivity of plant ^{14}C and indicates that this approach is a simple, yet effective method to monitor interannual changes in the $ffCO_2$ burden at the neighborhood scale. Thus, this approach could effectively track changes in local emissions if plants are periodically collected in direct proximity (< 20 m) from $ffCO_2$ emission sources. For instance, the Great Highway, a major north-south thoroughfare on San Francisco's western edge, was closed

to vehicles from April 2020 to August 2021. The road was converted into a car-free active transportation route, with access permitted only to pedestrians and bicyclists. Vehicle traffic was rerouted to 19th Avenue, a portion of CA State Route 1 less than 3 km east of the Great Highway. In 2020, plants collected along these two roads had very similar $\Delta^{14}C$ values (0.8‰ difference, which is within the measurement uncertainty). In 2021, a plant collected on the Great Highway was still statistically indistinguishable from the 2020 samples (0.7‰ difference), while a plant sample collected on 19th Avenue was significantly more depleted relative to the 2020 sample (-24.8‰ difference, equivalent to an increase of 10 ppm C_{ff}). This indicates higher $ffCO_2$ emissions on 19th Avenue where traffic increased in 2021, while $ffCO_2$ emission reductions near the Great Highway persisted while the roadway remained closed to vehicles.

All in all, we observed varying degrees of $ffCO_2$ reductions and rebound during the COVID-19 pandemic at various domains and spatiotemporal scales (Table 2.1). Year-to-year differences were more evident in urban domains (i.e., LA, Pasadena) than in statewide means or in coastal samples (e.g., Irvine).

2.3.4 Best practices and recommendations for future plant radiocarbon studies

Future work should conduct strategic experiments to better understand the correspondence between plant ^{14}C and other $ffCO_2$ atmospheric monitoring metrics. This will improve the applicability of plant ^{14}C analysis as a tool for monitoring decarbonization in cities around the world. Plant ^{14}C analysis reflected trends in ambient $\Delta^{14}CO_2$, with plant values having reasonable correspondence with air records from Irvine, CA and Pt. Barrow, AK (Fig. 2.3). However, our plant ^{14}C-based results contrast with our on-road CO_{2xs} observations where we observed a return to pre-pandemic conditions by July 2021. This is because the two datasets represent different emission sources and geographic regions. While the CO_{2xs} data specifically represents the LA area's on-road sector, our plant samples are mainly representative of statewide residential, open space and recreational areas, which showed a more heterogeneous response to the lifting of COVID-related restrictions. No plant samples were collected within 500-m of the roads surveyed with the mobile observatory (Fig. 2.1), so the two datasets were not directly comparable. A more strategic

sampling approach could reveal the relationship between these two approaches and the capacity of plants to monitor changes in transportation-sector emissions.

The spatial sensitivity ("footprint") of a plant is expected to be very localized (<100 m) but may vary for each sample depending on the local topography and air ventilation conditions. Previous work has shown that plants are predominantly influenced by emissions within 20 to 40 m (Lichtfouse et al., 2005; Turnbull et al., 2022). In contrast, atmospheric CO_2 measurements from rooftop/tower sites integrate signals over larger spatial scales (~10 km) since the inlet is higher above the ground (Kort et al., 2013). This makes tower sites well-suited for continuous monitoring of net $ffCO_2$ trends over an entire city using the CO_2 differential between a set of inflow- and outflow-representative sites. However, the localized spatial sensitivity of plants could be advantageous for studies seeking to investigate emissions at the neighborhood scale or from specific $ffCO_2$ sources (i.e. individual facilities or roads). Such analyses would require a strategic sampling design, targeting specific emission sources such as major roads (Turnbull et al., 2022). Without such targeted sampling, aggregated plant ^{14}C results in complex urban environments can be difficult to interpret since they represent highly local $ffCO_2$ emissions that may vary based on individual and immeasurable factors (i.e., human behaviors) within a neighborhood. With appropriately targeted sample pairs, however, plant ^{14}C can effectively reveal $ffCO_2$ reduction outcomes of local decarbonization measures (e.g., the Great Highway case described in Section 2.3.3). Plant-based monitoring of $ffCO_2$ emissions could also potentially be an appropriate proxy for exposure to co-emitted air pollutants such as from vehicle traffic and may be able to elucidate environmental justice concerns between neighborhoods. Future investigations are needed to assess this.

It is important to constrain the timing of carbon uptake as much as possible to distinguish spatially driven changes from temporal changes. Atmospheric $^{14}CO_2$ undergoes large temporal oscillations (Fig. 2.3) with the amplitude and seasonality driven by the timing of ^{14}C production and descendance into the troposphere, natural and anthropogenic CO_2 fluxes, and seasonal meteorology (wind and air mixing conditions). While the timing of flask sample collection is well-known, the timing of CO_2 uptake by plants is more uncertain. However, plant samples compensate for that by integrating over daytime hours of their

photosynthetic period, hence, reducing significant short-term variability observed in flask samples (e.g., Miller et al., 2020) to yield a seasonal average $ffCO_2$.

By sampling annual grasses, we have assumed that our $\Delta^{14}C$ analysis represents the growing season of these species in the region. We verified this assumption using downscaled remotely sensed observations of solar induced fluorescence (SIF, Fig. B8) (Turner, Köhler, et al., 2020) from the TROPOMI instrument onboard the Sentinel-5 Precursor satellite. Using the date of maximum SIF observance to represent the timing of peak growth, we found that all senesced plants had peak growth dates from March to May. We also observed some temporal agreement between plant $\Delta^{14}C$ and ambient $\Delta^{14}CO_2$ measured in Irvine, CA (Figs. B8 & B9), indicating potential applications of plant ^{14}C at the sub-seasonal scale. However, many $\Delta^{14}C$ values did not coincide with the Irvine trend and were more strongly driven by their distance to major roads (Fig. B8c), showing that the main driver of the samples' ^{14}C content is proximity to $ffCO_2$ emissions, with seasonality a secondary driver. SIF observations can help constrain the timing of plant growth for future studies to disentangle the spatial and temporal drivers of plant ^{14}C. Future studies could also potentially use purposely grown plants to monitor $ffCO_2$ (i.e., turfgrasses, Fig. B9), and actively manage the growing period to the timing of interest, which would allow similar analyses at smaller time scales and for other times of the year besides the annual grass growing season.

2.4 Conclusions

We quantified changes in fossil fuel consumption during the COVID-19 pandemic when California implemented aggressive mitigation measures, that included Stay-At-Home and work-from-home orders, travel limitations, and experienced widespread economic shutdown. On-road surveys of excess CO_2 demonstrated a drastic but temporary reduction in $ffCO_2$ emissions on LA freeways, with only about half the typical $ffCO_2$ emissions in July of 2020 and a return to pre-pandemic levels by July 2021. The analysis of ^{14}C in annual plants also revealed a measurable reduction in LA's $ffCO_2$ emissions in the spring of 2020

and 2021, indicated by a smaller offset between plant ^{14}C and ^{14}C of well-mixed northern hemispheric CO_2, and less variation in plant ^{14}C compared to previous years.

Our complementary approaches captured the heterogeneous reality of mandated and voluntary movement restrictions in California during the pandemic. Our study focused on a region rich in high quality datasets (i.e., previous ^{14}C records, a neighborhood scale bottom-up inventory, and an *in-situ* tower network) which allowed us to assess $ffCO_2$ emission reductions in the context of long-term trends. Mobile surveys can detect year-to-year differences in $ffCO_2$ trends from the on-road sector with high confidence, but further work is needed to relate on-road CO_2 enhancements to vehicle emissions and their drivers. Future research to constrain the spatial and temporal representation of periodically surveyed plants can support the tracking of decarbonization outcomes in cities and neighborhoods without investment in energy- and maintenance-demanding infrastructure. To account for the extreme variability of emissions sources in urban environments, however, plant-based $ffCO_2$ monitoring should focus on temporally repeated sampling of active plants in well-ventilated areas in the direct vicinity of specific emission sources.

2.5 Acknowledgements

The authors wish to thank all community scientists who submitted plant samples for this study and the Amigos de Bolsa Chica for helping with recruitment. Additionally, we thank A. Ocampo, C. Gurguis, V. Carranza, A. Odwuor, and C. Limón for their assistance with mobile surveys and W. M. Keck Carbon Cycle Accelerator Mass Spectrometer facility staff for supporting isotope analyses. We also thank A. Turner for his insight on this manuscript and for providing the downscaled solar induced fluorescence data to support the analysis. C. C. Yañez received support for this work from the National Science Foundation Graduate Research Fellowship Program (DGE-1839285). We also acknowledge helpful comments from three anonymous reviewers and editor E. Davidson.

Chapter 3 Plant Radiocarbon Across an Urban-Rural CO_2 Gradient Matches Surface and Column CO_2 Observations

Adapted from:

Yañez, C. C., Dubey, M., Hopkins, F.M, Meyer, A., Xu, X., Romero, J., Kim, J., Parker, H., & Czimczik, C.I. Plant Radiocarbon Across an Urban-Rural CO_2 Gradient Matches Surface and Column CO_2 Observations. *In Prep.*

3.1 Introduction

The majority of fossil fuel carbon dioxide ($ffCO_2$) emissions originate in urban areas, so decarbonizing cities is a priority for mitigating climate change (Crippa et al., 2021; Gurney et al., 2022). While many cities have ambitious plans to reach low- or net-zero emission targets within the next few decades (Seto et al., 2021), the lack of robust methods for quantifying urban $ffCO_2$ emissions makes the success of local emission reduction efforts uncertain (Duren & Miller, 2012). Ideally, urban $ffCO_2$ emissions should be quantified using methods that are both sensitive enough to detect spatiotemporal emission variations at scales relevant to policymakers (i.e., cities to neighborhoods) and accessible to cities around the world. However, these criteria are not met by any existing approach. Further development of $ffCO_2$ quantification approaches that are robust and operationally feasible is urgently needed to support climate change mitigation efforts.

To address this challenge, efforts to establish atmospheric CO_2 monitoring in cities have strengthened over the last decade, including investments in infrastructure to measure CO_2 mole fractions in (a) the lower troposphere (hereby referred to as "surface CO_2") and (b) total atmospheric columns of air ("XCO_2"). Surface CO_2 is measured on rooftops or towers in city networks (Karion et al., 2020; Mitchell et al., 2022; Verhulst et al., 2017; Xueref-Remy et al., 2018). Alternatively, XCO_2 can be measured remotely from the ground (Dietrich et al., 2021; Hedelius et al., 2018; Wunch et al., 2009) or from space (Eldering et al., 2019; Fang et al., 2023; Kiel et al., 2021) across urbanized regions. Surface CO_2 and XCO_2

each have their merits and limitations for $ffCO_2$ monitoring based on the distinct spatial and temporal scales at which they are sensitive to $ffCO_2$ emissions, meteorology, and atmospheric transport. Although significant enhancements of surface CO_2 and XCO_2 are detected in cities (Hakkarainen et al., 2016; Hedelius et al., 2018; Kort et al., 2012; Schwandner et al., 2017; Wunch et al., 2009), these measurements alone cannot disaggregate and directly quantify $ffCO_2$ emissions. Due to the well-mixed, long-lived nature of CO_2 in the atmosphere, the observed CO_2 signal is dominated by the changing background and fluxes arising from biospheric and oceanic interactions, while $ffCO_2$ emissions constitute a relatively small portion of the measured CO_2 mole fraction. Thus, additional information is needed to estimate $ffCO_2$ emission trends, such as prior emission estimates from bottom-up inventories (Lauvaux et al., 2020; Lian et al., 2023) or measurements of fossil fuel tracer species like nitrogen oxides, carbon monoxide, or carbon isotopes (Newman et al., 2016; Turnbull, Tans, et al., 2011; Wu et al., 2022; Yang et al., 2023b).

The "gold standard" tracer for $ffCO_2$ emissions is radiocarbon (^{14}C), a radioactive isotope of carbon with a half-life of 5,730 years (Graven et al., 2020b). Fossil fuels have a distinct ^{14}C signature because they originate from ancient plant material from which all initial ^{14}C has decayed away. Radiocarbon analysis of urban air $^{14}CO_2$ samples has been used to determine temporal variations in urban CO_2 contributions (Djuricin et al., 2010; Newman et al., 2016; Turnbull, Tans, et al., 2011), elucidate the presence of substantial biospheric CO_2 fluxes in cities (Miller et al., 2020), and evaluate $ffCO_2$ emission inventories (Basu et al., 2020). Plants provide time-integrated ambient ^{14}C information since they record the ^{14}C signature of CO_2 assimilated during photosynthesis. Previous studies used plant ^{14}C to map spatial patterns of urban $ffCO_2$ (Hsueh et al., 2007b; Riley et al., 2008; Santos et al., 2019; Wang & Pataki, 2010) and, more recently, measure temporal emission variations related to interannual changes in human activity (Turnbull et al., 2022; Yañez et al., 2022). In cities, plant ^{14}C offers some advantages over air $^{14}CO_2$ samples. Plants (a) provide high spatial resolution information about $ffCO_2$ emissions at the neighborhood scale since their sampling footprint is small (< 100 m) (Turnbull et al., 2022; Yañez et al., 2022) (b) have a much higher carbon content than air (40-50% vs.0.04% C, respectively), thus little material (1-2 mg of plant biomass vs. 5 L of air) is needed for ^{14}C analysis, and (c) are cheaper to ship and easier to process in the laboratory,

making routine operations more feasible. Despite these advantages, few studies have explored the capacity of plant ^{14}C to independently track urban $ffCO_2$ emission trends over time, especially on intra-annual timescales. This is because temporal and spatial uncertainties are not fully understood, and more work is needed to integrate plant ^{14}C data with surface CO_2 and XCO_2 observations.

In this study, we couple seasonal plant ^{14}C, XCO_2, and continuous surface CO_2 observations to quantify $ffCO_2$ emission patterns across the Los Angeles metropolitan area. Los Angeles is an ideal study location because it has established long-term, continuous atmospheric measurements with which to compare our plant ^{14}C observations, including air $^{14}CO_2$ (Xu, Pers. Comm., 2023), surface CO_2 (Verhulst et al., 2017), and XCO_2 (Wunch et al., 2009). Previous plant ^{14}C data in California only constrained $ffCO_2$ trends at annual resolution since they relied on the collection of annual invasive grasses that grow in the spring (Riley et al., 2008; Wang & Pataki, 2010; Yañez et al., 2022). In contrast, we repeatedly sampled irrigated turfgrasses, which are widely distributed across the region and reflect emission changes on time scales of 1-2 weeks year-round. We establish quantitative relationships between plant ^{14}C, surface CO_2, and XCO_2 and evaluate how plant ^{14}C fits into the current state of atmospheric CO_2 science by comparing with recent air $^{14}CO_2$ observations (Miller et al., 2020). Finally, we discuss the potential of plant ^{14}C to independently monitor $ffCO_2$ trends in other cities that are committed to lowering emissions but lack ground-based CO_2 measurement infrastructure to measure their progress.

3.2 Methods

3.2.1 Site characteristics

We measured turfgrass ^{14}C and atmospheric CO_2 in the Los Angeles (LA) area, focusing on five sites that span an urban to rural gradient (Table 3.1, Fig. 3.1). We repeated our sampling in three-month intervals between May 2022 and March 2023 to assess seasonal variations. The sites were selected based on their population density, location within the LA basin, and presence of long-term, continuous measurement infrastructure including surface CO_2 measurements via the LA Megacities (LAM) network

(Kim et al., 2022; Verhulst et al., 2017), ground-based XCO_2 measurements via the Total Carbon Column Observing Network (TCCON) (Wunch et al., 2009), and atmospheric $^{14}CO_2$ measurements (Xu, Pers. Comm., 2023). Most sites were located on university campuses where we could access electricity to power instruments and irrigated turfgrass lawns for plant ^{14}C sampling. We also periodically visited two secondary sites (MWO and SMM) to evaluate XCO_2 background conditions.

Table 3.1. Overview of CO_2 observation sites in the Los Angeles area in relation to existing Total Carbon Column Observing Network (TCCON) and LA Megacities (LAM) network sites.

ID	Site location	Population density*	Lat. (°N)	Long. (°W)	Elevation (m a.s.l.)	Existing instrumentation
Urban to rural gradient						
DLA	Downtown LA; University of Southern California	8304	34.02	118.28	59	LAM
PAS	Pasadena; California Institute of Technology	6040	34.14	118.13	240	LAM, TCCON
IRV	Irvine; University of California Irvine	4689	33.64	117.84	41	LAM, Air $^{14}CO_2$
RIV	Riverside; University of California Riverside	3878	33.98	117.32	330	LAM
BEA	Beaumont; Noble Creek Regional Park	1749	33.95	116.99	795	n.a.
Background Sites						
VIC	Victorville	1829	34.61	117.29	1370	LAM
SMM**	Santa Monica Mountains; Stunt Ranch Reserve	287	34.09	118.66	409	n.a.
AFRC	NASA Armstrong Flight Resource Center	7	34.96	117.88	700	TCCON
SCI	San Clemente Island	4	32.92	118.49	489	LAM
MWO***	Mount Wilson Observatory	2	34.22	118.06	1677	LAM

*City population density: persons per square mile in 2020 (www.census.gov). Population density for SMM, AFRC, SCI, MWO was determined by census tract (not city), since these locations have populations of less than 5000 people.
**SMM was only visited in August and November 2022
***MWO was only visited in August 2022

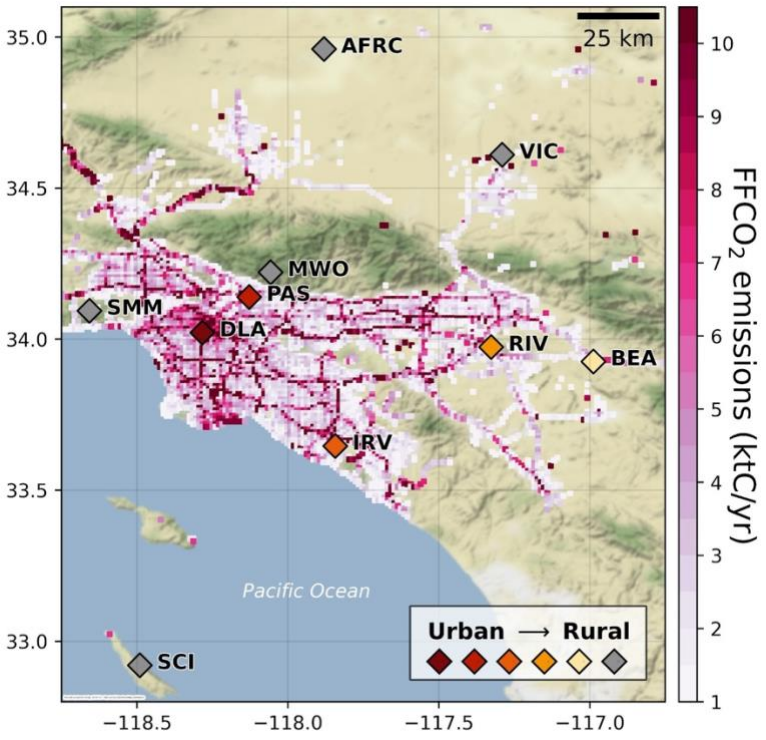

Figure 3.1. Map showing study sites in the Los Angeles area in Southern California, USA. Background colors indicate CO_2 emissions from the Hestia-LA annual 2015 emissions inventory, which has a spatial resolution of 1 km × 1 km (Gurney et al., 2019). Grid cells with less than 1 ktC emissions yr^{-1} were excluded for visualization purposes. Diamond symbols indicate site locations, with darker red colors indicating more urbanization. Sites that were used to estimate background CO_2 levels are in gray.

3.2.2 Plant radiocarbon (^{14}C) analysis

At each site, we collected a series of turfgrass samples for ^{14}C analysis up to 1 km away from where we conducted XCO_2 measurements (Fig. C4). During our first campaign in May 2022, we collected five samples in each cardinal direction in 100 to 500 m intervals but reduced the sampling for following campaigns (2-4 samples east and west of the XCO_2 measurements). We targeted landscaped turfgrasses in well-ventilated areas, avoiding local depressions to prevent biases that may arise from photosynthetic fixation of plant- or soil-respired CO_2. We used gardening shears to clip the top 2 cm of turfgrass and mixed several clippings within about 4 m^2. Samples were stored in paper envelopes until analysis. In the lab, samples were sonicated and rinsed with Milli-Q water and subsequently dried overnight at 60°C. We then homogenized the samples by either clipping them into small pieces or grinding to powder using a mortar

and pestle. We do not expect the two homogenizing techniques to have a strong effect on our results, but we did observe ^{14}C differences of up to 4‰ between the two methods, indicating the uncertainty due to sample heterogeneity (Fig. C5).

For ^{14}C analysis, approximately 4 mg were combusted with 80-100 mg cupric oxide in pre-baked quartz tubes for 3 hours at 900°C. The resulting CO_2 was purified cryogenically on a vacuum line, converted to graphite using a Zinc-reduction method (Xu et al., 2007), and analyzed for ^{14}C at the W. M. Keck Carbon Cycle Accelerator Mass Spectrometer (KCCAMS) facility at the University of California Irvine. We report our ^{14}C results using the $\Delta^{14}C$ notation (units of ‰), which represents the absolute amount of ^{14}C in the sample in the year it was measured, including a correction for the radioactive decay of the reference standard (Trumbore et al., 2016). The measurement uncertainty was less than 2‰ for all samples. Based on duplicate measurements, $\Delta^{14}C$ values varied by up to 4‰ (Fig. C5), which we use to quantify the uncertainty in our plant $\Delta^{14}C$ observations. We estimate that our $\Delta^{14}C$ measurements represent a temporal integration period of 1-2 weeks, based on the rate at which the grass grows and the frequency at which it is mowed. The spatial resolution is expected to be very localized, with a grass sample fixing CO_2 within 100 m (Turnbull et al., 2022).

We calculate local fossil fuel enhancements (C_{ff}), or the fossil fuel contribution to the total CO_2 signal, based on our plant ^{14}C measurements and a mass balance approach (Miller et al., 2020; Turnbull et al., 2022, 2006) [Eq. 3.1 – 3.2]:

$$C_{obs} = C_{bg} + C_{bio} + C_{ff} \quad \text{Eq. 3.1}$$

$$\Delta_{obs}C_{obs} = \Delta_{bg}C_{bg} + \Delta_{bio}C_{bio} + \Delta_{ff}C_{ff} \quad \text{Eq. 3.2}$$

Where C_{source} terms represent contributions to the total CO_2 mixing ratio in units of ppm, and Δ_{source} terms represent each of the sources' $\Delta^{14}C$ signatures in units of ‰. The sources of C are denoted in the subscripts of each term, where "obs" indicates our observations, "bg" the background, "ff" fossil fuel, and "bio" the terrestrial biosphere. Δ_{obs} are our turfgrass $\Delta^{14}C$ observations and C_{obs} are the observed surface CO_2 mole fractions at each site. For the Δ_{bg}, we use air $\Delta^{14}CO_2$ measurements collected at a remote site in

Utqiagvik, AK (Xu, Pers. Comm, 2023). We estimate C_{bg} based on daytime CO_2 mole fractions measured at two surface sites that have previously been determined to represent background during different times of the year in LA (Verhulst et al., 2017; Kim et al., 2023). The C_{bg} estimation is discussed in more detail in Section *3.2.5*. We consider Δ_{bio} as the mean Δ_{obs} since plants assimilate ambient $\Delta^{14}CO_2$ levels as in Miller et al. (2020). Δ_{ff} is -1000‰, the known $\Delta^{14}C$ signature of fossil fuels. In our analysis, we estimate and compare multiple versions of C_{ff} that either account for C_{bio} or neglect it. Under each case, the derivation is described in detail in Appendix C. The resulting C_{ff} equation when we neglect C_{bio} is:

$$C_{ff} = C_{bg}\,\frac{\Delta_{bg} - \Delta_{obs}}{\Delta_{obs} - \Delta_{ff}} \qquad \text{Eq. 3.3}$$

We also incorporate analysis of air $\Delta^{14}CO_2$ from samples collected in Irvine, CA (Xu, Pers. Comm, 2023) for comparison against the plant ^{14}C. The Irvine air samples are collected continuously in flasks over approximately 1 month periods. It is important to note that unlike the plants, these air samples represent both day- and nighttime conditions.

3.2.3 Surface CO_2 observations

Surface CO_2 measurements were taken from the LA Megacities (LAM) network at DLA, PAS, IRV, and RIV (Kim et al., 2022). At these sites, CO_2 mole fractions are measured *in situ* on rooftops or towers using cavity ringdown spectrometers. Instrumentation and calibration protocols have been described previously and CO_2 mole fraction measurement uncertainties were estimated to be 0.07 ppm (Verhulst et al., 2017). Only measurements collected between 10:00 to 16:00 local time (Pacific time zone) were used in our analysis to coincide with the timing of XCO_2 observations and plant ^{14}C datasets that only capture daytime conditions.

At BEA and SMM, we measured surface CO_2 using a Picarro G2401 cavity ringdown spectrometer. We set the sampling inlet approximately 3 m above the ground by attaching the tubing to the top of a canopy tent. To calibrate our measurements, we measured two NOAA standard compressed gas cylinders with known CO_2 mole fractions (410.4 to 507.0 ppm) matched to the WMO 2007 CO_2 scale. We then scaled our data based on the linear relationship between the measured and known CO_2 mole fractions. The correction

had a slope of 1.018 and a y-intercept of -2.7 ppm. Based on the standard deviation of the calibration measurements, the Picarro G2401 had a CO_2 measurement precision of 0.5 ppm. It is important to note that the sampling height at BEA and SMM was much lower than at the LAM sites (10-50 m), which is likely to result in different CO_2 mole fractions.

3.2.4 Total Column CO_2 (XCO_2) measurements

We measured the total atmospheric column averaged dry air mole fraction of CO_2 (XCO_2) using a portable sun-tracking Fourier transform infrared spectrometer (EM27/SUN, Bruker, Billerica, USA). Each site was visited at least twice during each campaign to gauge day-to-day variability. The EM27/SUN measures solar radiation in the near infrared wavelengths where CO_2 has known absorbance signatures. The instrument records solar interferograms approximately every eleven seconds. We also collected coinciding surface pressure measurements that are needed for XCO_2 retrievals using a portable ZENO weather station (Campbell Scientific, Logan, USA). Using the GGG2020 retrieval algorithm, the interferograms were subsequently transformed into spectra and XCO_2 values were calculated by fitting the observed spectra and forward-modeled solar spectra that are based on a priori vertical CO_2 profiles (Laughner et al., 2023; Wunch et al., 2015). These retrievals are automated for EM27/SUN measurements in the EGI software suite (Hedelius et al., 2016). The stability and measurement capabilities of EM27/SUN spectrometers are well documented in existing literature (Chen et al., 2016; Dietrich et al., 2021; Gisi et al., 2012; Hedelius et al., 2016).

For each sampling campaign, we calibrated our XCO_2 measurements against the PAS TCCON, which is maintained to a high measurement standard of 0.2% precision for CO_2 mole fractions, or a 0.8 ppm 2σ uncertainty for a single measurement (Wunch et al., 2010). We applied a correction to our data based on the slope of a linear fit forced through the origin between 10-minute averaged EM27 and TCCON measurements collected side by side, as done in previous work (Hedelius et al., 2016; Frausto-Vicencio et al., 2022). We found strong agreement between the EM27 and TCCON, with an R^2 value greater than 0.99 across all our measurements (Fig. C6). The slopes of the seasonal linear fits were applied as scaling factors

to correct the XCO_2 data from the EM27/SUN to the TCCON. The XCO_2 scaling factors were 1.0018, 1.0022, and 1.0022 in spring, summer and fall 2022, respectively and 1.0016 in winter 2023.

We considered whether our measurements were influenced by wildfire CO_2 emissions that may have been transported over long distances. Daily satellite imagery from MODIS suggests that we did not intercept any smoke plumes (Appendix C). Thus, the main contributors to variations in our XCO_2 enhancements are urban emissions, biospheric fluxes within the LA region, and the effects of advection and boundary layer dynamics.

3.2.5 Estimating the CO_2 background

Surface CO_2 background

Urban CO_2 enhancements (C_{xs}) were calculated by subtracting a background from the surface CO_2 observations (C_{obs}) as follows [Eq. 3.4]:

$$C_{xs} = C_{obs} - C_{bg} \quad \text{Eq. 3.4}$$

All values are in units of ppm. We calculate C_{bg} as the average daytime (10:00 to 16:00 local time) CO_2 mole fraction at a chosen background site. The choice of background site depends on prevailing wind conditions which vary seasonally. In LA, on-shore winds from the Pacific Ocean prevail during spring and summer, and periodic off-shore winds from the desert northeast of LA occur during fall and winter (Verhulst et al., 2017; Kim et al., 2023). Thus, we use either San Clemente Island (SCI) or Victorville (VIC) as the background site depending on wind flow and data availability (Table 3.1, Fig. 3.1).

We found that SCI was an adequate background site for most of the year (May to Dec). SCI had consistently stable and relatively low CO_2 mole fractions in these months, with average daily values (± SD) of 423.2 ± 1.1 ppm and 414.8 ± 2.0 ppm for the days in which we measured in the spring (May 2022) and summer (Jul to Aug, 2022), respectively. For Nov to Dec, CO_2 mole fractions at SCI were more variable, averaging (± SD) 423.7 ± 2.8 ppm, potentially because of episodic reversal of wind patterns. Although VIC could be a more suitable background site for some of these days, data was either not available or had average

CO_2 levels 2-7 ppm higher than SCI. Thus, we use SCI as the background for fall measurements, except on Nov 18 and 23 when VIC data was available and observed 1-6 ppm lower CO_2 values than SCI. For winter measurements (Feb to March), we used VIC to represent the background, resulting in an average daily background of 426.7 ± 1.8 ppm. There was no data available for either SCI or VIC from March 7, 9, 24 or 28 so we interpolated neighboring daily VIC averages to represent the background on those days, resulting in a mean C_{bg} of 426.5 ± 4.0 ppm.

XCO_2 background

To estimate urban XCO_2 enhancements, we subtract a background from our XCO_2 observations as follows [Eq. 3.5]:

$$\Delta XCO_2 = XCO_2 - XCO_{2bg} \qquad \text{Eq. 3.5}$$

We use a daily-varying background based on XCO_2 measurements collected at the AFRC TCCON site, located in a remote location in the Mojave Desert approximately 100 km north of LA (Table 3.1, Fig. 3.1). The applicability of AFRC as an XCO_2 background site relies on the diurnal mixed layer dynamics in the air basin. XCO_2 at the PAS TCCON site is similar to AFRC in the mornings but becomes enhanced in the afternoons when emissions have accumulated within the LA basin's surface mixed layer which is trapped by the surrounding mountains. By midday, XCO_2 values in PAS are typically enhanced by 2.3 ± 1.2 ppm relative to AFRC (Hedelius et al., 2017, 2018). Eventually the mixed layer height increases enough to allow the trapped, polluted air to flow out over the mountains and XCO_2 levels in PAS become similar to the free troposphere and at AFRC. To focus on the peak daily XCO_2 enhancement, we only use EM27/SUN measurements recorded between 12:00 to 15:00 (local time), when the differences between PAS and AFRC are most prominent.

3.3 Results and Discussion

3.3.1 Spatiotemporal Patterns of CO_2

Plant ^{14}C generally increased from DLA to PAS, RIV, IRV, and BEA respectively, capturing the expected urban to rural spatial gradient of $ffCO_2$ (Fig. 3.2a). For all the samples analyzed, mean $\Delta^{14}C$ values (± SD) were -53 ± 12‰ in DLA, -47 ± 7‰ in PAS, -31 ± 5‰ in RIV, -26 ± 9‰ in IRV, and -22 ± 5‰ in BEA. More negative values correspond to more $ffCO_2$ polluted air. For reference, the average ambient $\Delta^{14}CO_2$ observed at Utqiagvik, AK during the study period was -7 ± 2‰, which represents the ^{14}C background in a remote site with no local fossil fuel influence. We also compared against air $\Delta^{14}CO_2$ measurements at IRV which averaged -29 ± 12‰ over the study period in agreement with the IRV mean plant ^{14}C data.

The observed plant $\Delta^{14}C$ values translate into fossil fuel enhancements (C_{ff}, Eq. 3.3) of 2 to 26 ppm (Fig. C1). C_{ff} values generally decreased along the urban to rural gradient, with mean C_{ff} of 17 ± 6 ppm in DLA, 15 ± 3 ppm in PAS, 7 ± 2 ppm in RIV, 5 ± 4 ppm in IRV, and 3 ± 3 ppm in BEA, averaging across seasons. The lowest C_{ff} was observed in the rural site (BEA) for all seasons except summer when IRV was more enriched in ^{14}C. This is likely due to IRV's coastal location and strong onshore winds in the summer that transport its $ffCO_2$ emissions inland.

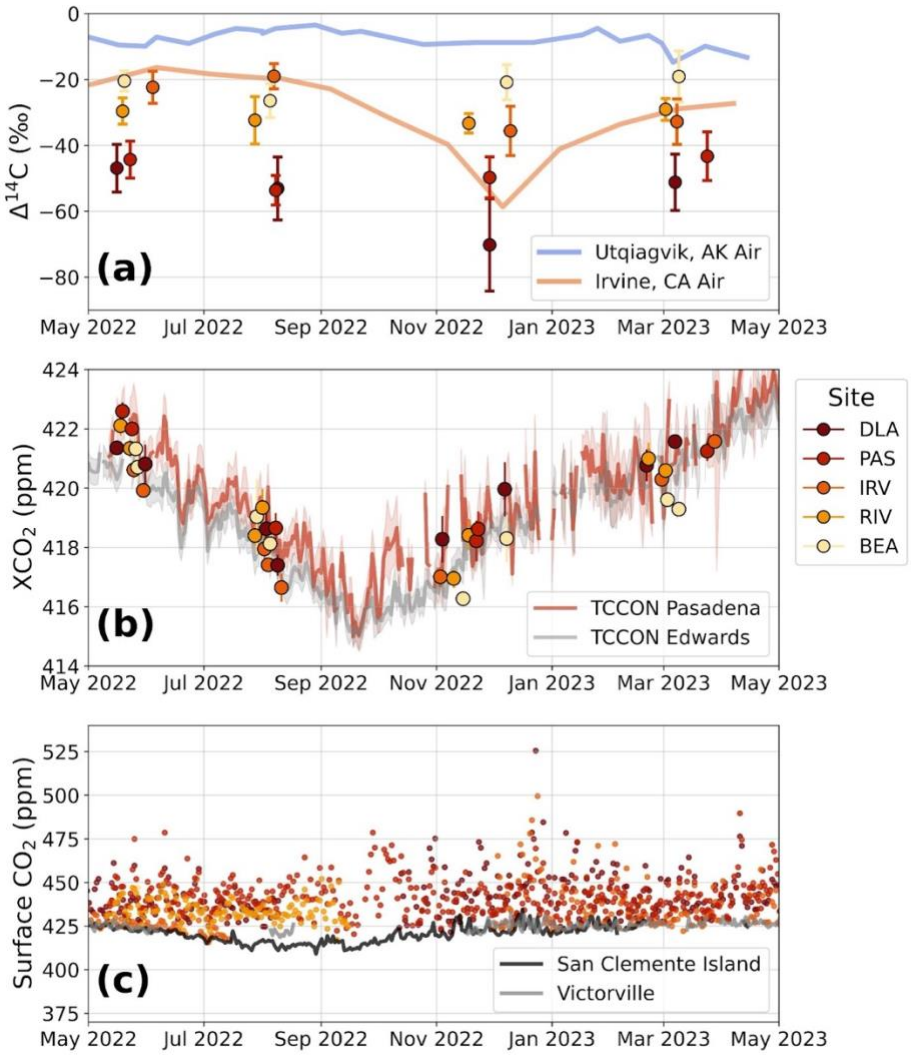

Figure 3.2. Temporal trends in $\Delta^{14}C$, XCO_2 and surface CO_2 measurements collected in and around the Los Angeles area. (a) Points are plant $\Delta^{14}C$ observations averaged and colored by site. Lines are ambient $\Delta^{14}CO_2$ measurements from air samples collected in Utqiagvik, AK (gray) and Irvine, CA (orange). (b) Points are daily-averaged XCO_2 observations colored by site, with error bars representing the daily standard deviation. Orange and black lines are daily-averaged XCO_2 observations from the TCCON PAS and AFRC sites, respectively. (c) Points are daytime (10:00 – 16:00 PT), daily-averaged surface CO_2 measurements colored by site. Lines are daytime daily-averaged surface CO_2 measurements at SCI and VIC background sites.

The seasonal differences between the plant $\Delta^{14}C$ observations, up to ~15‰, were dwarfed by the spatial differences, up to 50‰ (Fig. 3.2a). The seasonal mean $\Delta^{14}C$ (±SD) for all the samples taken together was -35 ± 12‰ in spring, -39 ± 16‰ in summer, -45 ± 18‰ in fall and -47 ± 12‰ in winter. Thus, the seasonal means are not significantly different. Previous studies have determined that seasonal changes in

$ffCO_2$ emissions are minor in LA, and that intra-annual differences in ambient $\Delta^{14}CO_2$ are primarily due to changing atmospheric dynamics (wind speeds and directions and planetary boundary layer height) that facilitate more trapping of $ffCO_2$ emissions (Hedelius et al., 2018; Miller et al., 2020; Newman et al., 2016). Thus, the lack of temporal variability in plant ^{14}C indicates that $ffCO_2$ patterns do not change substantially within the course of the year.

Across the study period, the lowest $\Delta^{14}C$ values (highest C_{ff}) were generally observed during Nov to Dec, especially at DLA, which is near many $ffCO_2$ emission sources. During the fall and winter (Nov to Feb), cooler temperatures and shorter days reduce the mixed layer height, trapping (^{14}C-depleted) emissions in the basin. This is exemplified by the air-based $\Delta^{14}CO_2$ measurements in IRV (Fig. 3.2a), which showed a sharp decline in Dec. However, we did not observe the same effect in the IRV plant samples, because plants do not capture CO_2 overnight when (^{14}C-depleted) CO_2 concentrations are most elevated. This suggests that temporal variability in plant ^{14}C is less sensitive to meteorological changes than to persistent local emission sources.

Generally, the XCO_2 and surface CO_2 observations also captured the expected urban to rural spatial gradient; however, the site-to-site differences were not as pronounced as those observed in the plant ^{14}C data. Daily daytime averages ranged from 416 to 526 ppm for surface CO_2 and 416 to 422 ppm for XCO_2. Surface CO_2 and XCO_2 measurements have a much larger sampling footprint than the plants, and thus, they are not as sensitive to fine scale (~100 m) variability like the plant samples. However, unlike plant ^{14}C, temporal variability (from daily to seasonal) in atmospheric CO_2 was considerably larger than the differences between sites (Fig. 3.2 b-c).

The different temporal variability between plant ^{14}C, surface CO_2, and XCO_2 is expected due to the different spatiotemporal characteristics inherent to each measurement. The maximum $ffCO_2$ contribution was observed in November based on plant ^{14}C, whereas the maximum excess XCO_2 occurred in May for all sites and was more randomly distributed in the surface CO_2 data. Surface CO_2 changes were noisier than $\Delta^{14}C$ and XCO_2 measurements, which made seasonality less prominent. This is expected because surface CO_2 measurements commonly intercept sporadic CO_2 plumes from local emissions that overpower

fluctuations in the background. Since the XCO_2 measurements incorporate CO_2 in the entire atmospheric column, local emissions at the surface are diluted and the overall signal is dominated by seasonality that is driven by meteorology and/or natural fluxes at the regional scale. As such, our data highlight an advantage of the temporally integrative nature of plants: their ^{14}C is more sensitive to local emissions than XCO_2 measurements while being less noisy than surface CO_2. This indicates that plant ^{14}C coupled with surface CO_2 and/or XCO_2 observations can serve complementary purposes since the atmospheric CO_2 measurements can better capture temporal variations while plant ^{14}C sampling can better capture local scale $ffCO_2$ patterns within a city or neighborhood.

3.3.2 Correlations between $ffCO_2$ metrics

By subtracting a background from the measurements presented in Fig. 3.2, we calculate first-order estimates of $ffCO_2$ patterns. Specifically, we use equations [Eq. 3.3 – 3.5] to estimate the urban enhancements of each $ffCO_2$ metric (i.e., plant ^{14}C, surface CO_2, and XCO_2). We treat each metric separately and assume we only have the plant ^{14}C, surface CO_2, or XCO_2 measurements and an estimate of the background for each. We consider these "first order" estimates because we neglect biospheric terms in order to make each equation solvable independently (i.e., so that plant C_{ff} can be solved without C_{obs} from the surface network). To calculate surface C_{xs}, we calculate the two-week average of the daily afternoon (12:00 to 15:00 local time) measurements. We use two-week averages to coincide with the time period that we expect the turfgrasses were integrating CO_2. Since the XCO_2 dataset is not continuous, we could not take two-week averages and instead aggregated the measurement days by site and season. Here, we only use XCO_2 measurements collected in the afternoon (12:00 to 15:00 local time), when the mixed layer is most developed and consequently when the XCO_2 average at the AFRC TCCON is the most representative of background conditions.

We then examine the relationship between each of these metrics (Fig. 3.3). Plant C_{ff} had a significant linear relationship with both surface CO_{2xs} and ΔXCO_2. This suggests that plant ^{14}C data can independently provide similar information as surface *in situ* CO_2 networks and has potential for validating

spatiotemporal XCO_2 trends in cities. These correlations indicate that despite their differences in spatiotemporal resolutions, plant C_{ff}, surface CO_{2xs}, and ΔXCO_2 all capture intra-region $ffCO_2$ emission patterns.

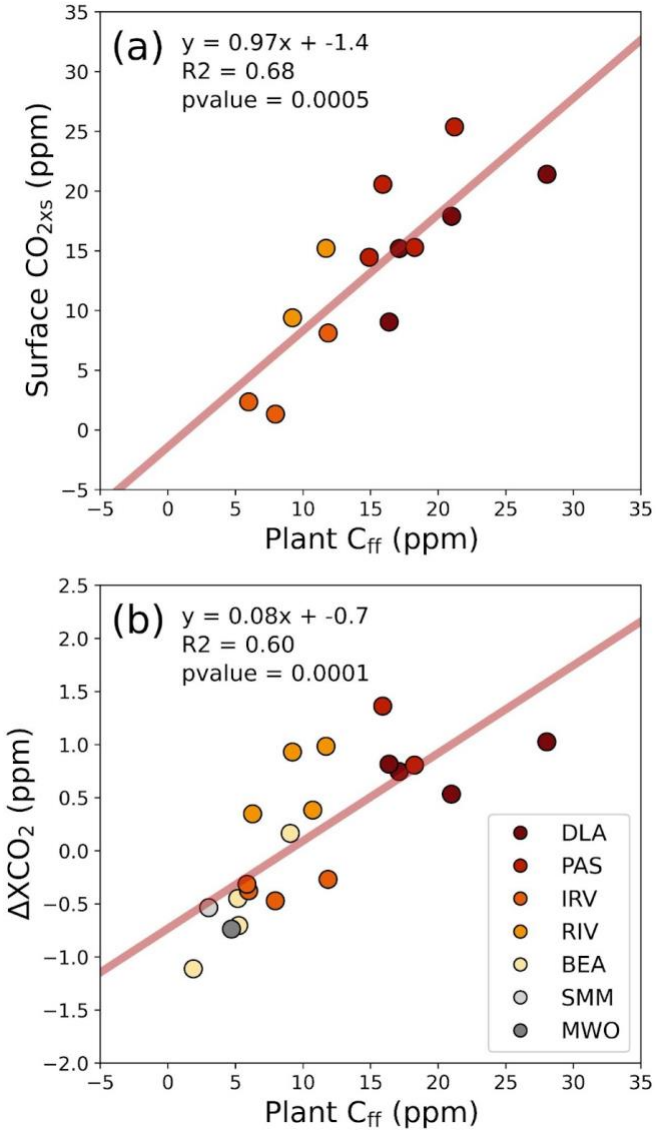

Figure 3.3. Correlations between plant fossil fuel enhancements derived from ^{14}C analysis ("Plant C_{ff}") and (a) excess surface CO_2 based on in situ measurements collected on rooftops/towers ("Surface CO_{2xs}") and (b) total column CO_2 enhancements (ΔXCO_2) based on ground-based solar spectra measurements. The colors of the points indicate the site, with darker red colors representing more urbanized sites.

Although these urban emission metrics were correlated, they each inform emissions characterizations with distinct sensitivity. Plant C_{ff} and surface CO_{2xs} are similar, with their values ranging

from 0 to 30 ppm (Fig. 3.3a). Therefore, plant ^{14}C sampling can create snapshots of surface $ffCO_2$ in cities that lack surface CO_2 networks or possibly supplement unmeasured locations in places that do have a ground network. ΔXCO_2 is a more diluted signal than the other two metrics, with the resulting values ranging by only about 2 ppm (-1.5 to 1.5 ppm, Fig. 3.3b). The uncertainty of the ΔXCO_2 values is at least 1.4 ppm, based on the root squared sum of the measurement uncertainties (1 ppm each from the EM27/SUN and TCCON AFRC). Thus, the $ffCO_2$ signal is relatively low for XCO_2 measurements relative to its uncertainty and poses a challenge for intra-city $ffCO_2$ monitoring using total column measurements. Among these three metrics, plant sampling is the most operationally feasible since the plants are highly sensitive to local $ffCO_2$ emissions, enabling monitoring at higher spatial resolution than surface CO_2 or XCO_2 measurements without the need for any infrastructure or instrumentation at the study site.

3.3.3 Source attribution using plant ^{14}C

In the previous section, we examined the use of plant ^{14}C to quantify $ffCO_2$ emission trends independently (without relying on atmospheric CO_2 observations at the study site). When both ^{14}C and CO_2 measurements are available at the same location and time, it becomes possible to apportion the biogenic and fossil contributions to the observed CO_2 signal. Previous work has estimated that biosphere fluxes can contribute approximately 25% of the annual C_{ff} enhancement in LA (Miller et al., 2020). Here, we consider the C_{bio} terms in the mass balance equations and solve them using the surface CO_2 measurements as C_{obs}, thereby allowing the surface CO_2 network to inform the plant ^{14}C analysis. Following the isotopic mixing analysis in Miller et al. (2020), we estimate the Δ_{source} of LA's emissions by rearranging the mass balance equations (Appendix C), which can subsequently be used to estimate the percentage of fossil and biospheric contributions [Eq. 3.6]:

$$\Delta_{source} = f_{ff}\,\Delta_{ff} + f_{bio}\,\Delta_{bio} \qquad \text{Eq. 3.6}$$

where f_{ff} is the fossil fraction, f_{bio} is the biospheric fraction, Δ_{ff} is the known fossil fuel $\Delta^{14}C$ signature of -1000‰, and Δ_{bio} is the biospheric $\Delta^{14}C$ signature. We assume Δ_{bio} is equal to the mean Δ_{obs} since plants up take ambient $\Delta^{14}CO_2$. Then, Δ_{source} is determined as the slope of a York linear regression

between $(\Delta \times C)_{xs}$ and C_{xs} (Fig. 3.4), based on a rearranging of the mass balance equations (Eq. 3.1 – 3.2; Appendix C). If Δ_{source} equals -1000‰ (the fossil fuel ^{14}C signature), this would indicate that fossil fuels are the only source of C_{xs}, and that biospheric fluxes are negligible. It is important to note that we expect the fossil fuel ^{14}C signature to be closer to -933‰ (not -1000‰) due to requirements that biogenic ethanol be blended into gasoline in California (Newman et al., 2016). For C_{obs}, we used the afternoon average of the surface CO_2 observations for the two weeks before the samples were collected at each site, to represent the expected temporal integration of turfgrass ^{14}C samples.

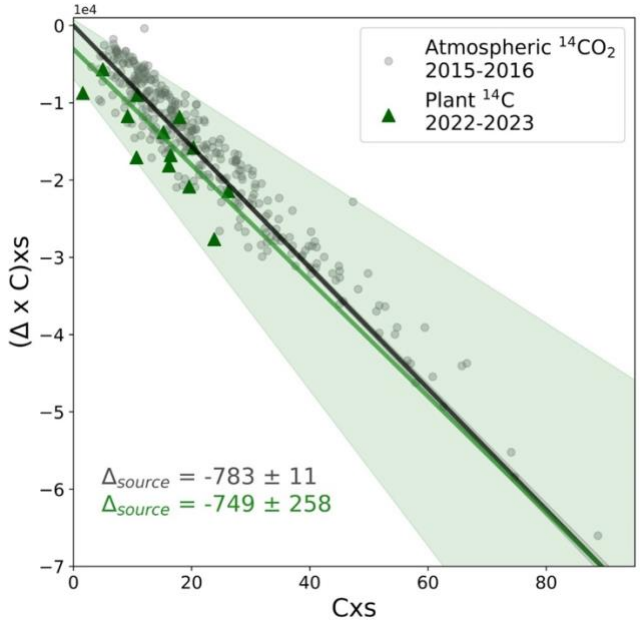

Figure 3.4. Isotopic mixing analysis used to determine Δ_{source}, following the same protocol as in Miller et al. (2020). Green triangles are calculated from plant $\Delta^{14}C$ and in situ CO_2 measurements aggregated by site and season (including DLA, PAS, IRV, and RIV). Gray points are measurements made by Miller et al. (2020) at three sites in LA using flask analysis of air $\Delta^{14}CO_2$ and CO_2 in 2015-2016. The linear fits were calculated using a York regression method (York et al., 2004), which considers the error in both x and y. The slope of the fit line (Δ_{source}) and its uncertainty for each dataset is shown on the lower left, with the green line/slope calculated based on the plant ^{14}C data and the black line/slope was calculated using air $^{14}CO_2$ data from Miller et al. (2020).

Using our turfgrass ^{14}C and CO_2 measurements averaged by site and season, we estimate Δ_{source} is -749 ± 258‰, which is similar to the results in Miller et al. (2020) (-783 ± 11‰), albeit with a much larger uncertainty (Fig. 3.4). Based on Δ_{source} derived from plant ^{14}C and assuming Δ_{ff} is -1000‰, we estimate C_{xs} fractions from fossil and biogenic sources of 74% and 26%, respectively. If we instead assume the fossil

fuel ^{14}C signature is -933‰ due to ethanol in gasoline, we calculate that 79% of the CO_2 enhancement is due to fossil fuels and 21% from the biosphere. This corresponds with Miller et al.'s finding that in LA, the fossil and biogenic fractions of C_{xs} are approximately 80% and 20%, respectively. This indicates that isotopic mixing analyses using urban plant samples can achieve similar results as air-based $\Delta^{14}CO_2$ measurements with larger uncertainty but less effort. The largest source of uncertainty in our Δ_{source} slope calculated with plant ^{14}C samples is the variability in C_{obs} over the two-week averaging period. We used the standard deviation of the daily afternoon means for two-weeks of data to represent the uncertainty of each C_{xs} value. This uncertainty is quite large (7 ppm on average), since C_{xs} varies substantially at two-week timescales at urban sites. In contrast, the uncertainty in C_{xs} for the air samples used in the Miller et al. analysis was only 0.9 ppm on average, based on the measurement uncertainty of flask CO_2 samples and the background. Thus, our uncertainty is larger because it considers atmospheric variability over a much longer temporal period than Miller et al.'s flask samples (two weeks vs minutes, respectively). Nonetheless, the overall results were still comparable, indicating that plants can trace $ffCO_2$ patterns and achieve similar results as atmospheric ^{14}C measurements.

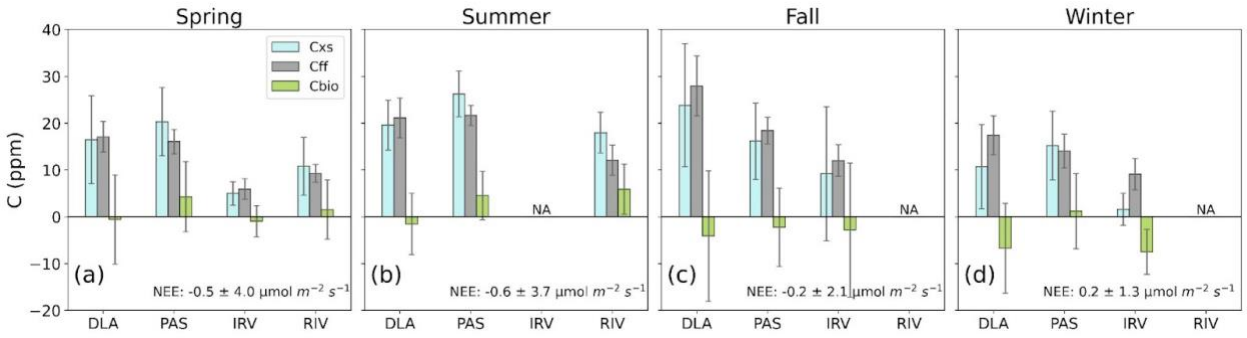

Figure 3.5. Source attribution of C_{xs} to C_{ff} and C_{bio} for each site in (a) spring, (b) summer, (c) fall and (d) winter. Bars represent the average C_{xs} (blue), C_{ff} (gray), and C_{bio} (green) for a site and season. Uncertainty is calculated using a Monte Carlo simulation described in Appendix C. Sites with "NA" indicate that surface CO_2 observations were not available for the calculation. The net ecosystem exchange (NEE) estimates were provided by the Solar Induced Fluorescence for Urban biogenic Fluxes (SMUrF) model (Wu et al., 2021). Hourly NEE estimates from SMUrF were averaged for the LA Basin region on a monthly basis for the most recent year available (2019), specifically, May, August, November, and March for spring, summer, fall, and winter, respectively.

Lastly, we calculate C_{xs}, C_{ff} and C_{bio} on a sample-by-sample basis and aggregate by site and season (Fig. 3.5). Our findings indicate that the majority of C_{xs} (70-100%) is attributable to $ffCO_2$ emissions. The error bars for C_{xs} and C_{ff} overlap, making them proxies for one another. Biospheric fluxes contribute a notable amount of the C_{xs} (on average 24% of the fossil fuel enhancement) but vary by site and season. It is important to note that the uncertainty in C_{bio} is large (larger than its magnitude), which propagates from the variability in C_{xs}. C_{bio} does not appear to have consistent spatial patterns between the sites. Generally, we observe that C_{bio} is a larger C sink in the fall and winter compared to the spring and summer. We compared our findings to modeled estimates of hourly net ecosystem exchange (NEE) from the Solar Induced Fluorescence for Urban Biogenic Fluxes (SMUrF) model (Wu & Lin, 2021; Wu et al., 2021), where positive NEE values indicate net emissions of CO_2 from biospheric sources (positive C_{bio}), while negative values indicate net CO_2 uptake from the biosphere (negative C_{bio}). On average over the LA region, NEE is estimated to be slightly negative (-0.6 to -0.2 μmol m^2 s^{-1}) during our study months, except in March (winter; Fig. 3.5d). Our ^{14}C analysis and SMUrF modeled NEE indicate that LA's biospheric fluxes are small with large uncertainty. Further analysis of plant ^{14}C and direct flux measurements along biogenic flux

gradients could help better understand urban biosphere fluxes and be impactful for guiding nature-based climate change solutions in cities.

3.4 Conclusions

Our analysis demonstrates that plant ^{14}C is a powerful tool for monitoring $ffCO_2$ emissions and supporting climate change mitigation efforts in cities. Compared to atmospheric measurements of surface CO_2 and XCO_2, plants offer the most localized $ffCO_2$ signal, making it possible to investigate urban emissions at high spatial resolution. We show that plant ^{14}C can provide insight to $ffCO_2$ sources in cities that lack surface CO_2 observing infrastructure and may help ground-truth spatiotemporal trends in XCO_2 observed by satellites, which struggle with quantifying $ffCO_2$ patterns at the local scale. In cities with ongoing surface CO_2 measurements, plant ^{14}C also offers similar insights to biogenic CO_2 sources as atmospheric $^{14}CO_2$ sampling at a fraction of the cost. However, more work is needed to understand spatiotemporal variations in urban biogenic fluxes and to guide nature-based climate solutions.

CONCLUSIONS

Summary of this work

The goal of this dissertation was to quantify spatial and temporal trends in air pollutant and $ffCO_2$ emissions in cities. The research was motivated by the pressing need to inform policymakers on the effectiveness of fossil fuel emission mitigation measures. In Chapter 1, I evaluated the progress of efforts intended to reduce carbon monoxide (CO) emissions from vehicles. I compared on-road CO/CO_2 levels measured with mobile laboratories in two cities (Los Angeles, CA and Salt Lake City, UT) across years between 2013 to 2021. The observations indicated that stringent regulations and advances in cleaner burning technology have effectively improved the vehicle combustion efficiency in Los Angeles between 2013 and 2019. However, combustion efficiency worsened in 2020 when traffic characteristics and fleet characteristics were drastically altered by the COVID-19 pandemic. Additionally, in Salt Lake City, combustion efficiency worsened between 2013 and 2019. These findings indicate that regulatory efforts to reduce vehicle CO emissions can be offset by less efficient traffic characteristics, such as aggressive driving styles and a less efficient fleet.

In Chapter 2, I demonstrated that plant radiocarbon (^{14}C) sampling captured $ffCO_2$ emission reductions associated with a drastic reduction in human activity during the COVID-19 pandemic. Analysis of plant ^{14}C samples collected in California revealed temporal $ffCO_2$ emission trends across years that aligned with the timing of social distancing measures. Further, plant ^{14}C indicated that emission trends varied at the neighborhood scale, with some communities maintaining emission reductions longer than others. The pandemic served as an analogy for a large-scale emissions reduction that we would expect to see over time with effective emission mitigation policies. The observed sensitivity of plant ^{14}C to changes in human activity implies that plant sampling can be an informative technique to gauge the success of climate action policies, especially in cities that lack operational CO_2 monitoring infrastructure.

In Chapter 3, I evaluated plant ^{14}C as an indicator of $ffCO_2$ trends against more established urban monitoring approaches: *in situ* surface CO_2 and remotely sensed total column CO_2 (XCO_2). I measured plant ^{14}C, surface CO_2, and XCO_2 along an urban to rural gradient in Southern California in three-month intervals for one year. Plant ^{14}C captured the strongest spatial contrast in CO_2 between the sites, advantaged by its sensitivity at local spatial scales. The plants did not indicate significant temporal changes in $ffCO_2$ within the year of measurements. Surface CO_2 and XCO_2 captured stronger temporal variability than the plants, but this variability was more likely because of meteorology and seasonality of natural CO_2 fluxes, not $ffCO_2$ emissions. Furthermore, mixing analysis combining the ^{14}C and surface CO_2 measurements revealed that biogenic CO_2 fluxes, such as from urban vegetation, respiration, and biofuel burning, contribute a notable but uncertain amount of excess CO_2. This research further strengthened the application of plant ^{14}C as an urban $ffCO_2$ monitoring technique since the observations showed that plants could provide similar information as other monitoring approaches but with higher spatial resolution.

Together, these three studies indicate that our capacity to monitor urban $ffCO_2$ trends is improving. My research suggests effective and detectable emission reductions regarding CO emissions from the on-road sector and $ffCO_2$ emissions during the COVID-19 pandemic. This work also uncovered ongoing complexities in reducing and monitoring emissions, such as the interplay of factors like traffic characteristics that can counter progress. Additionally, he heterogeneity of emission trends at highly local scales underscores the need for high resolution environmental measurements. This work can be used to support the implementation of practical $ffCO_2$ monitoring approaches in cities, such as plant ^{14}C analysis. All in all, this dissertation advanced our capacity to track urban $ffCO_2$ emission trends, enabling new opportunities for accessible and effective $ffCO_2$ information for future scientists, community members, and policy makers.

Future directions

As climate action policies take effect, large spatiotemporal changes in $ffCO_2$ emissions are anticipated over time. Through the investigations in this dissertation, I learned valuable lessons for most

effectively capturing these trends using atmospheric observations and supporting the success of emission mitigation efforts. Numerous opportunities remain to further extend this research and to continue improving quantification of urban $ffCO_2$ emissions.

On-road emissions. Chapter 1 revealed the complexity of vehicle combustion efficiency and how on-road CO emission reductions can be confounded by traffic characteristics and changes to the fleet characterization. The ongoing mystery that our dataset could not explicitly answer is what specifically caused those increases in CO/CO_2. We observed the net effect of policies, technology, and traffic conditions, but further measurements or modeling would be needed to detangle the drivers that led to the increased CO/CO_2. The worsened combustion efficiency during COVID-19 also contradicted EMFAC, California's official on-road emissions inventory that is used for mobile source regulations. Thus, additional work to better understand this could have major implications for the inventory and could lead to new recommendations for traffic regulations. The impacts of speed on CO/CO_2 were particularly complex. It would be beneficial to compare on-road measurements with a mobile laboratory like UCR's LIME/AVOCADO to emissions tests conducted with portable emission measurement systems that are installed on individual vehicles. The advantages of each approach would be complimentary and could elucidate the causes of high CO emissions under different driving conditions.

The observations in Chapter 1 also indicated that the application of the CO/CO_2 ratio as a fossil fuel tracer is weakening as vehicle combustion efficiency is improved. This finding could be further tested using radiocarbon measurements of vehicle exhaust emissions. Coinciding measurements of on-road CO, CO_2, and $^{14}CO_2$ would provide useful information about vehicle fuel, combustion efficiency, and inform mixing models of urban emissions. Up-to-date estimates of the $CO:CO_{2ff}$ ratio based on ^{14}C would allow studies using urban CO_2 measurements to attribute emissions from the transportation sector.

Plant ^{14}C Analysis: This work demonstrated that plant ^{14}C analysis is a robust tracer for spatial and temporal variations in $ffCO_2$ emissions in cities. By setting up that foundation, this work supports the application of such analyses for future urban $ffCO_2$ monitoring in new places and repeating periodically in the same places to track progress. Most of this work was conducted in the Los Angeles megacity, one of

the most equipped cities in the world for monitoring $ffCO_2$ emissions. Further research should now consider other cities that have less access to high quality datasets. For instance, many cities in the Global South are increasing $ffCO_2$ emissions with economic development. Although satellite measurements are expected to increase spatial coverage of XCO_2 data, many cities lack operational ground-truthing infrastructure to validate the trends observed remotely. As we observed in Chapter 3, plant-based CO_2 enhancements correlate with XCO_2 enhancements, indicating the potential of plants to cost-effectively validate CO_2 patterns observed by satellites. In such cities where emissions are expected to increase but there is a lack of existing data, it is particularly crucial to collect records now to set a baseline that we can evaluate emission reductions against in the future. We cannot go back in time to collect atmospheric data so plants are additionally useful because they can even be stored (i.e., in a herbarium) and analyzed later (Carbone et al., 2023).

The local scale sensitivity of plant ^{14}C analysis is currently an under-utilized advantage for urban $ffCO_2$ monitoring. In this work, we aggregated our plant sampling to regional scales, and only focused in on the hyperlocal information in a few cases (e.g., the Great Highway in Chapter 2). However, future work could repeat sample plants near a known emission source that is expected to be decarbonizing and track its emission reductions over time. For example, plants could be periodically collected next to a highway, and they would likely detect $ffCO_2$ reductions as more electric vehicles replace gasoline and diesel fueled vehicles. Additionally, the City of Los Angeles announced a goal for all buildings to have net zero emissions by 2050, and thus will be removing gas-powered appliances from residential and commercial buildings. Plant sampling could be used to track this progress, and to identify highest emitting buildings to prioritize. These are exciting opportunities to partner with community members and create clear demonstrations that could guide future policymaking.

Another important direction is using plant ^{14}C analysis to elucidate heterogeneity in $ffCO_2$ emissions at the census tract scale. Fossil fuel CO_2 emissions are usually co-emitted with emissions of hazardous air pollutants like CO, NO_x, and particulate matter, that are often harder to attribute their sources and interpret their measurements. Surveying plants in communities with racial or income-based disparities

could bring to light environmental injustice that should be considered when developing climate mitigation policy. Such projects can include community science opportunities that could empower historically marginalized communities by engaging them in monitoring their own air quality. This high-resolution tracking could inform on fine-scale disparities to air pollution exposure in urban areas and whether emission benefits of air pollution regulations are equitably distributed.

REFERENCES

Alessio, M., Anselmi, S., Conforto, L., Improta, S., Manes, F., & Manfra, L. (2002). Radiocarbon as a biomarker of urban pollution in leaves of evergreen species sampled in Rome and in rural areas (Lazio—Central Italy). *Atmospheric Environment*, *36*(34), 5405–5416. https://doi.org/10.1016/S1352-2310(02)00409-0

Ammoura, L., Xueref-Remy, I., Gros, V., Baudic, A., Bonsang, B., Petit, J.-E., Perrussel, O., Bonnaire, N., Sciare, J., & Chevallier, F. (2014). Atmospheric measurements of ratios between CO2 and co-emitted species from traffic: a tunnel study in the Paris megacity. *Atmospheric Chemistry and Physics*, *14*(23), 12871–12882. https://doi.org/10.5194/acp-14-12871-2014

Apte, J. S., Messier, K. P., Gani, S., Brauer, M., Kirchstetter, T. W., Lunden, M. M., Marshall, J. D., Portier, C. J., Vermeulen, R. C. H., & Hamburg, S. P. (2017). High-Resolution Air Pollution Mapping with Google Street View Cars: Exploiting Big Data. *Environmental Science & Technology*, *51*(12), 6999–7008. https://doi.org/10.1021/acs.est.7b00891

Archer, D., Eby, M., Brovkin, V., Ridgwell, A., Cao, L., Mikolajewicz, U., Caldeira, K., Matsumoto, K., Munhoven, G., Montenegro, A., & Tokos, K. (2009). *Atmospheric Lifetime of Fossil Fuel Carbon Dioxide*. https://doi.org/10.1146/annurev.earth.031208.100206

Baker, C. J. (1996). Outline of a novel method for the prediction of atmospheric pollution dispersal from road vehicles. *Journal of Wind Engineering and Industrial Aerodynamics*, *65*(1), 395–404. https://doi.org/10.1016/S0167-6105(97)00058-5

Bares, R., Lin, J. C., Hoch, S. W., Baasandorj, M., Mendoza, D. L., Fasoli, B., Mitchell, L., Catharine, D., & Stephens, B. B. (2018). The wintertime covariation of CO 2 and criteria pollutants in an urban valley of the western United States. *Journal of Geophysical Research*, *123*(5), 2684–2703. https://doi.org/10.1002/2017jd027917

Bares, R., Mitchell, L., Fasoli, B., Bowling, D. R., Catharine, D., Garcia, M., Eng, B., Ehleringer, J., & Lin, J. C. (2019). The Utah urban carbon dioxide (UUCON) and Uintah Basin greenhouse gas networks: instrumentation, data, and measurement uncertainty. *Earth System Science Data*, *11*(3), 1291–1308. https://doi.org/10.5194/essd-11-1291-2019

Basu, S., Lehman, S. J., Miller, J. B., Andrews, A. E., Sweeney, C., Gurney, K. R., Xu, X., Southon, J., & Tans, P. P. (2020). Estimating US fossil fuel CO_2 emissions from measurements of ^{14}C in atmospheric CO_2. *Proceedings of the National Academy of Sciences of the United States of America*, *117*(24), 13300–13307. https://doi.org/10.1073/pnas.1919032117

Boriboonsomsin, B., & Barth, M. (2008). Real-World CO 2 Impacts of Traffic Congestion. *Transportation Research Record*.

Buchwitz, M., Reuter, M., Noël, S., Bramstedt, K., Schneising, O., Hilker, M., Fuentes Andrade, B., Bovensmann, H., Burrows, J. P., Di Noia, A., Boesch, H., Wu, L., Landgraf, J., Aben, I., Retscher, C., O'Dell, C. W., & Crisp, D. (2021). Can a regional-scale reduction of atmospheric CO_2 during the COVID-19 pandemic be detected from space? A case study for East China using satellite XCO_2 retrievals. *Atmospheric Measurement Techniques*, *14*(3), 2141–2166. https://doi.org/10.5194/amt-14-2141-2021

Bush, S. E., Hopkins, F. M., Randerson, J. T., Lai, C.-T., & Ehleringer, J. R. (2015). Design and application of a mobile ground-based observatory for continuous measurements of atmospheric trace gas and criteria pollutant species. *Atmospheric Measurement Techniques*, *8*(8), 3481–3492. https://doi.org/10.5194/amt-8-3481-2015

California Air Resources Board. (2021). *Emissions Inventory (EMFAC)*. https://arb.ca.gov/emfac/

California Air Resources Board. (2022). *Advanced Clean Cars II*. https://ww2.arb.ca.gov/our-work/programs/advanced-clean-cars-program/advanced-clean-cars-ii

California Air Resources Board. (2023a). *Criteria Pollutant Emission Inventory Data*. https://ww2.arb.ca.gov/criteria-pollutant-emission-inventory-data

California Air Resources Board. (2023b). *Low-Emission Vehicle Regulations & Test Procedures*. https://ww2.arb.ca.gov/our-work/programs/advanced-clean-cars-program/lev-program/low-emission-vehicle-regulations-test

California Department of Transportation. (2023). *Performance Measurement System (PeMS)* [Data set]. https://pems.dot.ca.gov/

California State Government. (2022, February 14). *Essential Workforce*. Covid19.ca.gov. https://covid19.ca.gov/essential-workforce/

Carbone, M. S., Ayers, T. J., Ebert, C. H., Munson, S. M., Schuur, E. A. G., & Richardson, A. D. (2023). ATMOSPHERIC RADIOCARBON FOR THE PERIOD 1910–2021 RECORDED BY ANNUAL PLANTS. *Radiocarbon*, *65*(2), 357–374. https://doi.org/10.1017/RDC.2023.5

Carranza, V., Biggs, B., Meyer, D., Townsend-Small, A., Thiruvenkatachari, R. R., Venkatram, A., Fischer, M. L., & Hopkins, F. M. (2022). Isotopic signatures of methane emissions from dairy farms in California's San Joaquin valley. *Journal of Geophysical Research. Biogeosciences*, *127*(1). https://doi.org/10.1029/2021jg006675

Che, K., Liu, Y., Cai, Z., Yang, D., Wang, H., Ji, D., Yang, Y., & Wang, P. (2022). Characterization of Regional Combustion Efficiency using ΔXCO: ΔXCO2 Observed by a Portable Fourier-Transform Spectrometer at an Urban Site in Beijing. *Advances in Atmospheric Sciences*, *39*(8), 1299–1315. https://doi.org/10.1007/s00376-022-1247-7

Chen, J., Viatte, C., Hedelius, J. K., Jones, T., Franklin, J. E., Parker, H., Gottlieb, E. W., Wennberg, P. O., Dubey, M. K., & Wofsy, S. C. (2016). Differential column measurements using compact solar-tracking spectrometers. *Atmospheric Chemistry and Physics*, *16*(13), 8479–8498. https://doi.org/10.5194/acp-16-8479-2016

Chevallier, F., Zheng, B., Broquet, G., Ciais, P., Liu, Z., Davis, S. J., Deng, Z., Wang, Y., Bréon, F.-M., & O'Dell, C. W. (2020). Local anomalies in the column-averaged dry air mole fractions of carbon dioxide across the globe during the first months of the Coronavirus recession. *Geophysical Research Letters*, *47*(22), e2020GL090244. https://doi.org/10.1029/2020GL090244

Colmer, J., Hardman, I., Shimshack, J., & Voorheis, J. (2020). Disparities in PM2.5 air pollution in the United States. *Science*, *369*(6503), 575–578. https://doi.org/10.1126/science.aaz9353

Control of Air Pollution From Motor Vehicles: Tier 3 Motor Vehicle Emission and Fuel Standards, 79 FR 23413 23413 (2014). https://www.federalregister.gov/documents/2014/04/28/2014-06954/control-of-air-pollution-from-motor-vehicles-tier-3-motor-vehicle-emission-and-fuel-standards

Crippa, M., Guizzardi, D., Pisoni, E., Solazzo, E., Guion, A., Muntean, M., Florczyk, A., Schiavina, M., Melchiorri, M., & Hutfilter, A. F. (2021). Global anthropogenic emissions in urban areas: patterns, trends, and challenges. *Environmental Research Letters*, *16*(7), 074033. https://doi.org/10.1088/1748-9326/ac00e2

Davidson, L. (2014, November 15). Utah set to bump speed limit on urban freeways to 70 mph. *The Salt Lake Tribune*. https://www.sltrib.com/news/politics/2014/11/15/utah-set-to-bump-speed-limit-on-urban-freeways-to-70-mph/

Dietrich, F., Chen, J., Voggenreiter, B., Aigner, P., Nachtigall, N., & Reger, B. (2021). MUCCnet: Munich Urban Carbon Column network. *Atmospheric Measurement Techniques*, *14*(2), 1111–1126. https://doi.org/10.5194/amt-14-1111-2021

Djuricin, S., Pataki, D. E., & Xu, X. (2010). A comparison of tracer methods for quantifying CO_2 sources in an urban region. *Journal of Geophysical Research*, *115*(D11). https://doi.org/10.1029/2009jd012236

Dong, X., Xie, K., & Yang, H. (2022). How did COVID-19 impact driving behaviors and crash Severity? A multigroup structural equation modeling. *Accident; Analysis and Prevention*, *172*, 106687. https://doi.org/10.1016/j.aap.2022.106687

Duren, R. M., & Miller, C. E. (2012). Measuring the carbon emissions of megacities. *Nature Climate Change*, *2*(8), 560–562. https://doi.org/10.1038/nclimate1629

Eldering, A., Taylor, T. E., O'Dell, C. W., & Pavlick, R. (2019). The OCO-3 mission: measurement objectives and expected performance based on 1 year of simulated data. *Atmospheric Measurement Techniques*, *12*(4), 2341–2370. https://doi.org/10.5194/amt-12-2341-2019

Fang, J., Chen, B., Zhang, H., Dilawar, A., Guo, M., Liu, C., Liu, S., Gemechu, T. M., & Zhang, X. (2023). Global Evaluation and Intercomparison of XCO_2 Retrievals from GOSAT, OCO-2, and TANSAT with TCCON. *Remote Sensing*, *15*(20), 5073. https://doi.org/10.3390/rs15205073

Fitzmaurice, H. L., Turner, A. J., Kim, J., Chan, K., Delaria, E. R., Newman, C., Wooldridge, P., & Cohen, R. C. (2022). Assessing vehicle fuel efficiency using a dense network of CO2 observations. *Atmospheric Chemistry and Physics*, *22*(6), 3891–3900. https://doi.org/10.5194/acp-22-3891-2022

Flachsbart, P., & Ott, W. (2019). Trends in passenger exposure to carbon monoxide inside a vehicle on an arterial highway of the San Francisco Peninsula over 30 years: A longitudinal study. *Journal of the Air & Waste Management Association* , *69*(4), 459–477. https://doi.org/10.1080/10962247.2018.1548387

Friedlingstein, P., O'Sullivan, M., Jones, M. W., Andrew, R. M., Gregor, L., Hauck, J., Le Quéré, C., Luijkx, I. T., Olsen, A., Peters, G. P., Peters, W., Pongratz, J., Schwingshackl, C., Sitch, S., Canadell, J. G., Ciais, P., Jackson, R. B., Alin, S. R., Alkama, R., … Zheng, B. (2022). Global carbon budget 2022. *Earth System Science Data*, *14*(11), 4811–4900. https://doi.org/10.5194/essd-14-4811-2022

Gamage, L. P., Hix, E. G., & Gichuhi, W. K. (2020). Ground-Based Atmospheric Measurements of CO:CO2 Ratios in Eastern Highland Rim Using a CO Tracer Technique. *ACS Earth and Space Chemistry*, *4*(4), 558–571. https://doi.org/10.1021/acsearthspacechem.9b00322

Gamnitzer, U., Karstens, U., Kromer, B., Neubert, R. E. M., Meijer, H. A. J., Schroeder, H., & Levin, I. (2006). Carbon monoxide: A quantitative tracer for fossil fuel CO2? *Journal of Geophysical Research*, *111*(D22). https://doi.org/10.1029/2005jd006966

Gately, C. K., Hutyra, L. R., & Sue Wing, I. (2015). Cities, traffic, and CO2: A multidecadal assessment of trends, drivers, and scaling relationships. *Proceedings of the National Academy of Sciences of the United States of America*, *112*(16), 4999–5004. https://doi.org/10.1073/pnas.1421723112

Gensheimer, J., Turner, A. J., Shekhar, A., Wenzel, A., Keutsch, F. N., & Chen, J. (2021). What Are the Different Measures of Mobility Telling Us About Surface Transportation CO2 Emissions During the COVID-19 Pandemic? *Journal of Geophysical Research, D: Atmospheres*, *126*(11), e2021JD034664. https://doi.org/10.1029/2021JD034664

Gisi, M., Hase, F., Dohe, S., Blumenstock, T., Simon, A., & Keens, A. (2012). XCO_2-measurements with a tabletop FTS using solar absorption spectroscopy. *Atmospheric Measurement Techniques*, *5*(11), 2969–2980. https://doi.org/10.5194/amt-5-2969-2012

Graven, H., Keeling, R. F., & Rogelj, J. (2020a). Changes to Carbon Isotopes in Atmospheric CO_2 Over the Industrial Era and Into the Future. *Global Biogeochemical Cycles*, *34*(11), e2019GB006170. https://doi.org/10.1029/2019GB006170

Graven, H., Keeling, R. F., & Rogelj, J. (2020b). Changes to Carbon Isotopes in Atmospheric CO_2 Over the Industrial Era and Into the Future. *Global Biogeochemical Cycles*, *34*(11), e2019GB006170. https://doi.org/10.1029/2019GB006170

Gurney, K. R., Liang, J., Patarasuk, R., Song, Y., Huang, J., & Roest, G. (2020). The Vulcan version 3.0 high-resolution fossil fuel CO2 emissions for the United States. *Journal of Geophysical Research*, *125*(19), e2020JD032974. https://doi.org/10.1029/2020JD032974

Gurney, K. R., Patarasuk, R., Liang, J., Song, Y., O'Keeffe, D., Rao, P., Whetstone, J. R., Duren, R. M., Eldering, A., & Miller, C. (2019). The Hestia fossil fuel CO2 emissions data product for the Los Angeles megacity (Hestia-LA). *Earth System Science Data*, *11*(3), 1309–1335. https://doi.org/10.5194/essd-11-1309-2019

Gurney, K. R., Razlivanov, I., Song, Y., Zhou, Y., Benes, B., & Abdul-Massih, M. (2012). Quantification of fossil fuel CO2 emissions on the building/street scale for a large U.S. city. *Environmental Science & Technology*, *46*(21), 12194–12202. https://doi.org/10.1021/es3011282

Gurney, Kılkış, Ş., Seto, K. C., Lwasa, S., Moran, D., Riahi, K., Keller, M., Rayner, P., & Luqman, M. (2022). Greenhouse gas emissions from global cities under SSP/RCP scenarios, 1990 to 2100. *Global Environmental Change: Human and Policy Dimensions*, *73*, 102478. https://doi.org/10.1016/j.gloenvcha.2022.102478

Gurney, Liang, J., Roest, G., Song, Y., Mueller, K., & Lauvaux, T. (2021). Under-reporting of greenhouse gas emissions in U.S. cities. *Nature Communications*, *12*(1), 553. https://doi.org/10.1038/s41467-020-20871-0

Hakkarainen, J., Ialongo, I., & Tamminen, J. (2016). Direct space-based observations of anthropogenic CO 2 emission areas from OCO-2. *Geophysical Research Letters*, *43*(21). https://doi.org/10.1002/2016gl070885

Harkins, C., McDonald, B. C., Henze, D. K., & Wiedinmyer, C. (2021). A fuel-based method for updating mobile source emissions during the COVID-19 pandemic. *Environmental Research Letters: ERL [Web Site]*, *16*(6), 065018. https://doi.org/10.1088/1748-9326/ac0660

Hedelius, J. K., Feng, S., Roehl, C. M., Wunch, D., Hillyard, P. W., Podolske, J. R., Iraci, L. T., Patarasuk, R., Rao, P., O'Keeffe, D., Gurney, K. R., Lauvaux, T., & Wennberg, P. O. (2017). Emissions and topographic effects on column CO_2 (XCO2) variations, with a focus on the Southern California Megacity. *Journal of Geophysical Research*, *122*(13), 7200–7215. https://doi.org/10.1002/2017jd026455

Hedelius, J. K., Liu, J., Oda, T., Maksyutov, S., Roehl, C. M., Iraci, L. T., Podolske, J. R., Hillyard, P. W., Liang, J., Gurney, K. R., & Others. (2018). Southern California megacity CO_2, CH_4, and CO flux estimates using ground-and space-based remote sensing and a Lagrangian model. *Atmospheric Chemistry and Physics*, *18*(22), 16271–16291. https://acp.copernicus.org/articles/18/16271/2018/

Hedelius, J. K., Viatte, C., Wunch, D., Roehl, C. M., Toon, G. C., Chen, J., Jones, T., Wofsy, S. C., Franklin, J. E., Parker, H., & Others. (2016). Assessment of errors and biases in retrievals of XCO_2, XCH_4, XCO, and XN_2O from a 0.5 cm^{-1} resolution solar-viewing spectrometer. *Atmospheric Measurement Techniques*, *9*(8), 3527–3546. https://amt.copernicus.org/articles/9/3527/2016/

Held, A. E., Chang, D. P., & Niemeier, D. A. (2001). Observations and model simulations of carbon monoxide emission factors from a California highway. *Journal of the Air & Waste Management Association , 51*(1), 121–132. https://doi.org/10.1080/10473289.2001.10464248

Hopkins, F. M., Kort, E. A., Bush, S. E., Ehleringer, J. R., Lai, C.-T., Blake, D. R., & Randerson, J. T. (2016). Spatial patterns and source attribution of urban methane in the Los Angeles Basin. *Journal of Geophysical Research*, *121*(5), 2490–2507. https://doi.org/10.1002/2015jd024429

Hsueh, D. Y., Krakauer, N. Y., Randerson, J. T., Xu, X., Trumbore, S. E., & Southon, J. R. (2007a). Regional patterns of radiocarbon and fossil fuel-derived CO_2 in surface air across North America. *Geophysical Research Letters*, *34*(2). https://doi.org/10.1029/2006gl027032

Hsueh, D. Y., Krakauer, N. Y., Randerson, J. T., Xu, X., Trumbore, S. E., & Southon, J. R. (2007b). Regional patterns of radiocarbon and fossil fuel-derived CO_2 in surface air across North America. *Geophysical Research Letters*, *34*(2). https://doi.org/10.1029/2006gl027032

Hu, W. (2017). Raising the speed limit from 75 to 80mph on Utah rural interstates: Effects on vehicle speeds and speed variance. *Journal of Safety Research*, *61*, 83–92. https://doi.org/10.1016/j.jsr.2017.02.006

IPCC. (2023). *Summary for policymakers. In:Climate Change 2023: Synthesis Report. Contribution of Working Groups I, II, and III to the Sixth Assessment Report of the Intergovernmental Panel on Climate Change [Core Writing Team, H. Lee and J. Romero (eds)]*. https://doi.org/10.59327/IPCC/AR6-9789291691647.001

Jaikumar, R., Shiva Nagendra, S. M., & Sivanandan, R. (2017). Modeling of real time exhaust emissions of passenger cars under heterogeneous traffic conditions. *Atmospheric Pollution Research*, *8*(1), 80–88. https://doi.org/10.1016/j.apr.2016.07.011

Jaiprakash, Habib, G., Kumar, A., Sharma, A., & Haider, M. (2017). On-road emissions of CO, CO2 and NOX from four wheeler and emission estimates for Delhi. *Journal of Environmental Sciences , 53*, 39–47. https://doi.org/10.1016/j.jes.2016.01.034

Karion, A., Callahan, W., Stock, M., Prinzivalli, S., Verhulst, K. R., Kim, J., Salameh, P. K., Lopez-Coto, I., & Whetstone, J. (2020). Greenhouse gas observations from the Northeast Corridor tower network. *Earth System Science Data*, *12*(1). https://doi.org/10.5194/amt-7-647-2014

Kelp, M., Gould, T., Austin, E., Marshall, J. D., Yost, M., Simpson, C., & Larson, T. (2020). Sensitivity analysis of area-wide, mobile source emission factors to high-emitter vehicles in Los Angeles. *Atmospheric Environment*, *223*, 117212. https://doi.org/10.1016/j.atmosenv.2019.117212

Kiel, M., Eldering, A., Roten, D. D., Lin, J. C., Feng, S., Lei, R., Lauvaux, T., Oda, T., Roehl, C. M., Blavier, J.-F., & Iraci, L. T. (2021). Urban-focused satellite CO_2 observations from the Orbiting Carbon Observatory-3: A first look at the Los Angeles megacity. *Remote Sensing of Environment*, *258*, 112314. https://doi.org/10.1016/j.rse.2021.112314

Kim, J., Verhulst, K., Lueker, T., Salameh, P., Cox, A., Walker, S., Paplawsky, W., Prinzivalli, S., Fain, C., Stock, M., DiGangi, E., Biggs, B., Angel, B., Karion, A., Pongetti, T., Callahan, W., Weiss, R., Keeling, R., & Miller, C. (2022). *In Situ Carbon Dioxide, Methane, and Carbon Monoxide Mole Fractions from the Los Angeles Megacity Carbon Project, National Institute of Standards and Technology* [Data set]. https://doi.org/10.18434/mds2-2388

Konovalov, I. B., Berezin, E. V., Ciais, P., Broquet, G., Zhuravlev, R. V., & Janssens-Maenhout, G. (2016). Estimation of fossil-fuel CO2 emissions using satellite measurements of "proxy" species. *Atmospheric Chemistry and Physics*, *16*(21), 13509–13540. https://doi.org/10.5194/acp-16-13509-2016

Kort, Angevine, W. M., Duren, R., & Miller, C. E. (2013). Surface observations for monitoring urban fossil fuel CO2emissions: Minimum site location requirements for the Los Angeles megacity. *Journal of Geophysical Research*, *118*(3), 1577–1584. https://doi.org/10.1002/jgrd.50135

Kort, Frankenberg, C., & Miller, C. E. (2012). Space-based observations of megacity carbon dioxide. *Geophysical Research Letters*. https://doi.org/10.1029/2012GL052738

Lamb, W. F., Wiedmann, T., Pongratz, J., Andrew, R., Crippa, M., Olivier, J. G. J., Wiedenhofer, D., Mattioli, G., Al Khourdajie, A., House, J., Pachauri, S., Figueroa, M., Saheb, Y., Slade, R., Hubacek, K., Sun, L., Ribeiro, S. K., Khennas, S., de la Rue du Can, S., … Minx, J. (2021). A review of trends and drivers of greenhouse gas emissions by sector from 1990 to 2018. *Environmental Research Letters: ERL [Web Site]*, *16*(7), 073005. https://doi.org/10.1088/1748-9326/abee4e

Laughner, J. L., Roche, S., Kiel, M., Toon, G. C., Wunch, D., Baier, B. C., Biraud, S., Chen, H., Kivi, R., Laemmel, T., & Others. (2023). A new algorithm to generate a priori trace gas profiles for the GGG2020 retrieval algorithm. *Atmospheric Measurement Techniques*, *16*(5), 1121–1146. https://amt.copernicus.org/articles/16/1121/2023/

Lauvaux, T., Gurney, K. R., Miles, N. L., Davis, K. J., Richardson, S. J., Deng, A., Nathan, B. J., Oda, T., Wang, J. A., Hutyra, L., & Turnbull, J. (2020). Policy-Relevant Assessment of Urban CO2 Emissions. *Environmental Science & Technology*, *54*(16), 10237–10245. https://doi.org/10.1021/acs.est.0c00343

Le Quéré, C., Jackson, R. B., Jones, M. W., Smith, A. J. P., Abernethy, S., Andrew, R. M., De-Gol, A. J., Willis, D. R., Shan, Y., Canadell, J. G., Friedlingstein, P., Creutzig, F., & Peters, G. P. (2020). Temporary reduction in daily global CO2 emissions during the COVID-19 forced confinement. *Nature Climate Change*, *10*(7), 647–653. https://doi.org/10.1038/s41558-020-0797-x

Le Quéré, C., Peters, G. P., Friedlingstein, P., Andrew, R. M., Canadell, J. G., Davis, S. J., Jackson, R. B., & Jones, M. W. (2021). Fossil CO2 emissions in the post-COVID-19 era. *Nature Climate Change*, *11*(3), 197–199. https://doi.org/10.1038/s41558-021-01001-0

Lee, S., Fulper, C. R., Cullen, D., McDonald, J., Fernandez, A., Doorlag, M. H., Sanchez, L. J., & Olechiw, M. (2020). On-Road Portable Emission Measurement Systems Test Data Analysis and Light-Duty Vehicle In-Use Emissions Development. *SAE International Journal of Electrified Vehicles*, *9*(2), 111–132. https://www.jstor.org/stable/27041198

Levin, I., Kromer, B., Schmidt, M., & Sartorius, H. (2003). A novel approach for independent budgeting of fossil fuel CO2over Europe by14CO2observations. *Geophysical Research Letters*, *30*(23). https://doi.org/10.1029/2003gl018477

Li, Y., Ma, Z., Han, T., Quan, W., Wang, J., Zhou, H., He, D., & Dong, F. (2022). Long-term declining in carbon monoxide (CO) at a rural site of Beijing during 2006–2018 implies the improved combustion efficiency and effective emission control. *Journal of Environmental Sciences* , *115*, 432–442. https://doi.org/10.1016/j.jes.2020.11.011

Lian, J., Lauvaux, T., Utard, H., Bréon, F.-M., Broquet, G., Ramonet, M., Laurent, O., Albarus, I., Chariot, M., Kotthaus, S., & Others. (2023). Can we use atmospheric CO_2 measurements to verify emission trends reported by cities? Lessons from a six-year atmospheric inversion over Paris. *Atmospheric Chemistry and Physics*, *23*(15), 8823–8835. https://doi.org/10.5194/acp-23-8823-2023

Libby, W. F. (1955). *Radiocarbon Dating* (2nd ed.). Chicago: The University of Chicago Press.

Lichtfouse, E., Lichtfouse, M., Kashgarian, M., & Bol, R. (2005). 14C of grasses as an indicator of fossil fuel CO2 pollution. *Environmental Chemistry Letters*, *3*(2), 78–81. https://doi.org/10.1007/s10311-005-0100-4

Liu, Ciais, P., Deng, Z., Lei, R., Davis, S. J., Feng, S., Zheng, B., Cui, D., Dou, X., Zhu, B., Guo, R., Ke, P., Sun, T., Lu, C., He, P., Wang, Y., Yue, X., Wang, Y., Lei, Y., … Schellnhuber, H. J. (2020). Near-real-time monitoring of global CO2 emissions reveals the effects of the COVID-19 pandemic. *Nature Communications*, *11*(1), 5172. https://doi.org/10.1038/s41467-020-18922-7

Liu, Sun, W., Zeng, N., Han, P., Yao, B., Liu, Z., Wang, P., Zheng, K., Mei, H., & Cai, Q. (2021). Observed decreases in on-road CO2 concentrations in Beijing during COVID-19 restrictions. *Atmospheric Chemistry and Physics*, *21*(6), 4599–4614. https://doi.org/10.5194/acp-21-4599-2021

Lopez, M., Schmidt, M., Delmotte, M., Colomb, A., Gros, V., Janssen, C., Lehman, S. J., Mondelain, D., Perrussel, O., Ramonet, M., Xueref-Remy, I., & Bousquet, P. (2013). CO, NOx and 13CO2 as tracers for fossil fuel CO2: results from a pilot study in Paris during winter 2010. *Atmospheric Chemistry and Physics*, *13*(15), 7343–7358. https://doi.org/10.5194/acp-13-7343-2013

Lopez-Coto, I., Ren, X., Karion, A., McKain, K., Sweeney, C., Dickerson, R. R., McDonald, B. C., Ahn, D. Y., Salawitch, R. J., He, H., Shepson, P. B., & Whetstone, J. R. (2022). Carbon Monoxide Emissions from the Washington, DC, and Baltimore Metropolitan Area: Recent Trend and COVID-19 Anomaly. *Environmental Science & Technology*, *56*(4), 2172–2180. https://doi.org/10.1021/acs.est.1c06288

Mackey, K. R. M., Stragier, S., Robledo, L., Cat, L. A., Xu, X., Capps, S., Treseder, K. K., Czimczik, C. I., & Faiola, C. (2021). Seasonal variation of aerosol composition in Orange County, Southern California. *Atmospheric Environment*, *244*, 117795. https://doi.org/10.1016/j.atmosenv.2020.117795

Maier, F. M., Levin, I., Conil, S., Gachkivskyi, M., Denier van der Gon, H., & Hammer, S. (2023). Uncertainty of continuous ΔCO-based ΔffCO2 estimates derived from 14C flask and bottom-up ΔCO / ΔffCO2 ratios. In *EGUsphere* (pp. 1–31). https://doi.org/10.5194/egusphere-2023-1237

Maier, F. M., Rödenbeck, C., Levin, I., Gerbig, C., Gachkivskyi, M., & Hammer, S. (2023). Potential of 14C-based versus ΔCO-based ΔffCO2 observations to estimate urban fossil fuel CO2 (ffCO2) emissions. In *EGUsphere* (pp. 1–30). https://doi.org/10.5194/egusphere-2023-1239

Maness, H. L., Thurlow, M. E., McDonald, B. C., & Harley, R. A. (2015). Estimates of CO2 traffic emissions from mobile concentration measurements. *Journal of Geophysical Research*, *120*(5), 2087–2102. https://doi.org/10.1002/2014jd022876

Masson-Delmotte, V., Zhai, P., Pirani, A., Connors, S. L., Péan, C., Berger, S., Caud, N., Chen, Y., Goldfarb, L., Gomis, M. I., Huang, M., Leitzell, K., Lonnoy, E., Matthews, J. B. R., Maycock, T. K., Waterfield, T., Yelekçi, O., Yu, R., & Zhou, B. (2021). *Climate Change 2021: The Physical Science Basis. Contribution of Working Group I to the Sixth Assessment Report of the Intergovernmental Panel on Climate Change : Summary for Policymakers*. Cambridge University Press. doi:10.1017/9781009157896.001

McDonald, B. C., Gentner, D. R., Goldstein, A. H., & Harley, R. A. (2013). Long-term trends in motor vehicle emissions in u.s. urban areas. *Environmental Science & Technology*, *47*(17), 10022–10031. https://doi.org/10.1021/es401034z

Mei, H., Wang, L., Wang, M., Zhu, R., Wang, Y., Li, Y., Zhang, R., Wang, B., & Bao, X. (2021). Characterization of Exhaust CO, HC and NOx Emissions from Light-Duty Vehicles under Real Driving Conditions. *Atmosphere*, *12*(9), 1125. https://doi.org/10.3390/atmos12091125

Miller, Actkinson, B., Padilla, L. J., Griffin, R. J., Moore, K., Lewis, G., Gardner-Frolick, R. P., Craft, E., Portier, C., & Alvarez, R. (2019). *Characterizing elevated urban air pollution spatial patterns near sources with Google Street View mobile monitoring in Houston, Texas*. *2019*, A23Q-2932. https://ui.adsabs.harvard.edu/abs/2019AGUFM.A23Q2932M

Miller, Lehman, S. J., Verhulst, K. R., Miller, C. E., Duren, R. M., Yadav, V., Newman, S., & Sloop, C. D. (2020). Large and seasonally varying biospheric CO2 fluxes in the Los Angeles megacity revealed by atmospheric radiocarbon. *Proceedings of the National Academy of Sciences of the United States of America*, *117*(43), 26681–26687. https://doi.org/10.1073/pnas.2005253117

Mitchell, L. E., Lin, J. C., Bowling, D. R., Pataki, D. E., Strong, C., Schauer, A. J., Bares, R., Bush, S. E., Stephens, B. B., Mendoza, D., Mallia, D., Holland, L., Gurney, K. R., & Ehleringer, J. R. (2018). Long-term urban carbon dioxide observations reveal spatial and temporal dynamics related to urban characteristics and growth. *Proceedings of the National Academy of Sciences of the United States of America*, *115*(12), 2912–2917. https://doi.org/10.1073/pnas.1702393115

Mitchell, L. E., Lin, J. C., Hutyra, L. R., Bowling, D. R., Cohen, R. C., Davis, K. J., DiGangi, E., Duren, R. M., Ehleringer, J. R., Fain, C., Falk, M., Guha, A., Karion, A., Keeling, R. F., Kim, J., Miles, N. L., Miller, C. E., Newman, S., Pataki, D. E., … Wofsy, S. C. (2022). A multi-city urban atmospheric greenhouse gas measurement data synthesis. *Scientific Data*, *9*(1), 361. https://doi.org/10.1038/s41597-022-01467-3

Mouteva, G. O., Randerson, J. T., Fahrni, S. M., Bush, S. E., Ehleringer, J. R., Xu, X., Santos, G. M., Kuprov, R., Schichtel, B. A., & Czimczik, C. I. (2017). Using radiocarbon to constrain black and organic carbon aerosol sources in Salt Lake City. *Journal of Geophysical Research: Atmospheres*, *122*(18), 9843–9857. https://doi.org/10.1002/2017JD026519

Newman, S., Xu, X., Affek, H. P., Stolper, E., & Epstein, S. (2008). Changes in mixing ratio and isotopic composition of CO_2in urban air from the Los Angeles basin, California, between 1972 and 2003. *Journal of Geophysical Research*, *113*(D23). https://doi.org/10.1029/2008jd009999

Newman, S., Xu, X., Gurney, K. R., Hsu, Y. K., Li, K. F., Jiang, X., Keeling, R., Feng, S., O'Keefe, D., Patarasuk, R., Wong, K. W., Rao, P., Fischer, M. L., & Yung, Y. L. (2016). Toward consistency between trends in bottom-up CO_2 emissions and top-down atmospheric measurements in the Los Angeles megacity. *Atmospheric Chemistry and Physics*, *16*(6), 3843–3863. https://doi.org/10.5194/acp-16-3843-2016

NHTSA. (2021). *Update to Special Reports on Traffic Safety during the COVID-19 Public Health Emergency: Fourth Quarter Data [Traffic Safety Facts]* (DOT HS 813 135). https://doi.org/10.21949/1526015

Nicolini, G., Antoniella, G., Carotenuto, F., Christen, A., Ciais, P., Feigenwinter, C., Gioli, B., Stagakis, S., Velasco, E., Vogt, R., Ward, H. C., Barlow, J., Chrysoulakis, N., Duce, P., Graus, M., Helfter, C., Heusinkveld, B., Järvi, L., Karl, T., … Papale, D. (2022). Direct observations of CO2 emission reductions due to COVID-19 lockdown across European urban districts. *The Science of the Total Environment*, *830*, 154662. https://doi.org/10.1016/j.scitotenv.2022.154662

Oda, T., Haga, C., Hosomi, K., Matsui, T., & Bun, R. (2021). Errors and uncertainties associated with the use of unconventional activity data for estimating CO2 emissions: the case for traffic emissions in Japan. *Environmental Research Letters: ERL [Web Site]*, *16*(8), 084058. https://doi.org/10.1088/1748-9326/ac109d

Park, S., Rakha, H., Farzaneh, M., Zietsman, J., & Lee, D.-W. (2010). Development of fuel and emission models for high speed heavy duty trucks, light duty trucks, and light duty vehicles. *13th International IEEE Conference on Intelligent Transportation Systems*, 25–32.

Park, S. S., Kozawa, K., Fruin, S., Mara, S., Hsu, Y.-K., Jakober, C., Winer, A., & Herner, J. (2011). Emission factors for high-emitting vehicles based on on-road measurements of individual vehicle exhaust with a

mobile measurement platform. *Journal of the Air & Waste Management Association* , *61*(10), 1046–1056. https://doi.org/10.1080/10473289.2011.595981

Patarasuk, R., Gurney, K. R., O'Keeffe, D., Song, Y., Huang, J., Rao, P., Buchert, M., Lin, J. C., Mendoza, D., & Ehleringer, J. R. (2016). Urban high-resolution fossil fuel CO2 emissions quantification and exploration of emission drivers for potential policy applications. *Urban Ecosystems*, *19*(3), 1013–1039. https://doi.org/10.1007/s11252-016-0553-1

Pavley, F. (2002). AB-1493: Vehicular emissions: greenhouse gases. *California Assembly Bill*. https://leginfo.legislature.ca.gov/faces/billNavClient.xhtml?bill_id=200120020AB1493

Pickers, P. A., Manning, A. C., Le Quéré, C., Forster, G. L., Luijkx, I. T., Gerbig, C., Fleming, L. S., & Sturges, W. T. (2022). Novel quantification of regional fossil fuel CO2 reductions during COVID-19 lockdowns using atmospheric oxygen measurements. *Science Advances*, *8*(16), eabl9250. https://doi.org/10.1126/sciadv.abl9250

Popa, M. E., Vollmer, M. K., Jordan, A., Brand, W. A., Pathirana, S. L., Rothe, M., & Röckmann, T. (2014). Vehicle emissions of greenhouse gases and related tracers from a tunnel study: CO: CO 2, N 2 O: CO 2, CH 4: CO 2, O 2: CO 2 ratios, and the stable isotopes 13 C and 18 O in CO 2 and CO. *Atmospheric Chemistry and Physics*, *14*(4), 2105–2123. https://acp.copernicus.org/articles/14/2105/2014/

Rao, P., R. Gurney, K., Patarasuk, R., Song, Y., E. Miller, C., M. Duren, R., & Eldering, A. (2017). Spatio-temporal variations in on-road CO_2 emissions in the Los Angeles megacity. *AIMS Geosciences*, *3*(2), 239–267. https://doi.org/10.3934/geosci.2017.2.239

Riley, W. J., Hsueh, D. Y., Randerson, J. T., Fischer, M. L., Hatch, J. G., Pataki, D. E., Wang, W., & Goulden, M. I. (2008). Where do fossil fuel carbon dioxide emissions from California go? An analysis based on radiocarbon observations and an atmospheric transport model. *Journal of Geophysical Research: Biogeosciences*, *113*(G4). https://doi.org/10.1029/2007JG000625

Rosenzweig, C., Solecki, W., Hammer, S. A., & Mehrotra, S. (2010, October 20). *Cities lead the way in climate–change action*. Nature Publishing Group UK. https://doi.org/10.1038/467909a

Santos, G. M., Oliveira, F. M., Park, J., Sena, A. C. T., Chiquetto, J. B., Macario, K. D., & Grainger, C. S. G. (2019). Assessment of the regional fossil fuel CO_2 distribution through Δ14C patterns in ipê leaves: The case of Rio de Janeiro state, Brazil. *City and Environment Interactions*, *1*, 100001. https://doi.org/10.1016/j.cacint.2019.06.001

Schuur, E. A. G., Druffel, E. R. M., & Trumbore, S. E. (2016). *Radiocarbon and Climate Change: Mechanisms, Applications and Laboratory Techniques*. Springer. https://play.google.com/store/books/details?id=ZvI0DAAAQBAJ

Schwandner, F. M., Gunson, M. R., Miller, C. E., Carn, S. A., Eldering, A., Krings, T., Verhulst, K. R., Schimel, D. S., Nguyen, H. M., Crisp, D., O'Dell, C. W., Osterman, G. B., Iraci, L. T., & Podolske, J. R. (2017). Spaceborne detection of localized carbon dioxide sources. *Science*, *358*(6360). https://doi.org/10.1126/science.aam5782

Seto, K. C., Cervero, R., Torres Martinez, J., Christensen, P., Dhakal, S., Bigio, A., Blanco, H., Delgado, G. C., Dewar, D., Huang, L., Inaba, A., Kansal, A., Lwasa, S., Mcmahon, J. E., Müller, D. B., Murakami, J., Nagendra, H., & Ramaswami, A. (2014). Human settlements, infrastructure, and spatial planning. *In Climate Change 2014 Mitigation of Climate Change. Contribution of Working Group III Too the Fifth Assessment Report of the Intergovernmental Panel on Climate Change (Pp. 923–1000).* https://escholarship.org/content/qt7kz997d2/qt7kz997d2.pdf

Seto, K. C., Churkina, G., Hsu, A., Keller, M., Newman, P. W. G., Qin, B., & Ramaswami, A. (2021). From Low- to Net-Zero Carbon Cities: The Next Global Agenda. *Annual Review of Environment and Resources*, *46*(1), 377–415. https://doi.org/10.1146/annurev-environ-050120-113117

Sharma, R., Kunchala, R. K., Ojha, S., Kumar, P., Gargari, S., & Chopra, S. (2023). Spatial distribution of fossil fuel derived CO2 over India using radiocarbon measurements in crop plants. *Journal of Environmental Sciences* , *124*, 19–30. https://doi.org/10.1016/j.jes.2021.11.003

Silva, S. J., Arellano, A. F., & Worden, H. M. (2013). Toward anthropogenic combustion emission constraints from space-based analysis of urban CO_2/CO sensitivity. *Geophysical Research Letters*, *40*(18), 4971–4976. https://doi.org/10.1002/grl.50954

Suarez-Bertoa, R., Astorga, C., Franco, V., Kregar, Z., Valverde, V., Clairotte, M., Pavlovic, J., & Giechaskiel, B. (2019). *On-road Vehicle Emissions Beyond RDE Conditions: Experimental Assessment Addressing EU Real-Driving Emission (RDE)*. Publications Office of the European Union. https://play.google.com/store/books/details?id=xbNazQEACAAJ

Sullivan, T. J., Driscoll, C. T., Beier, C. M., Burtraw, D., Fernandez, I. J., Galloway, J. N., Gay, D. A., Goodale, C. L., Likens, G. E., Lovett, G. M., & Watmough, S. A. (2018). Air pollution success stories in the United States: The value of long-term observations. In *Environmental Science & Policy* (Vol. 84, pp. 69–73). https://doi.org/10.1016/j.envsci.2018.02.016

Suntharalingam, P. (2004). Improved quantification of Chinese carbon fluxes using CO2/CO correlations in Asian outflow. *Journal of Geophysical Research*, *109*(D18). https://doi.org/10.1029/2003jd004362

Thiruvenkatachari, R. R., Carranza, V., Ahangar, F., Marklein, A., Hopkins, F., & Venkatram, A. (2020). Uncertainty in using dispersion models to estimate methane emissions from manure lagoons in dairies. *Agricultural and Forest Meteorology*, *290*, 108011. https://doi.org/10.1016/j.agrformet.2020.108011

Trumbore, S. E., Sierra, C. A., & Hicks Pries, C. E. (2016). Radiocarbon Nomenclature, Theory, Models, and Interpretation: Measuring Age, Determining Cycling Rates, and Tracing Source Pools. In E. A. G. Schuur, E. Druffel, & S. E. Trumbore (Eds.), *Radiocarbon and Climate Change: Mechanisms, Applications and Laboratory Techniques* (pp. 45–82). Springer International Publishing. https://doi.org/10.1007/978-3-319-25643-6_3

Turnbull, J. C., Domingues, L. G., & Turton, N. (2022). Dramatic Lockdown Fossil Fuel CO_2 Decrease Detected by Citizen Science-Supported Atmospheric Radiocarbon Observations. *Environmental Science & Technology*, *56*(14), 9882–9890. https://doi.org/10.1021/acs.est.1c07994

Turnbull, J. C., Karion, A., Davis, K. J., Lauvaux, T., Miles, N. L., Richardson, S. J., Sweeney, C., McKain, K., Lehman, S. J., Gurney, K. R., Patarasuk, R., Liang, J., Shepson, P. B., Heimburger, A., Harvey, R., & Whetstone, J. (2019). Synthesis of Urban CO2 Emission Estimates from Multiple Methods from the Indianapolis Flux Project (INFLUX). *Environmental Science & Technology*, *53*(1), 287–295. https://doi.org/10.1021/acs.est.8b05552

Turnbull, J. C., Karion, A., Fischer, M. L., Faloona, I., Guilderson, T., Lehman, S. J., Miller, B. R., Miller, J. B., Montzka, S., Sherwood, T., Saripalli, S., Sweeney, C., & Tans, P. P. (2011). Assessment of fossil fuel carbon dioxide and other anthropogenic trace gas emissions from airborne measurements over Sacramento, California in spring 2009. *Atmospheric Chemistry and Physics*, *11*(2), 705–721. https://doi.org/10.5194/acp-11-705-2011

Turnbull, J. C., Miller, J. B., Lehman, S. J., Tans, P. P., Sparks, R. J., & Southon, J. (2006). Comparison of $^{14}CO_2$, CO, and SF6 as tracers for recently added fossil fuel CO_2 in the atmosphere and implications for biological CO_2 exchange. *Geophysical Research Letters*, *33*(1). https://doi.org/10.1029/2005gl024213

Turnbull, J. C., Tans, P. P., Lehman, S. J., Baker, D., Conway, T. J., Chung, Y. S., Gregg, J., Miller, J. B., Southon, J. R., & Zhou, L.-X. (2011). Atmospheric observations of carbon monoxide and fossil fuel CO2emissions from East Asia. *Journal of Geophysical Research*, *116*(D24). https://doi.org/10.1029/2011jd016691

Turner, A. J., Kim, J., Fitzmaurice, H., Newman, C., Worthington, K., Chan, K., Wooldridge, P. J., Köehler, P., Frankenberg, C., & Cohen, R. C. (2020). Observed impacts of COVID-19 on urban CO 2 emissions. *Geophysical Research Letters*, *47*(22). https://doi.org/10.1029/2020gl090037

Turner, A. J., Köhler, P., Magney, T. S., Frankenberg, C., Fung, I., & Cohen, R. C. (2020). A double peak in the seasonality of California's photosynthesis as observed from space. *Biogeosciences* , *17*(2), 405–422. https://doi.org/10.5194/bg-17-405-2020

Tzirakis, E., Zannikos, F., & Stournas, S. (2007). Impact of driving style on fuel consumption and exhaust emissions: defensive and aggressive driving style. *Proceedings of the 10th International Conference on Environmental Science and Technology*, 1497–1504.

UDEQ. (2023). *Air Quality Incentive Programs*. Utah Department of Environmental Quality. https://deq.utah.gov/air-quality/incentive-programs-aq/air-quality-incentive-programs#individuals.

United States Environmental Protection Agency. (2017). *National Emissions Inventory* [Data set]. https://gispub.epa.gov/neireport/2017/

United States Environmental Protection Agency. (2023). Inventory of U.S. Greenhouse Gas Emissions and Sinks: 1990-2021 [Data set]. In *EPA 430-R-23-002*. https://www.epa.gov/ghgemissions/inventory-us-greenhouse-gas-emissions-and-sinks-1990-2021.

Utah Department of Transportation (UDOT). (2023). *Performance Measurement System (PeMS)* [Data set]. https://udot.iteris-pems.com/

Vargas, R., Trumbore, S. E., & Allen, M. F. (2009). Evidence of old carbon used to grow new fine roots in a tropical forest. *The New Phytologist*, *182*(3), 710–718. https://doi.org/10.1111/j.1469-8137.2009.02789.x

Verhulst, K. R., Karion, A., Kim, J., Salameh, P. K., Keeling, R. F., Newman, S., Miller, J., Sloop, C., Pongetti, T., Rao, P., Wong, C., Hopkins, F. M., Yadav, V., Weiss, R. F., Duren, R. M., & Miller, C. E. (2017). Carbon dioxide and methane measurements from the Los Angeles Megacity Carbon Project–Part 1: calibration,

urban enhancements, and uncertainty estimates. *Atmospheric and Climate Sciences*. https://doi.org/10.5194/acp-17-8313-2017

Vogel, F., Hamme, S., Steinhof, A., Kromer, B., & Levin, I. (2010). Implication of weekly and diurnal 14C calibration on hourly estimates of CO-based fossil fuel CO2 ata moderately polluted site in southwestern Germany. *Tellus. Series B, Chemical and Physical Meteorology*, *62*(5), 512–520. https://doi.org/10.1111/j.1600-0889.2010.00477.x

Wang, W., & Pataki, D. E. (2010). Spatial patterns of plant isotope tracers in the Los Angeles urban region. *Landscape Ecology*, *25*(1), 35–52. https://doi.org/10.1007/s10980-009-9401-5

Ware, J., Kort, E. A., DeCola, P., & Duren, R. (2016). Aerosol lidar observations of atmospheric mixing in Los Angeles: Climatology and implications for greenhouse gas observations. *Journal of Geophysical Research, D: Atmospheres*, *121*(16), 9862–9878. https://doi.org/10.1002/2016JD024953

Warneke, C., de Gouw, J. A., Holloway, J. S., Peischl, J., Ryerson, T. B., Elliot Atlas, Blake, D., Trainer, M., & Parrish, D. D. (2012). Multiyear trends in volatile organic compounds in Los Angeles, California: Five decades of decreasing emissions. *Journal of Geophysical Research*, *117*(D21). https://doi.org/10.1029/2012jd017899

Wen, Y., Wang, H., Larson, T., Kelp, M., Zhang, S., Wu, Y., & Marshall, J. D. (2019). On-highway vehicle emission factors, and spatial patterns, based on mobile monitoring and absolute principal component score. *The Science of the Total Environment*, *676*, 242–251. https://doi.org/10.1016/j.scitotenv.2019.04.185

Winkler, S. L., Anderson, J. E., Garza, L., Ruona, W. C., Vogt, R., & Wallington, T. J. (2018). Vehicle criteria pollutant (PM, NOx, CO, HCs) emissions: how low should we go? *Npj Climate and Atmospheric Science*, *1*(1), 1–5. https://doi.org/10.1038/s41612-018-0037-5

Wu, D., & Lin, J. C. (2021). *Urban biogenic CO2 fluxes: GPP, Reco and NEE estimates from SMUrF, 2010-2019. ORNL DAAC, Oak Ridge, Tennessee, USA* [Data set]. https://doi.org/10.3334/ORNLDAAC/1899

Wu, D., Lin, J. C., Duarte, H. F., Yadav, V., Parazoo, N. C., Oda, T., & Kort, E. A. (2021). A model for urban biogenic CO_2 fluxes: Solar-Induced Fluorescence for Modeling Urban biogenic Fluxes (SMUrF v1). *Geoscientific Model Development*, *14*(6), 3633–3661. https://doi.org/10.5194/gmd-14-3633-2021

Wu, D., Liu, J., Wennberg, P. O., Palmer, P. I., Nelson, R. R., Kiel, M., & Eldering, A. (2022). Towards sector-based attribution using intra-city variations in satellite-based emission ratios between CO_2 and CO. *Atmospheric Chemistry and Physics*, *22*(22), 14547–14570. https://doi.org/10.5194/acp-22-14547-2022

Wunch, D., Toon, G. C., Sherlock, V., Deutscher, Nicholas M, Liu, C., Feist, D. G., & Wennberg, P. O. (2015). The total carbon column observing network's GGG2014 data version. *Carbon Dioxide Information Analysis Center, Oak Ridge National Laboratory, Oak Ridge, Tennessee, USA, Available at: Doi*, *10*.

Wunch, D., Toon, G. C., Wennberg, P. O., Wofsy, S. C., Stephens, B. B., Fischer, M. L., Uchino, O., Abshire, J. B., Bernath, P., Biraud, S. C., Blavier, J.-F. L., Boone, C., Bowman, K. P., Browell, E. V., Campos, T., Connor, B. J., Daube, B. C., N. M. Deutscher, Diao, M., … Zondlo, M. A. (2010). Calibration of the Total Carbon Column Observing Network using aircraft profile data. *Atmospheric Measurement Techniques*, *3*(5), 1351–1362. https://doi.org/10.5194/amt-3-1351-2010

Wunch, D., Wennberg, P. O., Toon, G. C., Keppel-Aleks, G., & Yavin, Y. G. (2009). Emissions of greenhouse gases from a North American megacity. *Geophysical Research Letters*, *36*(15). https://doi.org/10.1029/2009gl039825

Xi, X., Ding, X., Fu, D., Zhou, L., & Liu, K. (2011). Regional Δ14C patterns and fossil fuel derived CO2 distribution in the Beijing area using annual plants. *Chinese Science Bulletin = Kexue Tongbao*, *56*(16), 1721–1726. https://doi.org/10.1007/s11434-011-4453-8

Xu, X., Trumbore, S. E., Zheng, S., Southon, J. R., McDuffee, K. E., Luttgen, M., & Liu, J. C. (2007). Modifying a sealed tube zinc reduction method for preparation of AMS graphite targets: Reducing background and attaining high precision. *Nuclear Instruments & Methods in Physics Research. Section B, Beam Interactions with Materials and Atoms*, *259*(1), 320–329. https://doi.org/10.1016/j.nimb.2007.01.175

Xueref-Remy, I., Dieudonné, E., Vuillemin, C., Lopez, M., Lac, C., Schmidt, M., Delmotte, M., Chevallier, F., Ravetta, F., Perrussel, O., Ciais, P., Bréon, F.-M., Broquet, G., Ramonet, M., Spain, T. G., & Ampe, C. (2018). Diurnal, synoptic and seasonal variability of atmospheric CO_2 in the Paris megacity area. *Atmospheric Chemistry and Physics*, *18*(5), 3335–3362. https://doi.org/10.5194/acp-18-3335-2018

Yadav, V., Ghosh, S., Mueller, K., Karion, A., Roest, G., Gourdji, S. M., Lopez-Coto, I., Gurney, K. R., Parazoo, N., Verhulst, K. R., Kim, J., Prinzivalli, S., Fain, C., Nehrkorn, T., Mountain, M., Keeling, R. F., Weiss, R. F., Duren, R., Miller, C. E., & Whetstone, J. (2021). The impact of COVID-19 on CO2 emissions in the Los Angeles and Washington DC/Baltimore metropolitan areas. *Geophysical Research Letters*, *48*(11), e2021GL092744. https://doi.org/10.1029/2021GL092744

Yañez, C. C., Hopkins, F. M., Xu, X., Tavares, J. F., Welch, A., & Czimczik, C. I. (2022). Reductions in California's urban fossil fuel CO_2 emissions during the COVID-19 pandemic. *AGU Advances*, *3*(6). https://doi.org/10.1029/2022av000732

Yang, E. G., Kort, E. A., Ott, L. E., Oda, T., & Lin, J. C. (2023a). Using space-based CO_2 and NO_2 observations to estimate urban CO_2 emissions. *Journal of Geophysical Research*, *128*(6). https://doi.org/10.1029/2022jd037736

Yang, E. G., Kort, E. A., Ott, L. E., Oda, T., & Lin, J. C. (2023b). Using space-based CO_2 and NO_2 observations to estimate urban CO_2 emissions. *Journal of Geophysical Research*, *128*(6). https://doi.org/10.1029/2022jd037736

Zhang, Y., West, J. J., Mathur, R., Xing, J., Hogrefe, C., Roselle, S. J., Bash, J. O., Pleim, J. E., Gan, C.-M., & Wong, D. C. (2018). Long-term trends in the ambient PM2.5- and O3-related mortality burdens in the United States under emission reductions from 1990 to 2010. *Atmospheric Chemistry and Physics*, *18*(20), 15003–15016. https://doi.org/10.5194/acp-18-15003-2018

Zheng, B., Chevallier, F., Yin, Y., Ciais, P., Fortems-Cheiney, A., Deeter, M. N., Parker, R. J., Wang, Y., Worden, H. M., & Zhao, Y. (2019). Global atmospheric carbon monoxide budget 2000–2017 inferred from multi-species atmospheric inversions. *Earth System Science Data*, *11*(3), 1411–1436. https://doi.org/10.5194/essd-11-1411-2019

Zheng, B., Geng, G., Ciais, P., Davis, S. J., Martin, R. V., Meng, J., Wu, N., Chevallier, F., Broquet, G., Boersma, F., van der A, R., Lin, J., Guan, D., Lei, Y., He, K., & Zhang, Q. (2020). Satellite-based estimates of decline and rebound in China's CO2 emissions during COVID-19 pandemic. *Science Advances*, *6*(49). https://doi.org/10.1126/sciadv.abd4998

Zhou, Y., Smith, S. J., Zhao, K., Imhoff, M., Thomson, A., Bond-Lamberty, B., Asrar, G. R., Zhang, X., He, C., & Elvidge, C. D. (2015). A global map of urban extent from nightlights. *Environmental Research Letters*, *10*(5), 054011. https://doi.org/10.1088/1748-9326/10/5/054011

Zhu, X.-H., He, H.-D., Lu, K.-F., Peng, Z.-R., & Gao, H. O. (2022). Characterizing carbon emissions from China V and China VI gasoline vehicles based on portable emission measurement systems. *Journal of Cleaner Production*, *378*, 134458. https://doi.org/10.1016/j.jclepro.2022.134458

APPENDIX A

Supporting Information for Ch 1: Contrasting trends in vehicle combustion efficiency in Los Angeles, CA and Salt Lake City, UT

Section A1. Wildfire influence

Wildfires emit CO and CO_2 and thus could have caused elevated mixing ratios in both gases, but especially for CO, if smoke was present in the study areas. To assess the potential influence of wildfires on our measurements, we evaluated daily satellite imagery captured by MODIS sensors onboard NASA's Aqua and Terra satellites, which detect fires, thermal anomalies and smoke plumes (https://worldview.earthdata.nasa.gov/). We found that there were no wildfires near the sites on the majority of the study days. The only measurement day when the satellite imagery captured a nearby fire and smoke reaching the study area was on August 16, 2013 in SLC. Our measurements may have detected this smoke plume. We observed elevated CO and CO_{xs}/CO_{2xs} values on August 16, 2013 compared to the other SLC 2013 measurement days (Fig. A1). Average CO levels were 928 ppb on August 16, whereas on the other measurement days, the mean CO mixing ratio was between 328 to 440 ppb. CO_{xs}/CO_{2xs} values were similarly elevated on this day, with a mean value of 10.9 ppb/ppm on August 16, 2013 whereas on other days the mean ranged from 4.5 to 6.2 ppb/ppm. We assume that these enhancements were due to wildfire smoke and thus excluded this day from the analysis.

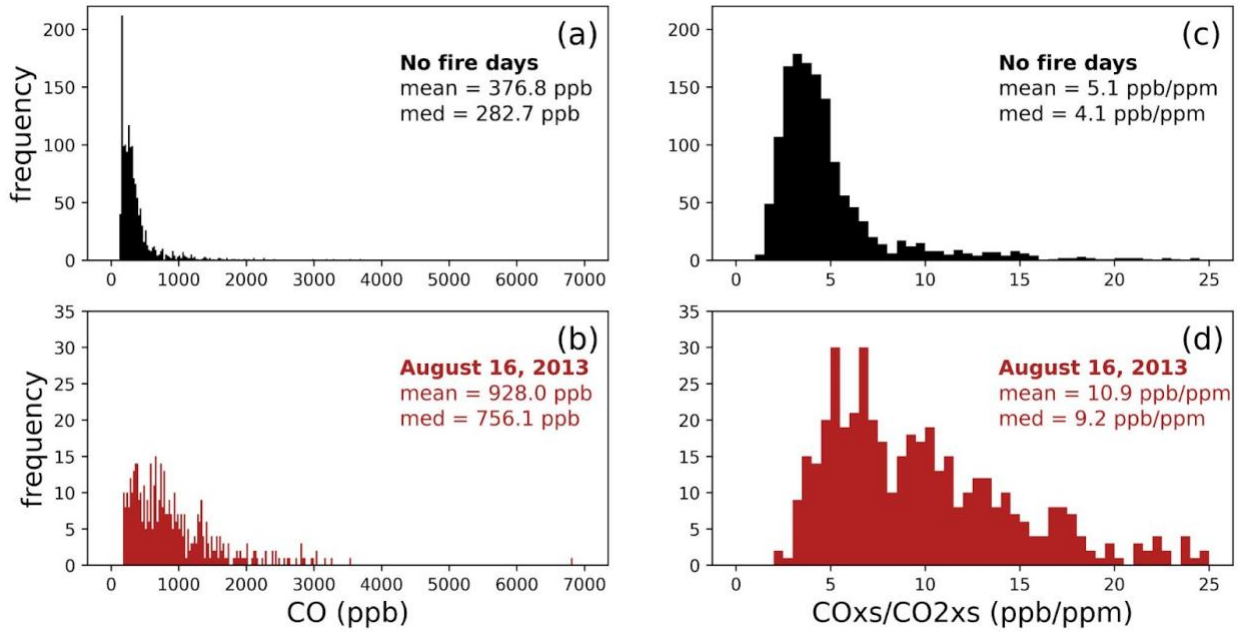

Figure A1. Histograms showing the distribution of on-road CO mixing ratios measured during the SLC 2013 survey on (a) days when we do not see wildfire influence (August 8, 13, and 15, 2013) and (b) on a day when the area was visibly contaminated with wildfire smoke (August 16, 2013). Similarly, (c) shows the distribution of CO_{xs}/CO_{2xs} ratios on non-fire days and (d) shows the distribution of CO_{xs}/CO_{2xs} ratios on the fire day.

Table A1. Dates and estimated CO and CO_2 background values for each survey.

Year	City	Dates	CO_2 (ppm)	CO (ppb)
2013	Los Angeles	June 14 - July 7	395.2 ± 3.6	75.6 ± 30.3
2013	Salt Lake City	August 8-16	377.1 ± 4.8	62.5 ± 36.5
2019	Los Angeles	July 15-31	407.9 ± 1.7	91.2 ± 11.0
2019	Salt Lake City	August 14-29	390.1 ± 5.9	67.5 ± 16.9
2020	Los Angeles	July 9-31	413.7 ± 6.7	72.2 ± 36.8
2021	Los Angeles	July 15-17	418.4 ± 20.6	87.3 ± 34.0

Background values were calculated by averaging the lowest 20% of the daily minimum measurements for all surveys except LA 2019. Because we did not sample background conditions and only measured on city streets or freeways in LA 2019, we instead characterized the background using the monthly average of measurements at San Clemente Island, an offshore tower site upwind of Los Angeles (J. Kim, Pers. Comm., 2020).

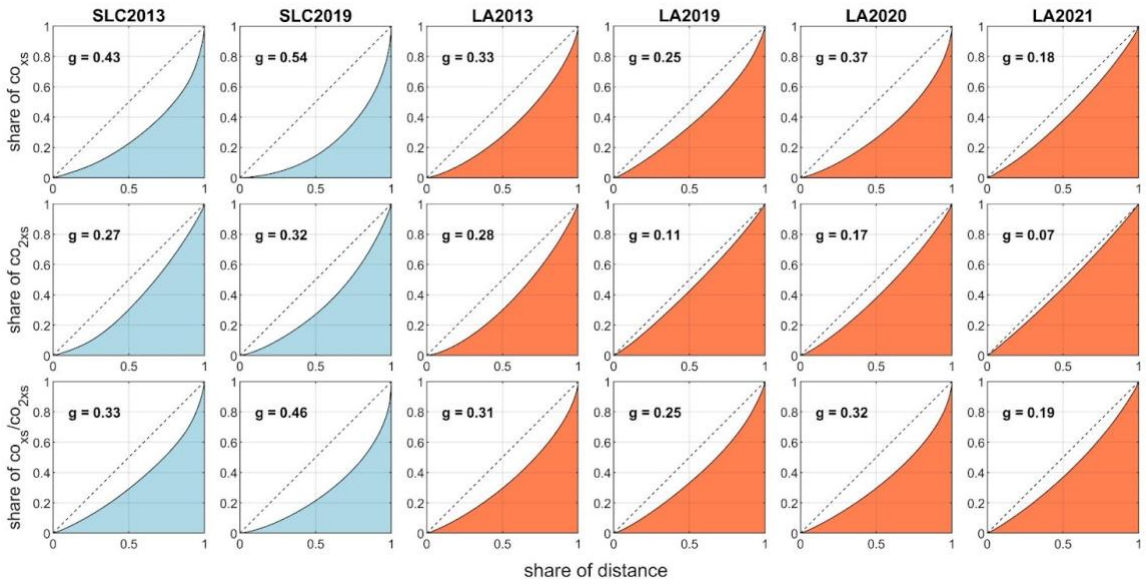

Figure A2. Lorenz curves showing the disproportionality of CO_{xs} (top panels), CO_{2xs} (middle panels), and CO_{xs}/CO_{2xs} (bottom panels) for each mobile survey in Salt Lake City (SLC) and Los Angeles (LA) between 2013 and 2021. The Gini index (g) is a measure of inequality, where larger g values indicate a more skewed distribution (i.e., few road segments having a large share of CO_{xs} values).

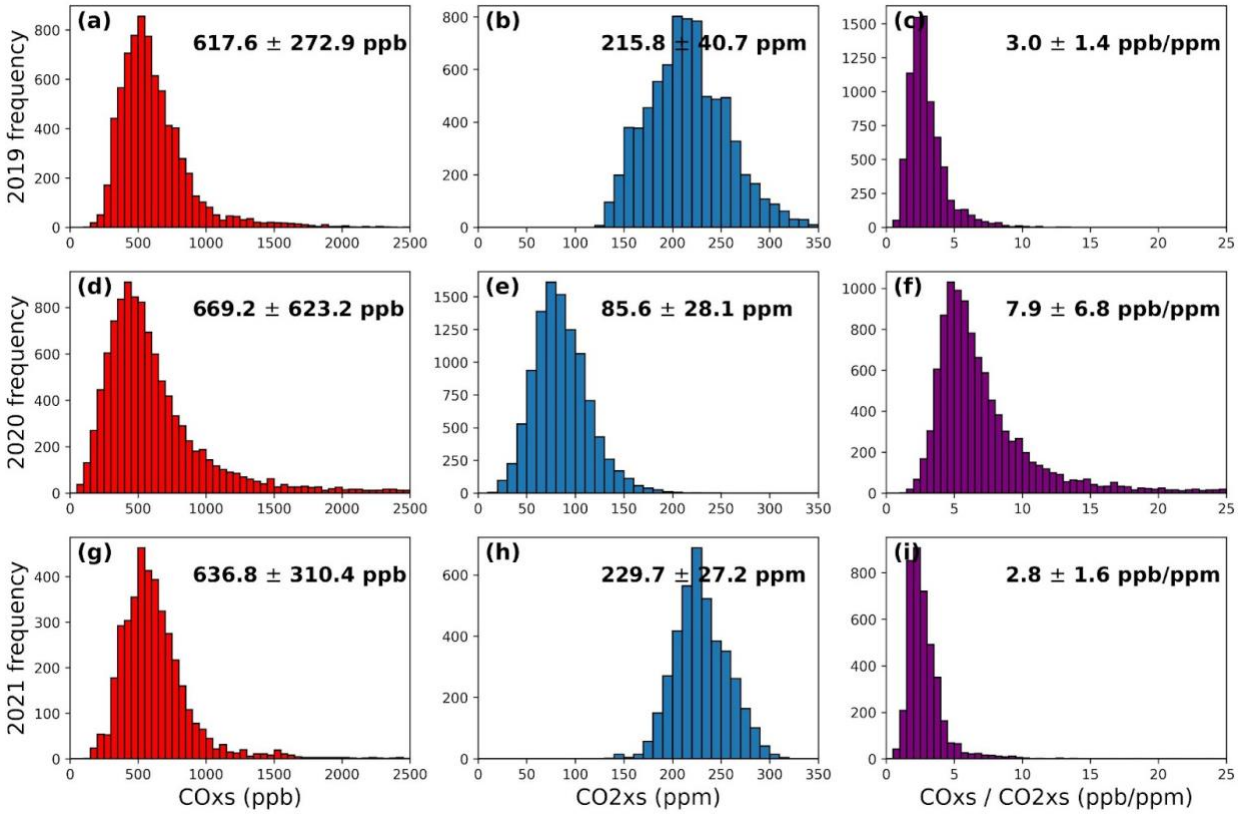

Figure A3. Frequency distributions of on-road CO_{xs}, CO_{2xs}, and the ratio CO_{xs}/CO_{2xs} before (a-c), during (d-f) and after (g-i) COVID-19-related traffic reductions in Los Angeles, CA. The values in the plots are the mean ± standard deviation.

Table A2. Results of simulated traffic fleet changes on on-road CO and CO_2 emissions based on the EMFAC 2021 model (CARB, 2021).

Scenario	Changes made to default 2020 fleet	Annual CO emissions (g)	Annual CO_2 emissions (g)	CO/CO_2 ratio (g/g)	CO/CO_2 ratio (1000 mol CO/ mol CO_2)	Percent change relative to default
Default EMFAC 2020 conditions	None	360.23	104229.6	0.003456	5.43	**0.00%**
Increase heavy-duty vehicle miles	Keep total VMT the same, but assign light duty passenger vehicles (LDA) VMT to zero, and redistribute the LDA miles to the other vehicle categories proportionally. Essentially, this is a scenario where there are **zero LDA vehicles** but the fleetwide VMT stays the same.	469.8	137430.59	0.003418	5.37	**-1.09%**
Faster speeds	Default VMT and fleet composition but made all vehicles drive faster by forcing all vehicle categories to drive in their "nighttime" (1AM) conditions all the time.	313.12	102751.99	0.003047	4.79	**-11.83%**
Older vehicle fleet	Ran EMFAC with the 2013 vehicle fleet instead of the 2020 fleet. Forced the speed conditions to be the same as 2020 and VMT to be the 2020 values for each vehicle category. Thus, speed, VMT and fleet composition is the same as the default, but with older vehicles on the road.	720.95	113280.62	0.006364	10.00	**84.14%**

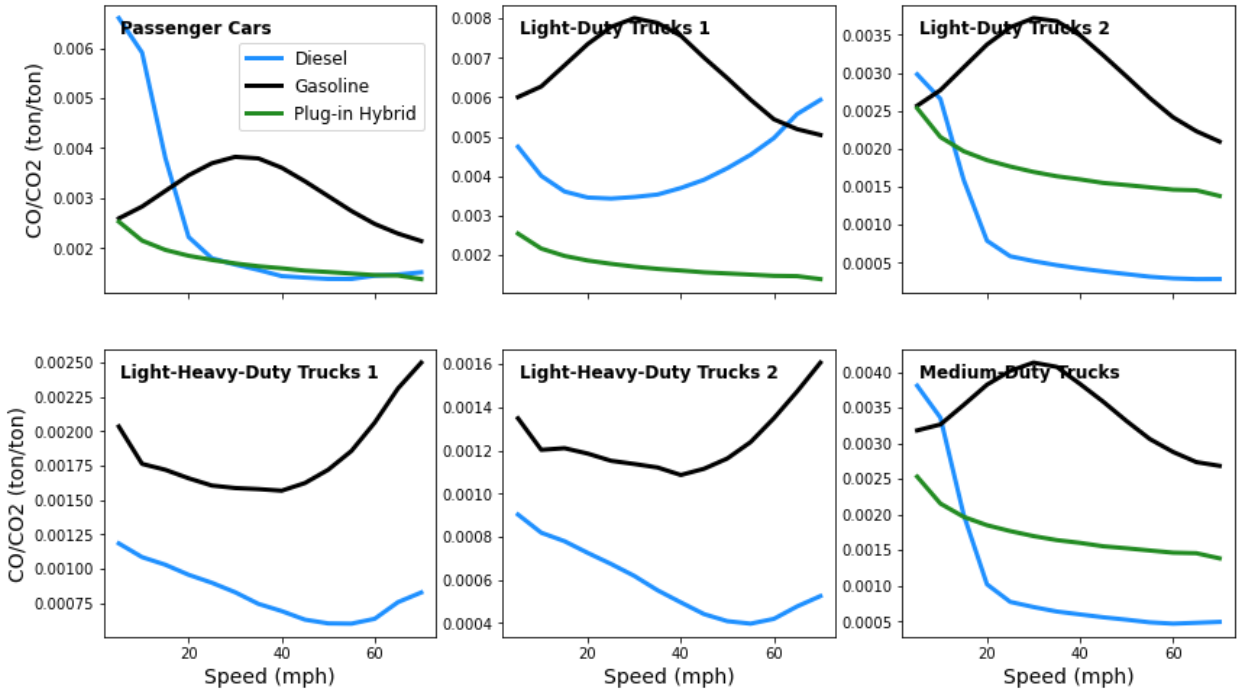

Figure A4. Effect of speed on CO and CO_2 emission rates (CO/CO_2) for light-duty vehicle categories. Data is from EMFAC 2021, is aggregated by vehicle age, and is based on the fleet characterization in the year 2020 in the South Coast Air Basin. Colors represent different fuel types (diesel, gasoline, and plug-in hybrid).

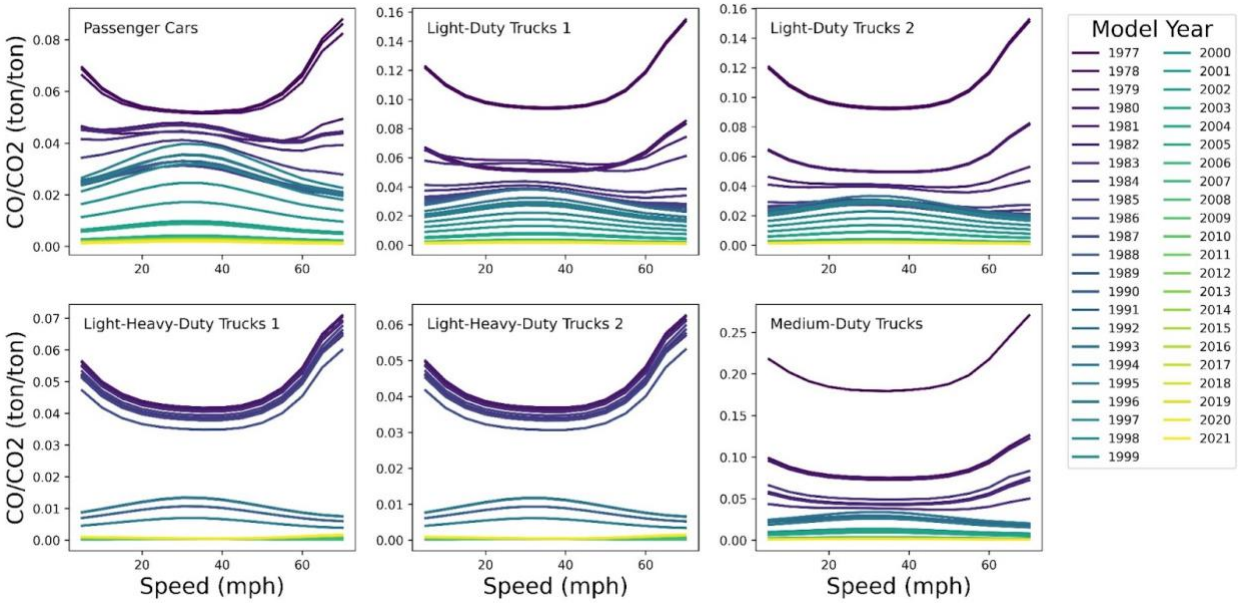

Figure A5. Effect of speed on CO and CO_2 emission rates by vehicle age, with lighter colors indicating newer model years. The data was downloaded from EMFAC 2021, using annual emissions from the year 2020 in the South Coast Air Basin. Only gasoline-powered light-duty vehicle categories are shown.

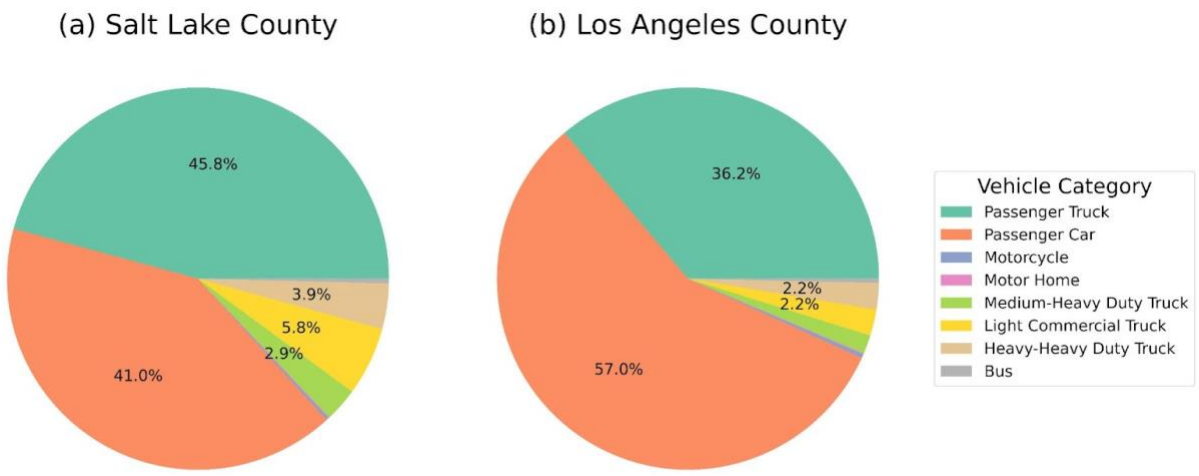

Figure A6. Fleet composition (% of vehicle miles traveled (VMT) by vehicle category) of (a) Salt Lake County and (b) Los Angeles County in 2017. The SLC data was compiled by the Department of Air Quality (UDAQ, pers. Comm. 2023) and is what is used to run the EPA MOVES model. The LA County data was downloaded from EMFAC2021 (https://arb.ca.gov/emfac/). Vehicle categories were simplified and reclassified for direct comparison between EMFAC and MOVES classifications.

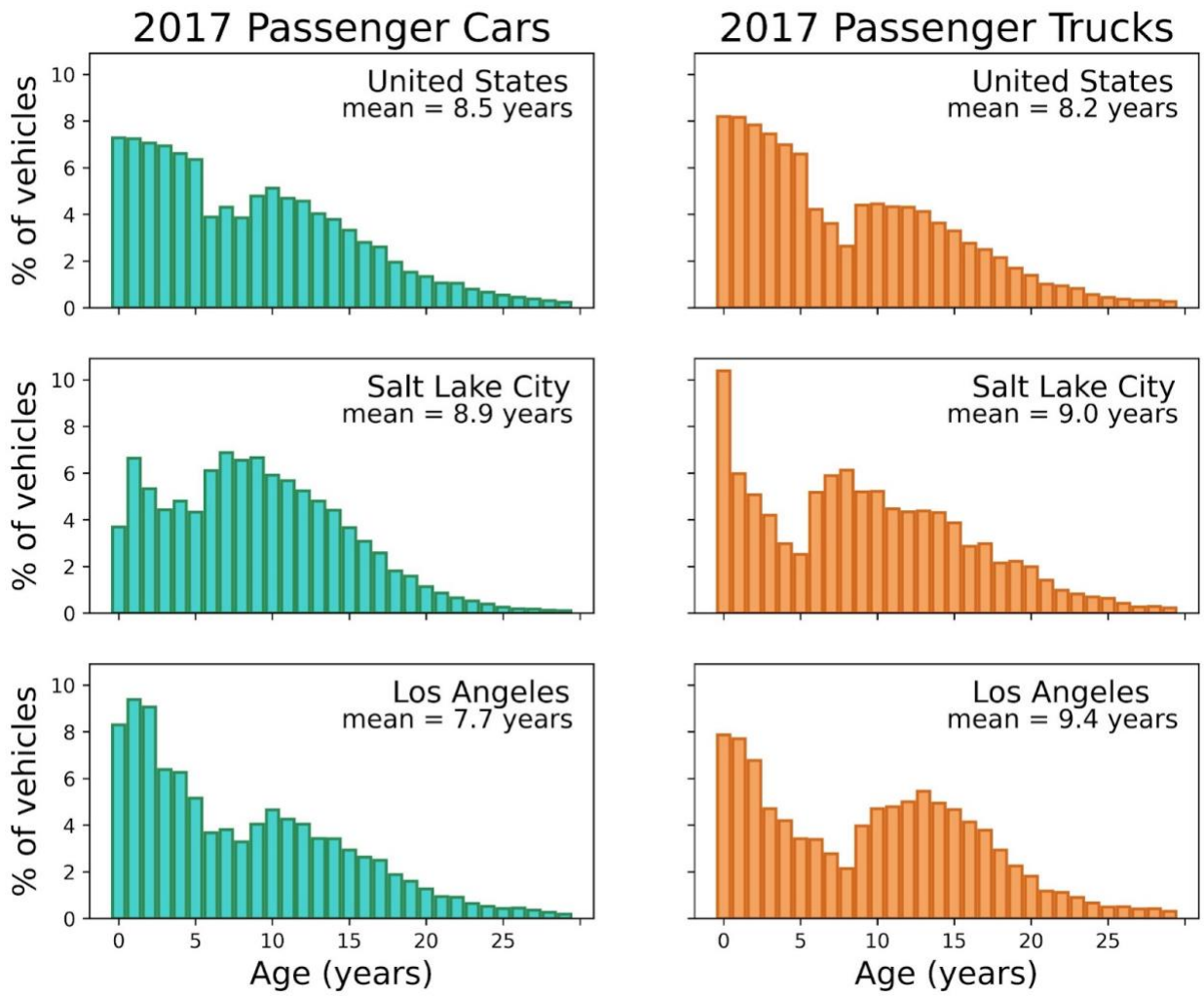

Figure A7. The 2017 vehicle age distributions of (left) passenger cars and (right) passenger trucks for (top row) the U.S. nationwide fleet, (middle row) the Salt Lake County fleet and (bottom row) the Los Angeles County fleet. The national age distribution is the 2017 default input used in EPA MOVES, downloaded from https://www.epa.gov/moves/previous-moves-versions-and-documentation. The Salt Lake County age distribution data was compiled by the Utah Department of Air Quality for use in the Ozone State Implementation Plan (UDAQ, pers. Comm. 2023). The LA County data was derived from the 2017 vehicle population in EMFAC2021 and is based on vehicle registration data from the California Department of Motor Vehicles (https://arb.ca.gov/emfac/fleet-db/). Note that 30+ year old vehicles were excluded (model years 1988 and older) to more realistically represent the vehicles being driven on the highways. 30+ year old passenger vehicles are expected to contribute a minimal fraction of vehicle miles traveled.

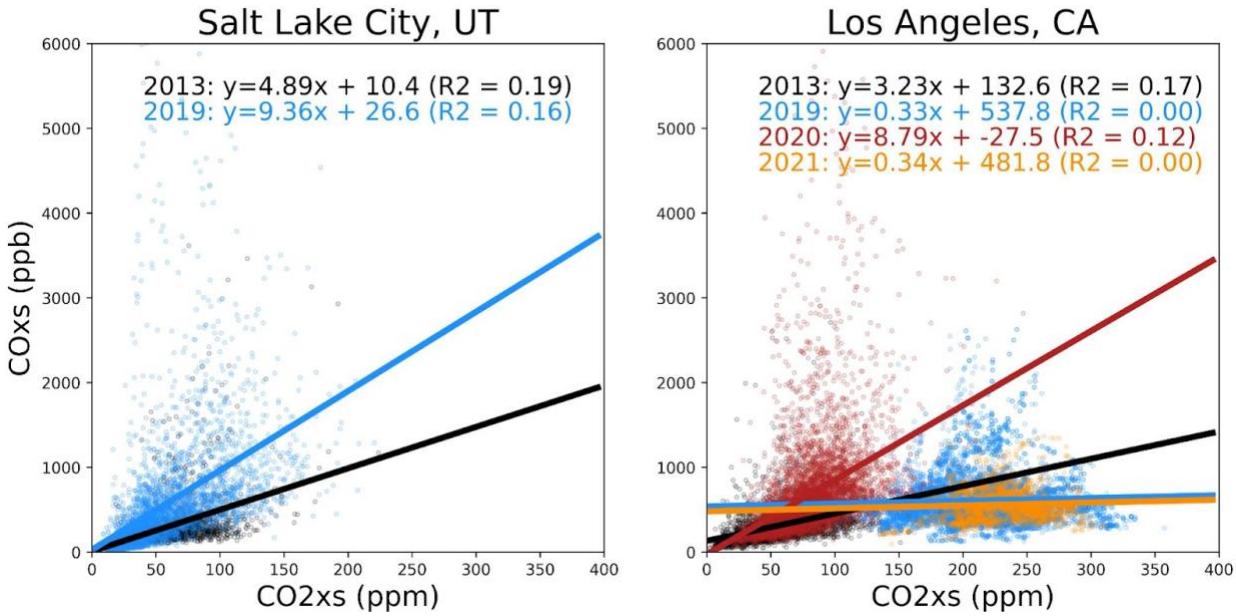

Figure A8. Linear correlation between CO_{2xs} and CO_{xs} for each survey in (left) Salt Lake City, UT and (right) Los Angeles, CA. Points and regression lines are colored by year, as indicated by the color of the linear equation text. The y-axis has been truncated for visualization purposes. The window captures >99% of the data, but CO_{xs} values between 6000-14000 ppb are not included in the figure. All linear regressions had a p-value < 0.05.

APPENDIX B

Supporting information for Ch 2: Reductions in California's fossil fuel carbon dioxide emissions during the COVID-19 pandemic

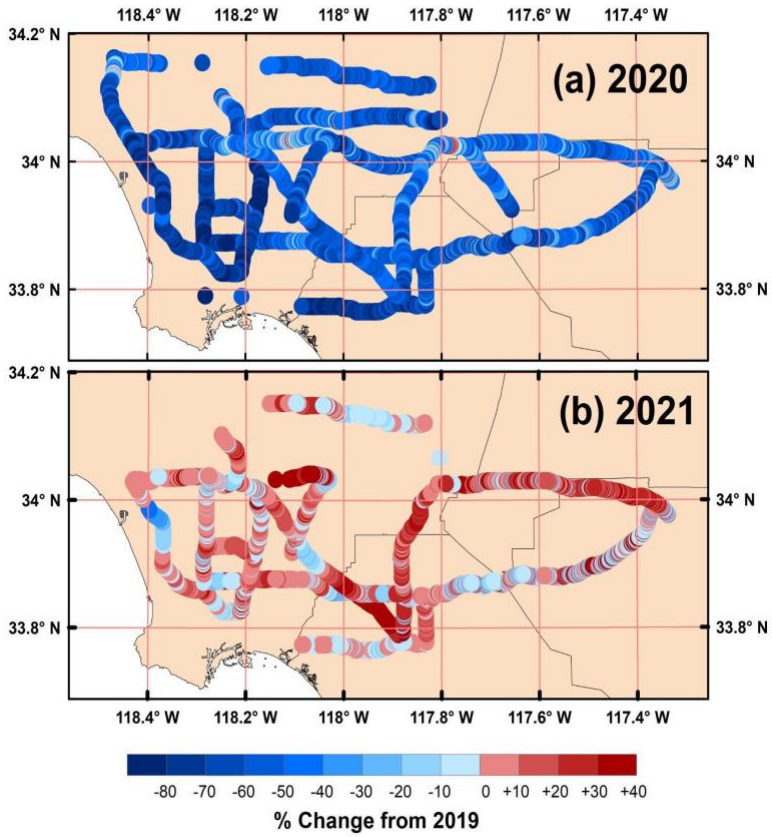

Figure B1. The percent change in CO_{2XS} in the Los Angeles metropolitan area in July relative to 2019 for a) 2020 and b) 2021 calculated from on-road surveys.

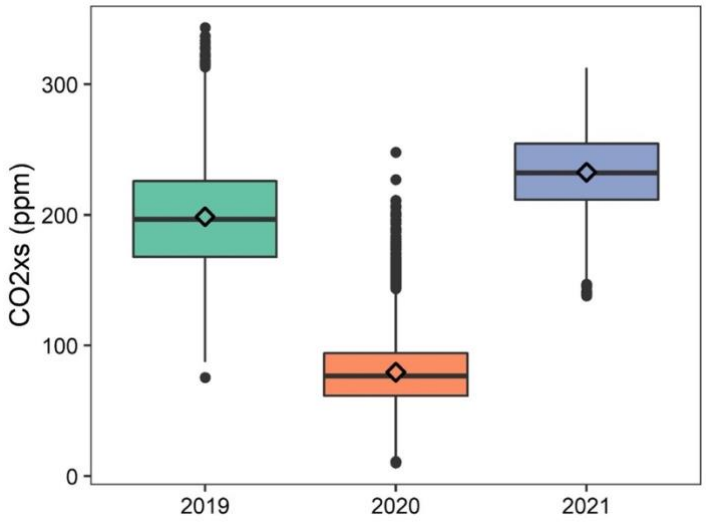

Figure B2. Boxplots showing the distribution of on-road CO_{2XS} values measured on Los Angeles freeways before the COVID-19 pandemic (2019) and during the pandemic (2020 and 2021). Diamond symbols indicate the mean of each year.

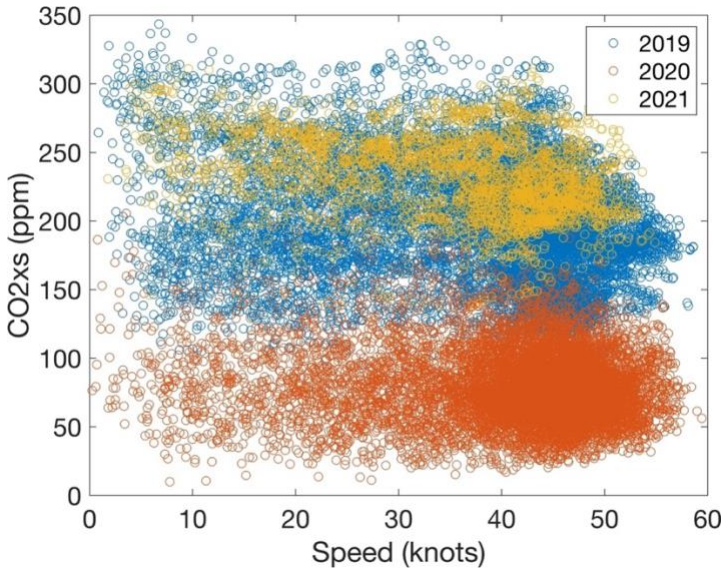

Figure B3. The relationship between vehicle speed and CO_{2xs} values measured for each year's mobile surveys.

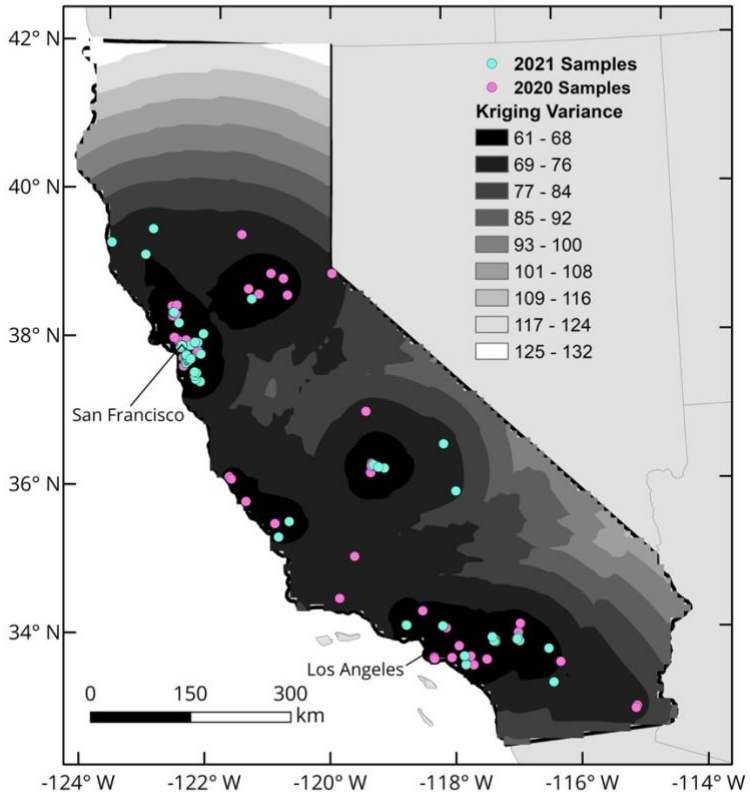

Figure B4. The variance in the ordinary kriging interpolation of the plant ^{14}C values across California. Areas with higher variance have larger uncertainty in the interpolation prediction showed in Figure 2.2.

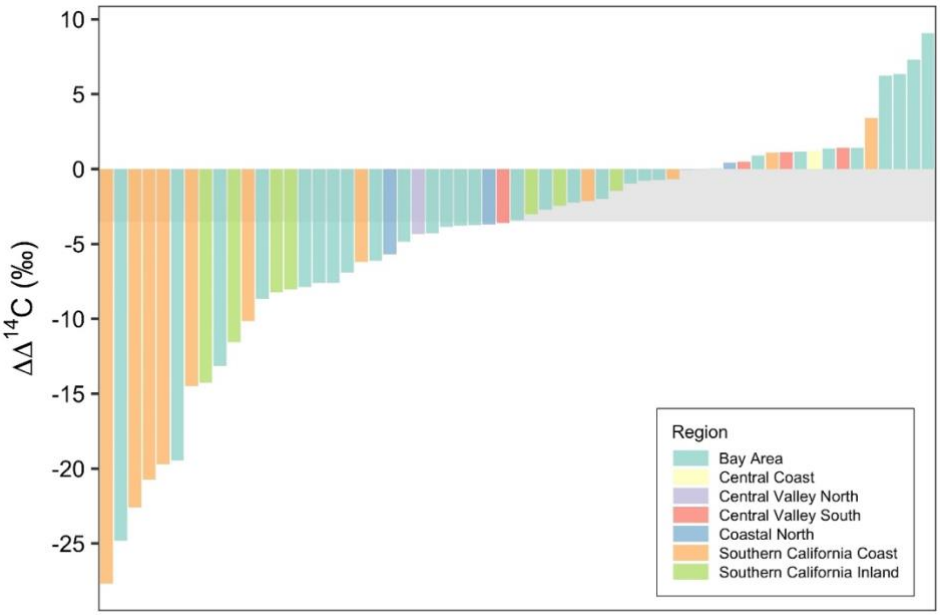

Figure B5. Difference in radiocarbon values of plant samples collected in the same locations in California in 2020 and 2021. Each bar represents the difference between samples collected within 500 m of each other ($\Delta\Delta^{14}C = \Delta^{14}C_{2021} - \Delta^{14}C_{2020}$, N=59 pairs). The shaded region indicates -3.5‰, the expected annual global change in atmospheric $^{14}CO_2$, hence any $\Delta\Delta$ value more negative than -3.5‰ indicates an increase in fossil fuel CO_2 from 2020 to 2021

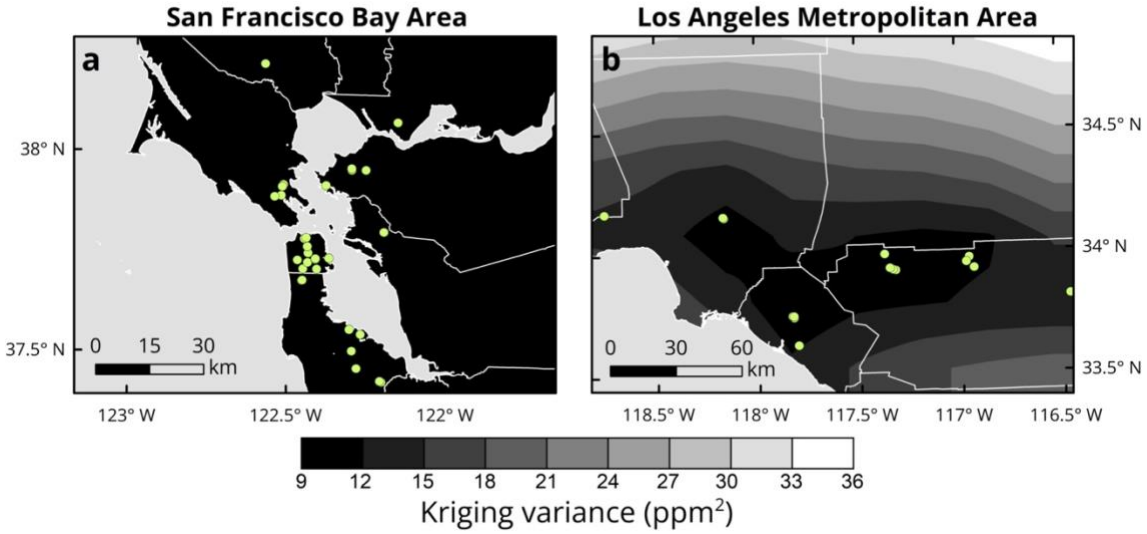

Figure B6. The variance in the ordinary kriging interpolation of the change in C_{ff} in the San Francisco Bay Area (a) and the Los Angeles Metropolitan Area (b). Areas with higher variance indicate larger uncertainty in the predicted kriging values presented in Figure 3.

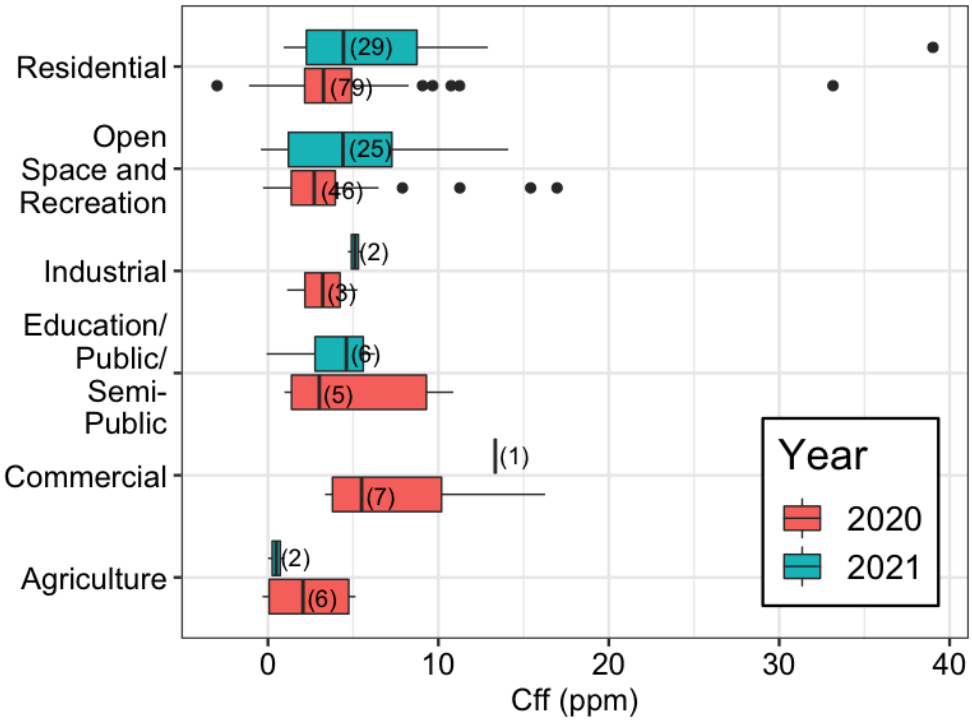

Figure B7. Boxplots showing the distribution of fossil fuel contributions by sector for the full dataset (all samples, not just co-located as in Fig. 2.3).

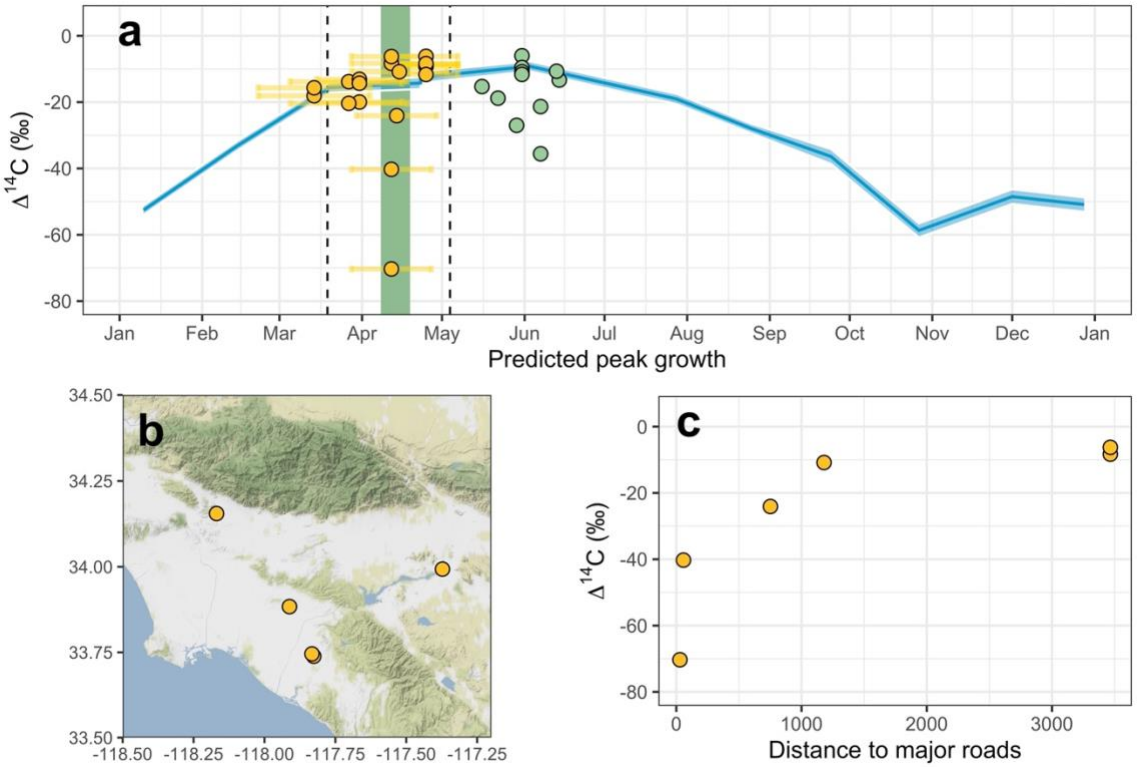

Figure B8. An attempt to use remotely sensed measurements of solar induced fluorescence (SIF) to better predict the timing of plant sample growth. (a) $\Delta^{14}C$ of plants collected in 2020, with the timing of peak growth predicted by SIF if the plant was already senesced during collection (yellow points) or predicted by the collection date if the plant was green (green points). Error bars surrounding the yellow points show the range of dates when 30% of peak plant growth occurred. Blue line shows $\Delta^{14}CO_2$ of air samples collected in Irvine, CA (Xu, pers. Com). Vertical dashed lines indicate the period where the Stay-At-Home Order was in effect. (b) Locations of plant samples that had similar predicted peak growth dates (April 15, 2020 ± 2 days) but vastly different $\Delta^{14}C$ values from each other. (c) $\Delta^{14}C$ increased nonlinearly with distance from major roads for the same set of samples from panel (b).

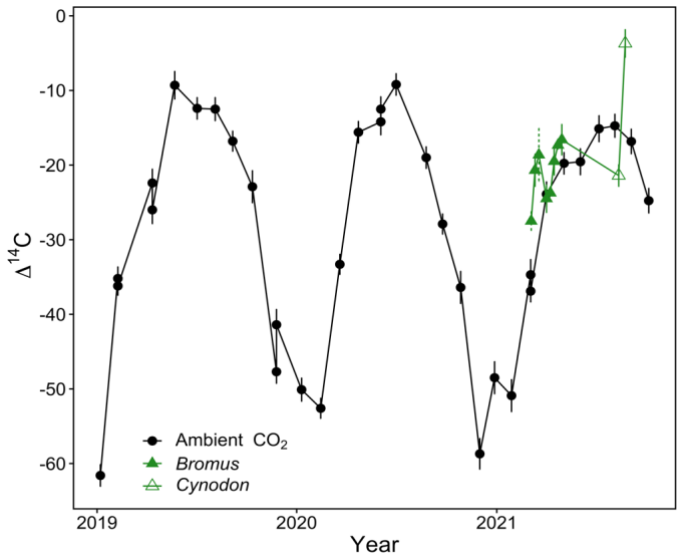

Figure B9. The $\Delta^{14}C$ of ambient CO_2 and plant samples collected at the University of California in Irvine, CA. Solid error bars show the measurement error and dashed error bars show SD of replicated samples. Open triangles are Bermuda turfgrass samples (*Cynodon dactylon*) while closed triangles are annual grass species (*Bromus diandrus* Roth).

Table B1. Mobile survey dates and calibration parameters used to correct on-road CO_2 data measured using a Picarro G2401 analyzer.

Year	Survey dates	Standard 1 (ppm CO_2)	Standard 2 (ppm CO_2)	Slope (mean ± SD)	Intercept (mean ± SD)	Precision* (ppm CO_2)
2019	July 15-17, 19, 23-26, 29-31	564	1021	0.985 ± 0.001	19.0 ± 0.4	0.5
2020	July 9-10, 23-24, 30-31	551	1028	1.00 ± 0.01	3.2 ± 8.0	0.9
2021	July 16-17	420.4	551	1.00 ± 0.001	-1.1 ± 0.3	0.1

*****Precision was defined as the average standard deviation of all calibration runs

Table B2. $\Delta^{14}C$ and background values used to calculate the results in Table 2.1 of the main text.

Region	Year	Type	Study	n	Δ_{obs} (‰)	Δ_{bg} (‰)	C_{bg} (ppm)	C_{ff}
CA	2005	plant	Riley et al. (2008)	128	47.6 ± 13.7	57.5 ± 3.1	384.5 ± 1.9	4 ± 5
CA	2020	plant	This study	188	-11.3 ± 8.6	-2.8 ± 1.3	416.7 ± 1.1	4 ± 4
CA	*2020*	*plant*	*This study (co-located)*	*49*	*-13.5 ± 11.0*	*-2.8 ± 1.3*	*416.7 ± 1.1*	*5 ± 5*
CA	2021	plant	This study	82	-16.6 ± 12.0	-6.2 ± 1.7	419.4 ± 0.8	5 ± 5
CA	*2021*	*plant*	*This study (co-located)*	*49*	*-17.5 ± 13.0*	*-6.2 ± 1.7*	*419.4 ± 0.8*	*5 ± 6*
LA	2005	plant	Wang & Pataki (2010)	79	31.2 ± 25.4	57.5 ± 3.1	384.5 ± 1.9	10 ± 10
LA	2015	air	Miller et al. (2020)	76	-10.3 ± 19.5	14.8 ± 1.1	405.2 ± 2.8	10 ± 8
LA	2016	air	Miller et al. (2020)	24	-17.2 ± 18.3	13.0 ± 1.9	407.7 ± 1.0	13 ± 8
LA	2020	plant	This study	53	-15.9 ± 12.5	-2.8 ± 1.3	416.7 ± 1.1	6 ± 5
LA	*2020*	*plant*	*This study (co-located)*	*10*	*-22.8 ± 21.1*	*-2.8 ± 1.3*	*416.7 ± 1.1*	*9 ± 9*
LA	2021	plant	This study	27	-25.7 ± 15.4	-6.2 ± 1.7	419.4 ± 0.8	9 ± 7
LA	*2021*	*plant*	*This study (co-located)*	*10*	*-31.7 ± 21.9*	*-6.2 ± 1.7*	*419.4 ± 0.8*	*11 ± 10*
Pasadena	2020[a]	air	Newman et al. (2016)	n/a	-55.5 ± 8.8	-2.8 ± 1.3	416.7 ± 1.1	23 ± 4
Pasadena	2020	plant	This study	1	-10.8	-2.8 ± 1.3	416.7 ± 1.1	3 ± 1
Pasadena	2021	plant	This study	6	-35.7 ± 4.5	-6.2 ± 1.7	419.4 ± 0.8	13 ± 2
Irvine	2019	air	Xu (pers. comm)	4	-17.5 ± 8.0	-2.2 ± 2.1	415.2 ± 1.0	7 ± 4
Irvine	2020	plant	This study	1	-15.9	-2.8 ± 1.3	416.7 ± 1.1	6 ± 1
Irvine	2021	plant	This study	3	-16.5 ± 1.6	-6.2 ± 1.7	419.4 ± 0.8	4 ± 1

Note: To calculate changes in C_{ff} from ^{14}C observations, we use Eq. 2.4 with the background characterized by ^{14}C observations in Pt. Barrow, AK (Xu, pers. comm) and the CO_2 background characterized by observations at Cape Kumukahi, HI (Dlugokencky et al., 2021). All air ^{14}C data is subset to the annual grass growing season (March to May) to match the temporal integration of the plant samples. Uncertainties are represented by the standard deviation unless n =1. Italicized rows indicate subsets of the data in the previous row where only co-located samples (plants collected in both 2020 and 2021 within 150 m apart) are included in the calculation.

[a]The 2020 Pasadena value is a hypothetical no-pandemic scenario and was estimated based on a linear extrapolation of 2006-2013 air ^{14}C data (Newman et al., 2016)

APPENDIX C

Supporting Information for Ch 3: Plant Radiocarbon across an Urban-Rural CO_2 Gradient Matches Surface and Column CO_2 Observations

Isotope mass balance calculations

Our estimates of C_{ff} are based on the following two mass balance equations (Turnbull et al., 2011; Miller et al., 2020):

$$C_{obs} = C_{bg} + C_{ff} + C_{bio}$$

$$\Delta_{obs}C_{obs} = \Delta_{bg}C_{bg} + \Delta_{ff}C_{ff} + \Delta_{bio}C_{bio}$$

where C_i terms indicate CO_2 mixing ratios (in units ppm) and Δ_i terms indicate $\Delta^{14}C$ values (in units of ‰). The subscripts indicate the source, where "obs" are our observations, "bg" is the background, "ff" is from fossil fuels, and "bio" is from the biosphere. We use two different approaches in the manuscript to estimate the fossil contributions to our observations: one neglecting the biosphere terms (Section 3.3.3) and one including them (Section 3.3.4). The latter follows a two end member mixing analysis that is described in Miller et al. (2020) to estimate the fossil fraction (f_{ff}) of our aggregated samples. Below, we show the derivations under both cases.

Calculating C_{ff}, ignoring C_{bio} terms	Calculating f_{ff}, including C_{bio} terms
Mass balance equations: $$C_{obs} = C_{bg} + C_{ff}$$ $$\Delta_{obs}C_{obs} = \Delta_{bg}C_{bg} + \Delta_{ff}C_{ff}$$ Treating C_{obs} as an unknown, we substitute the C_{obs} term from the first equation to the second to eliminate it: $$\Delta_{obs}(C_{bg} + C_{ff}) = \Delta_{bg}C_{bg} + \Delta_{ff}C_{ff}$$ Now we can solve for C_{ff} since all other terms are measured or known:	Mass balance equations: $$C_{obs} = C_{bg} + C_{ff} + C_{bio}$$ $$\Delta_{obs}C_{obs} = \Delta_{bg}C_{bg} + \Delta_{ff}C_{ff} + \Delta_{bio}C_{bio}$$ Assuming we measured C_{obs} at the locations where the plants were collected, the unknowns in this case are C_{ff} and C_{bio}. Following Miller et al. (2020), we re-arranged the equations in terms of "excess" values above background as follows:

$$C_{ff} = C_{bg}\frac{(\Delta_{bg} - \Delta_{obs})}{(\Delta_{obs} - \Delta_{ff})}$$	$$C_{xs} = C_{ff} + C_{bio}$$ $$C_{xs} = C_{obs} - C_{bg}$$ $$\Delta_{obs}C_{obs} = \Delta_{bg}C_{bg} + (\Delta \times C)_{xs}$$ $$(\Delta \times C)_{xs} = \Delta_{source}C_{xs}$$ We estimate Δ_{source} as the slope of a linear regression of $(\Delta \times C)_{xs}$ and C_{xs}. Where Δ_{source} is the flux-weighted average isotopic signature of the fossil and biogenic fractions $$\Delta_{source} = (f_{ff}\Delta_{ff}) + (f_{bio}\Delta_{bio})$$ We can then solve for f_{ff} (the fraction of C_{xs} that is contributed by fossil fuels) using the following substitution: $$f_{ff} = 1 - f_{bio}$$ Subsequently, we can also solve for f_{bio}.

Additionally, we can calculate C_{ff} and C_{bio} sample by sample based on the following derivation, assuming we know C_{obs}, Δ_{obs}, C_{bg}, Δ_{bg}. This approach was taken for the analysis presented in Figure 3.5 of the main text. We start with the same mass balance equation, except now we separate the C_{bio} term into respiration and photosynthesis terms: $C_{bio} = C_r + C_p$.

$$C_{obs} = C_{bg} + C_{ff} + C_r + C_p$$

$$\Delta_{obs}C_{obs} = \Delta_{bg}C_{bg} + \Delta_{ff}C_{ff} + \Delta_r C_r + \Delta_p C_p$$

We solve for C_{ff} by substituting the C_p term from the first equation into the second and setting $\Delta_p = \Delta_{bg}$. The rearranged equation then becomes:

$$C_{ff} = C_{obs}\frac{(\Delta_{obs} - \Delta_{bg})}{(\Delta_{ff} - \Delta_{bg})} - C_r\frac{(\Delta_r - \Delta_{bg})}{(\Delta_{ff} - \Delta_{bg})}$$

Following Miller et al. (2020), we assume the biospheric disequilibrium (Δ_r - Δ_{bg}) is 50‰ and that C_r = 5 ppm. Thus, the second term is 0.25 ppm. All values in the first term are known so we can solve for C_{ff}. Subsequently, we can estimate C_{bio} as:

$$C_{bio} = C_{obs} - C_{bg} - C_{ff}$$

Uncertainty analysis

To quantify the uncertainty in our plant ^{14}C-derived C_{ff} and C_{bio} estimates (Fig. 3.5 of the main text), we consider the uncertainty in the C_i and Δ_i terms in the mass balance equations as described in the table below. These quantities are also used as inputs for the York regression in Figure 3.4 of the main text.

Term	Estimation approach	Uncertainty range (varies)
C_{obs}	Standard deviation of two-week averages (the integration period of turfgrasses)	2 to 13 ppm
C_{bg}	Standard deviation of monthly average C_{obs} at chosen background site (SCI or VIC).	1 to 4 ppm
$C_r \frac{(\Delta_r - \Delta_{bg})}{(\Delta_{ff} - \Delta_{bg})}$	Following Miller et al. (2020), we assign 100% uncertainty to this term.	0.25 ppm
Δ_{obs}	Standard deviation of average Δ_{obs} of samples collected at a given site and season (e.g., DLA in Spring).	4 to 14 ‰
Δ_{bg}	The larger of either (a) the standard deviation of the monthly average Δ_{obs} at Utqiagvik, AK or (b) the maximum measurement uncertainty of Δ_{obs} at Utqiagvik, AK within the month	1.5 to 3.5‰
Δ_{ff}	Zero uncertainty because fossil fuels have no radiocarbon	0‰

To estimate the uncertainty in the mean C_{ff} and C_{bio} for a given site and season, we consider three approaches: (1) the standard deviation of the mean C_{ff} and C_{bio} by site and season, (2) propagating the uncertainty through the mass balance equations using a standard partial derivative approach, and (3) estimating uncertainty based on a Monte Carlo simulation with 10,000 randomized runs. In Figure 3.5 of

the main text, we chose the Monte Carlo approach, but also include the results for the other two approaches here.

The first uncertainty option simply considered the uncertainty as the standard deviation of the C_{ff} and C_{bio} averages. However, this approach does not capture the uncertainty that should propagate from C_{obs} and C_{bg}, and we think underestimates the uncertainty. The alternative error bars are shown below and are smaller than the error bars in the main text.

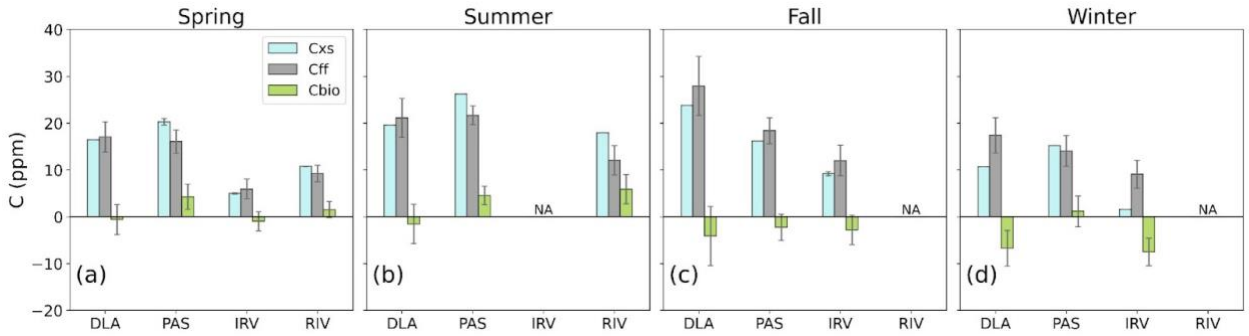

Figure C1. An alternative of Figure 3.5 of the main text, but the error bars are represented by the standard deviation of the means instead of the Monte Carlo-propagated uncertainties.

The second uncertainty option is derived using a standard error propagation approach: calculating the partial derivatives of each term in the equation and taking the root of the squared sums. The resulting uncertainty equations for C_{xs}, C_{ff} and C_{bio} are as follows.

Uncertainty in C_{xs}:

$$\sigma_{Cxs} = \sqrt{(\sigma_{Cobs})^2 + (\sigma_{Cbg})^2}$$

Uncertainty in C_{ff}, where "*dise*" is the biospheric disequilibrium term:

$$\sigma_{C_{ff}} = \sqrt{\left(\frac{\partial Cff}{\partial Cobs}\sigma_{Cobs}\right)^2 + \left(\frac{\partial Cff}{\partial \Delta bg}\sigma_{\Delta bg}\right)^2 + \left(\frac{\partial Cff}{\partial \Delta obs}\sigma_{\Delta obs}\right)^2 + \left(\frac{\partial Cff}{\partial dise}\sigma_{dise}\right)^2}$$

$$\sigma_{Cff} = \sqrt{\left(\left(\frac{(\Delta obs - \Delta bg)}{(-1000 - \Delta bg}\right) \cdot \sigma_{Cobs}\right)^2 + \left(\left((Cobs(\Delta obs - \Delta bg) - Cobs\frac{(-1000 - \Delta bg)}{(-1000 - \Delta bg)^2}\right) \cdot \sigma_{\Delta_{bg}}\right)^2 + \left(\left(\frac{Cobs}{(-1000 - \Delta bg)}\right) \cdot \sigma_{\Delta obs}\right)^2 + ((1) \cdot \sigma_{dise})^2}$$

Uncertainty in C_{bio}:

$$\sigma_{Cbio} = \sqrt{(\sigma_{Cobs})^2 + (\sigma_{Cbg})^2 + (\sigma_{Cff})^2}$$

Using these equations, we calculate uncertainty ranges of 2-6 ppm for C_{ff} and 3-14 ppm for C_{bio}. We also cross referenced these results with a Monte Carlo simulation (uncertainty approach #3), where we randomly sampled 10,000 artificial data points within the uncertainty ranges of C_{obs}, Δ_{obs}, C_{bg}, and Δ_{bg} and calculated the standard deviations of the mean C_{ff}, C_{xs}, and C_{bio} of all runs. We arrived at nearly identical uncertainty in C_{xs}, C_{ff}, and C_{bio} as resulted from the error propagation equations above.

Influence of wildfires

We considered whether wildfire emissions may have been captured by our data by examining daily fire anomalies and smoke plume imagery captured by the MODIS sensor on board NASA's Terra and Aqua satellites. The product (Satellite Detections of Fire, 2021 update) is publicly available online at https://worldview.earthdata.nasa.gov/. Only two measurement days had relevant thermal anomalies with smoke potentially being transported to our sites (May 26, 2022 and August 1, 2022, photos below). However, we did not observe anomalous CO_2 or CO values on these days, so we do not think our measurements were affected by these events.

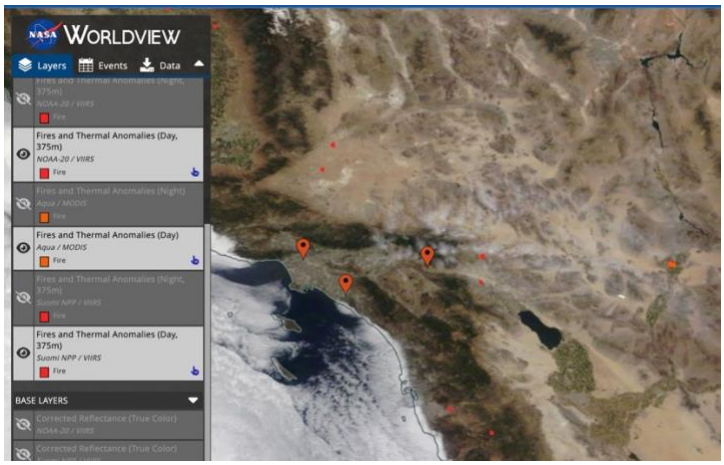

Figure C2. Thermal anomalies detected by MODIS on May 26, 2022 (BEA), showing some smoke coming from the east.

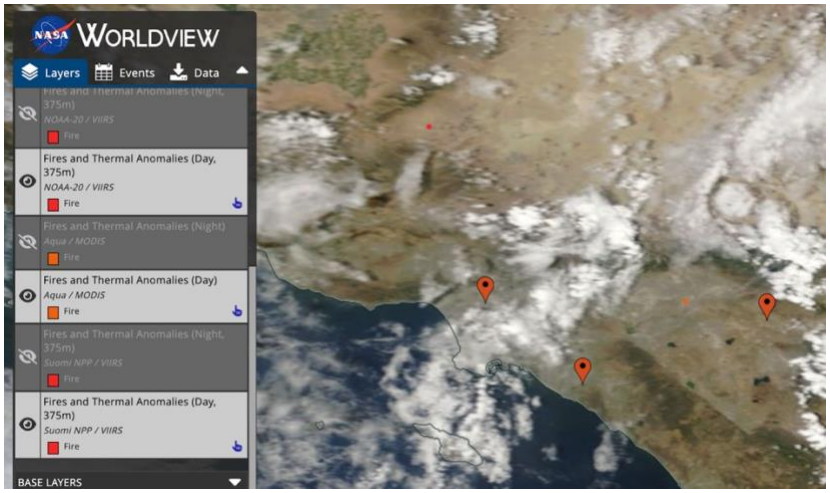

Figure C3. August 1, 2022 (RIV) - A fire anomaly within the LA basin, with some smoke possibly being mixed with clouds.

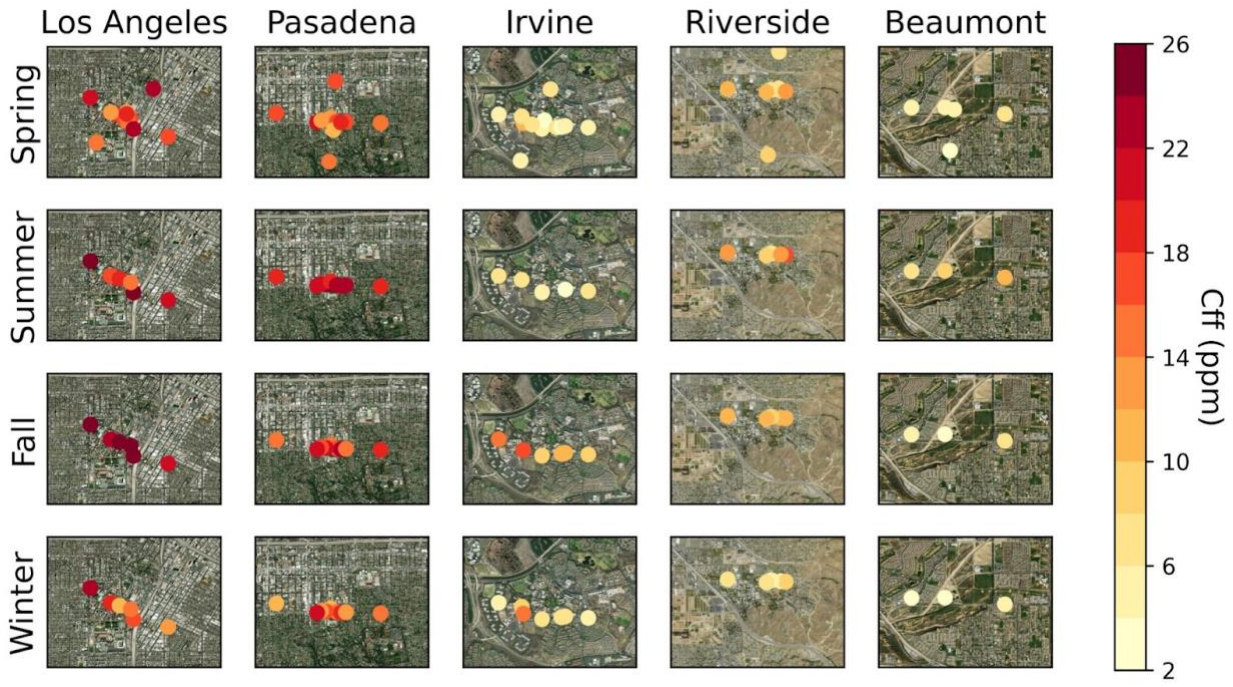

Figure C4. Maps showing turfgrass sampling locations at five sites along an urban to rural gradient. Colors indicate the fossil fuel enhancement (C_{ff}) derived from analysis of the plant ^{14}C content.

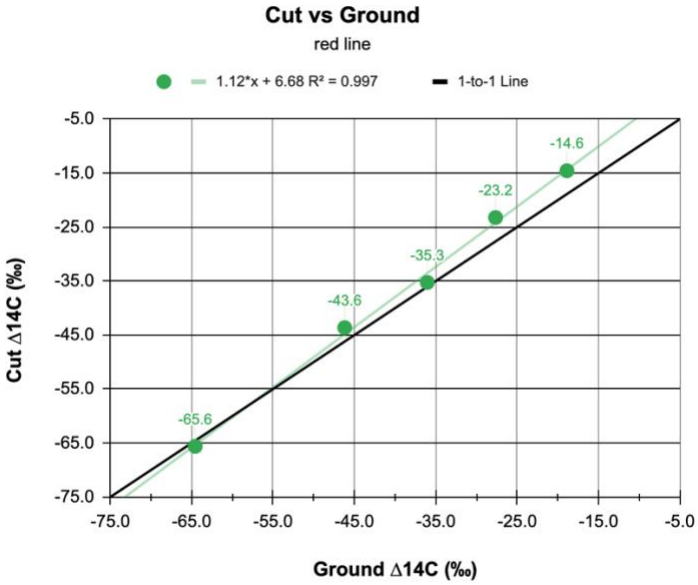

Figure C5. Correlation between $\Delta^{14}C$ of duplicate plant samples that were homogenized using different methods (cutting into small pieces on the y-axis versus grinding into powder using mortar and pestle on the x-axis). The maximum difference between the $\Delta^{14}C$ results was 4.4‰, which we use to quantify the uncertainty in our $\Delta^{14}C$ measurements based on intra-sample heterogeneity.

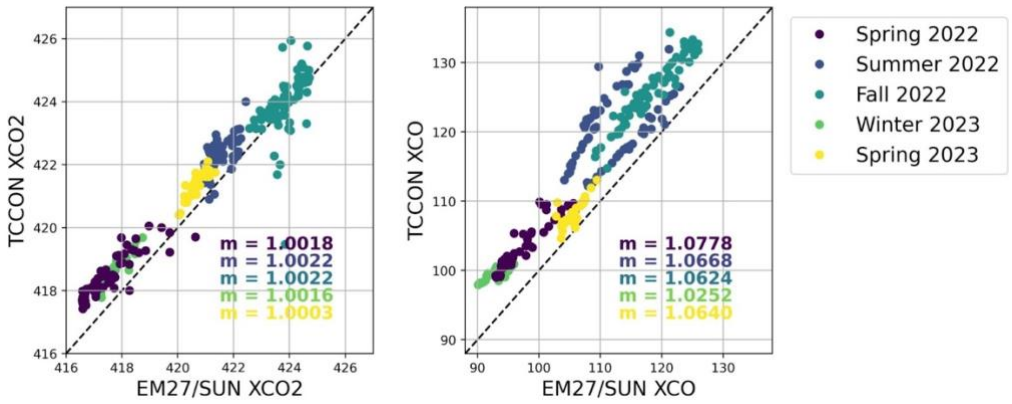

Figure C6. Calibration of XCO_2 (ppm) and XCO (ppb) measured with the EM27/SUN against the Caltech TCCON. Measurements were collected side-by-side for 1-2 days per season. The data shows the ten-minute averages of coinciding measurements. Colors indicate different seasons, with "m" being the slope of the linear fits for each season. The slopes were used as correction factors to calibrate the EM27/SUN data. The dashed line shows the 1-to-1 line.